AN EXPERIMENTAL AND THEORETICAL STUDY OF THE ELECTRONIC STATES OF CAFFEINE

John Nicolaas Kikkert, B.Sc. (Hons.)

Department of Physical and Inorganic Chemistry,
University of Adelaide.

Thesis presented for the degree of
Doctor of Philosophy

August, 1971

SUMMARY

The aggregation of caffeine in aqueous solution has been studied by means of absorption spectroscopy. Caffeine in aqueous solution was found to consist of equilibrium mixtures of monomers, dimers and tetramers, and the absorption spectra for these species were obtained from numerical analysis of the spectral changes on dilution.

A Gaussian analysis was carried out on the 36,600 cm^{-1} absorption band of the caffeine molecule to determine the vibrational spacing for the excited state.

Oriented films of caffeine in polyvinyl alcohol were studied. The dichroic spectrum was separated into bands and the transition dipole directions for the main transitions were determined.

A CNDO/2 total electron calculation was performed to determine the caffeine σ and π electron distributions. A PPP-SCF calculation was performed on the caffeine π electrons and electronic energies and oscillator strengths were obtained for the $\pi^* \leftarrow \pi$ transitions. Charge distributions and transition monopoles were calculated, and from these the interaction energy between the monomer units were calculated using the monopole-monopole approximation. The coupling coefficient was estimated both from the monopole-monopole and the dipole-dipole approximations.

The experimental dimer spectrum is compared with the dimer spectrum obtained from theoretical calculations for various values of the exciton coupling coefficient.

A high resolution fluorimeter was built, and the fluorescence spectrum of caffeine was studied in aqueous solution.

To the best of my knowledge and belief, this thesis contains no material previously published or written by another person, nor any material previously submitted for a degree or diploma at any University, except where due reference is made in the text.

ACKNOWLEDGEMENTS

I wish to thank Dr. T. Kuruoev for his encouragement and guidance during the course of this project.

I wish to thank the technical staff, especially Mr. K. Shepherdson and Mr. R. Byrne, for their help in the construction, maintenance and use of the apparatus required for this project. I am also indebted to Mrs. D. Newish for the typing of this thesis, and to my father for preparing the diagrams for xeroxing.

The award of a C.S.I.R.O. Postgraduate Studentship is also acknowledged.

J.N. Kilkart

Department of Physical and
Inorganic Chemistry,
The University of Adelaide,
South Australia.

August, 1971.

CONTENTS

CONTENTS (contd.) Page

CHAPTER 3

POLARIZED ABSORPTION SPECTROSCOPY

CONTENTS (contd.) Page

CHAPTER 4

THEORETICAL CALCULATIONS

CONTENTS (contd.) Page

CONTENTS (contd.) Page

1. INTRODUCTION

The interaction between purine and pyrimidine molecules has been the subject of considerable research in recent years. This interest arises from hopes that, firstly, the study of interactions and associated modes of aggregation in these molecules will throw light on the forces responsible for the organization in nucleic acids, and secondly, a knowledge of the nature of the interaction of radiation with these molecules and their aggregates will give an understanding of the radiobiological damage and other biological processes involving excited states of nucleic acids.

Caffeine (1:3:7 trimethyl xanthine) is a water soluble purine derivative that has been shown to aggregate in aqueous solution (Guttman and Higuchi, 1957). It was selected for study because it is obtainable relatively pure, is soluble in water and shows no pH or salt effects since there are no acidic hydrogens in the compound (Cavalieri et al, 1954). Fig. 1.1 shows the caffeine molecule drawn to scale according to the crystallographic data of Sutor (1958), with the usual numbering system used for purine molecules.

Aggregation has been studied by a variety of methods. These include:

1) Vapour Pressure Osmometry.

Measurement is made of the temperature difference between a drop of solvent and a drop of solution. This difference is directly

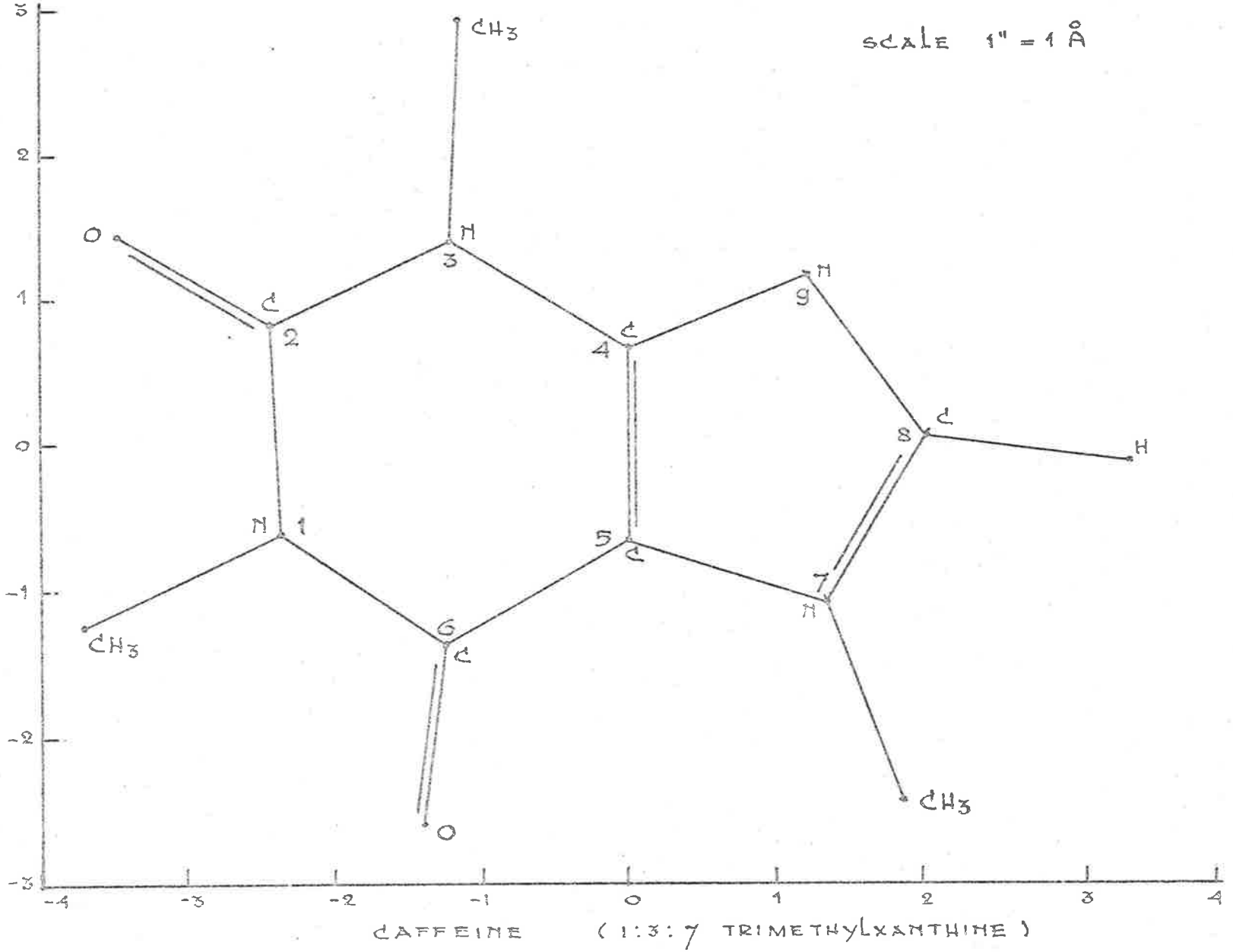

CAFFEINE (1:3:7 TRIMETHYLXANTHINE)

FIG. 1.1.

proportional to the number of solute particles per unit volume in the solution. For aggregating systems the number of solute particles per unit volume is less than if no aggregation occurs, which will result in a reduction in the temperature difference. This reduction can be related to the equilibrium constant for the aggregation process. Vapour pressure osmometry is discussed in more detail in Appendix 8.

2) Absorption Spectroscopy.

Since the monomer, dimer, trimer, etc. will be chemically distinct, although related, species, changes in the absorption spectrum will occur when aggregation takes place. When there are major changes in the spectrum such as shifts of the relative positions and intensities of the bands, then the system is said to show metachromacy. On the other hand, if the only noticeable change in the spectrum is a relative drop in the intensity of the bands, then the system is said to show hypochromicity. By studying the changes in the spectrum as a function of concentration, a measure of the amount of aggregation can be obtained. These changes will also give an indication as to the type of aggregates formed.

3) Microcalorimetry.

It is assumed that all heat of dilution effects are due to dissociation of complex species of the form A_n related to the equilibria

$$A_n \rightleftharpoons A_{n-1} + A$$

If equal equilibrium constants and equal enthalpies of dissociation

for each step are assumed the following relation is found (Stoesser and Gill, 1967):

$$\phi_L = \Delta H^o - \left(\frac{\Delta H^o}{K}\right)^{\frac{1}{2}} \left(\frac{\phi_L}{m}\right)^{\frac{1}{2}} \qquad 1.1$$

where m is the molarity and ϕ_L is the relative molal enthalpy. The enthalpy of reaction and the aggregation equilibrium constant can therefore be found from a plot of ϕ_L versus $(\phi_L/m)^{\frac{1}{2}}$. Equilibrium constants and enthalpies of dissociation are given for a number of purines, including caffeine, by Gill, Downing and Sheats (1967).

4) Partition Equilibria.

The distribution of the aggregating molecules between water and a non-miscible organic solvent is studied over a range of concentrations. It is assumed that a reversible equilibrium exists in the aqueous phase, while no aggregation occurs in the organic phase. The monomer concentration in the organic phase is directly proportional to the monomer concentration in the aqueous phase, since the chemical potential of the monomer in both phases must be equal (Denbigh). Guttman and Higuchi (1957) have derived the following equations:

$$(P.C)/(P.C)_m = 1 + 2K_1(X)_m + 3K_2(X)_m^2 + \ldots + nK_{n-1}(X)_m^{n-1} \qquad 1.2$$

where $(X)_m$ is the monomeric concentration of X, and P.C is the partition coefficient equal to the molar concentration of X in water divided by the molar concentration of X in the organic layer and $(P.C)_m$ is the partition coefficient when only monomers are present, i.e. at infinite dilution. Guttman and Higuchi showed that in the case of caffeine a

reasonable fit to 1.2 is obtained only if a monomer-dimer-tetramer equilibrium is assumed in which case 1.2 reduces to

$$((P.C)/(P.C)_m - 1)/CAF_m = 2K_1 + 4K_3(CAF)_m^2 \qquad 1.3$$

In this case a plot of the left-hand side versus $(CAF)_m^2$ gave a straight line. The intercept was K_1 and the slope K_3. The results on interpolation showed that K_3 approximates K_1^3 with K_1 equal to 13.5 litre $mole^{-1}$ at 23°C.

5) N.M.R.

When the environment around protons changes, changes in the NMR spectrum occur due to a change in the shielding of the proton by the surrounding electrons. Because of this, NMR is a sensitive indicator of aggregation and the type of interaction causing the aggregation. T'so et al (1964B, 1965, 1967) showed that the NMR shifts observed in purines on aggregation are likely to be caused by π electron interactions due to vertical stacking of the planes. An intermolecular distance of 3-4 Å was found to be most likely. Thakkar et al (1970) studied the NMR shifts in the caffeine molecule on aggregation and from the relative shift in the proton resonance peaks concluded that a configuration of the caffeine dimer known in group symmetry as C_2 is most likely. An equilibrium constant of 8.6 was calculated although the accuracy of the value is extremely doubtful since no tetramers were included in the calculations. The C_2 configuration of the caffeine dimer is shown in Fig. 1.2.

CAFFEINE DIMER MODEL BASED ON THE C_2 CONFIGURATION.

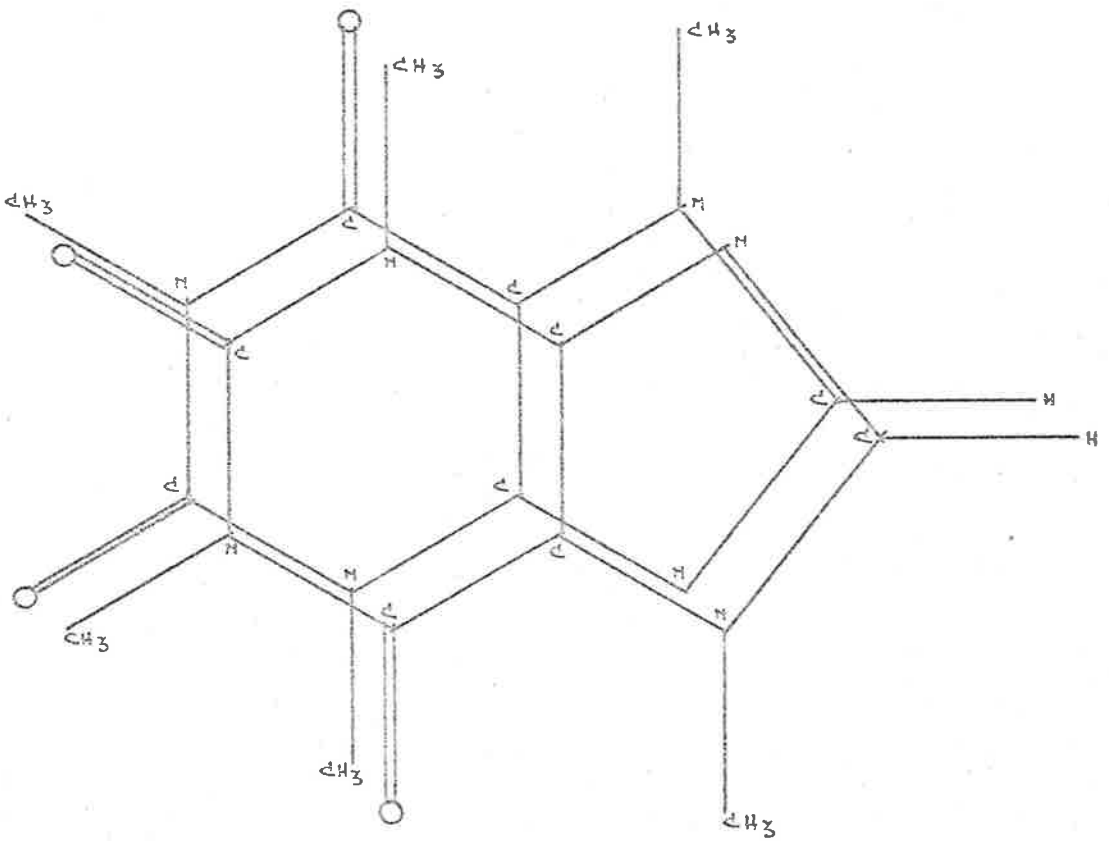

FIG. 1.2.

2. ABSORPTION SPECTRA

2.1 INTRODUCTION

Absorption spectroscopy has been used extensively as a tool in the study of the interactions of molecules in solution. The presence of molecular interactions can be observed by a change in the spectrum when the concentration of the solution is increased. If only one solute species is present, these spectral changes are due to the combination of these molecules to form aggregates. By studying these spectral changes as a function of concentration, the type of aggregates and the equilibrium constant for the aggregation can be determined (e.g. Ramette and Sandell, 1956; and Haugen and Melhuish, 1964).

The type of spectral changes observed on aggregation will indicate the degree of exciton coupling between the units of the aggregate. Strong coupling results in considerable changes in the spectral structure, such as changes in the relative intensity of bands, and the splitting of bands. Kuruesev and Strauss (1970) studied the changes in the spectrum of acridine orange hydrochloride on aggregation, and explained these changes in terms of strong exciton coupling in the dimer. For weak or intermediate coupling small changes in the spectrum are observed; mainly a slight broadening of the bands (due to splitting) or small changes of the relative intensities.

2.2 THEORY

Electromagnetic radiation, such as light, interacts with matter

through inducing an oscillating moment. For an harmonic oscillating dipole, the dipole moment at any given instant may be expressed as

$$\underline{\mu} = \underline{\mu}_0 \cos(2\pi\nu t) \qquad 2.1$$

where ν is the frequency of the oscillating dipole, and $\underline{\mu}_0$ is the amplitude vector. The total energy emitted per unit time by such an oscillating dipole, is given by Gilbert as

$$\frac{dE}{dt} = \frac{16\nu^4 \mu_0^2}{3c^3} \qquad 2.2$$

where c is the velocity of light.

In the classical picture a transition can only be expected when the frequency of the oscillating dipole is equal to the frequency of the oscillation of the electric field vector. In quantum mechanics the instantaneous dipole moment is replaced by the expectation value if the time averaged dipole for the initial and final states is different. The dipole moment associated with the change of state is

$$\underline{\mu}_{ab} = 2e \cos(2\pi\nu_{ab})\underline{r}_{ab} \qquad 2.3$$

where $\underline{r}_{ab} = \int \psi_a^* \underline{r} \psi_b \, d\tau$ in which a denotes the highest state and b denotes the lowest state. Substituting 2.3 in 2.2 yields

$$\frac{dE}{dt} = \frac{64\pi^4 \nu_{ab}^4 e^2}{3c^3} (\underline{r}_{ab})^2 \qquad 2.4$$

From this it follows that the absorption and instantaneous re-emissions associated with scattering depends on the fourth power of the frequency. Equation 2.4 is often written in the form:

$$\frac{dE}{dt} = h\nu_{ab} A_{ab} \qquad 2.5$$

where A_{ab} is the Einstein coefficient of spontaneous emission. It can be shown (Bauman) that A_{ab} is related to B_{ab}, the Einstein coefficient of induced emission, by

$$B_{ab} = \frac{c^3}{8\pi\nu_{ab}^3} A_{ab} \qquad 2.6$$

The Einstein coefficient of induced emission can be shown (Bauman) to be related to the extinction coefficient by the relation

$$\varepsilon = \frac{h\nu_{ab} B_{ab}}{c} \qquad 2.7$$

2.3 THE CAFFEINE SPECTRA

The ultraviolet absorption spectra of purine and pyrimidine bases have been studied extensively by many authors such as Mason (1954), Stewart and Davidson (1964), Voet, Gratzer, Cox and Doty (1963) and Clark and Tinoco (1965). These spectra show three or four $\pi^* \leftarrow \pi$ transitions in the region 30,000-40,000 cm^{-1}, in addition to a weak $\pi^* \leftarrow n$ transition which has been observed in some purine and pyrimidine bases (Kelly, 1970; Drobnik et al, 1966, 1967; Rich and Kasha, 1960).

Clark and Tinoco (1965) have correlated the spectra of these bases with the spectrum of pyrimidine, whose electronic states may be derived from benzene. On this basis, spectral bands of the bases can be separated into one band in the 36,000-40,000 cm^{-1} region, one band in

the 40,000-44,000 cm^{-1} region, and two bands in the 47,000-55,000 cm^{-1} region, which can be correlated to the benzene B_{2u}, B_{1u} and the E_{1u} transitions respectively.

The spectrum of caffeine in aqueous solution is shown in Fig. 2.1. It shows a peak at 36,600 cm^{-1} (B_{2u}), a small peak at 43,500 cm^{-1} (B_{1u}), and a large peak at 48,000 cm^{-1}, which may be due to two bands (B_{1u}), and a possible weak $\pi^*\leftarrow n$ transition in the 35,000 cm^{-1} region.

If caffeine is considered to be a perturbed benzene system, some indication of the polarisation directions of the transitions can be obtained. The theory of the intensity changes and polarisation directions of forbidden benzene transitions on substitution have been discussed by Platt (1951). In caffeine the main perturbers of the system are the two keto groups. The B_{2u} band is likely to be polarized along the line joining these groups, while the B_{1u} band would be perpendicular to this line. The strong perturbation required in this case leaves the usefullness of the correlation open to doubt. For this reason the bands in purine spectra are often referred to by number in preference to the label derived from the benzene bands. (e.g. Chen and Clark, 1969; and Stewart and Jensen, 1964) The weak $\pi^*\leftarrow n$ band is labelled band I, while the four $\pi^*\leftarrow\pi$ bands are labelled II-V in the order of their transition energies, starting at the low end. The B_{2u} band (36,600 cm^{-1}) is called band II while the B_{1u} band (43,500 cm^{-1}) is labelled band III. The two E_{1u} bands in the far ultraviolet (47,000-53,000 cm^{-1}) will be referred to as bands IV and V.

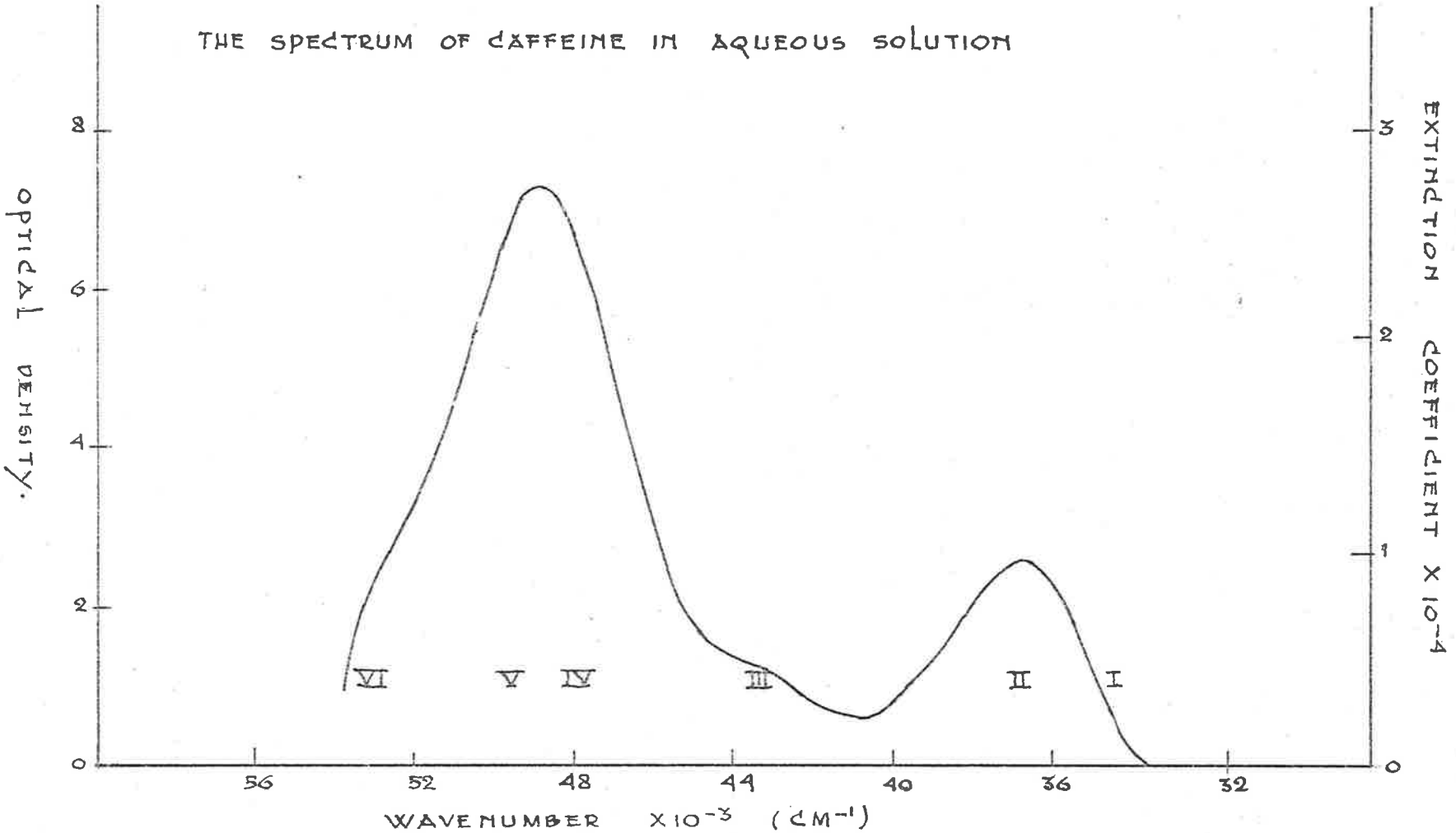
THE SPECTRUM OF CAFFEINE IN AQUEOUS SOLUTION
OPTICAL DENSITY.
EXTINCTION COEFFICIENT X 10⁻⁴
0
2
4
6
8
0
1
2
3
56
52
48
44
40
36
32
WAVENUMBER X10⁻³ (CM⁻¹)
VI
V
IV
III
II
I

FIG. 2.1

2.4 GAUSSIAN ANALYSIS

The vibronic band for caffeine at 36,600 cm^{-1} consists of a number of vibrational bands. It can be assumed that one vibration (the symmetric one) dominates, and that this vibration is harmonic. These assumptions have been made many times and they are the basic assumptions in many of the exciton theories (Siebrand, 1964; McRae, 1962). The band can then be considered to consist of a number of vibrational bands whose centres are given by

$$w_n = w_o + n\nu_o \quad cm^{-1} \qquad 2.8$$

The shape of the bands can be described by a large number of mathematical functions, many of which are described by Jones and Sandorfy (1956). The most commonly used of these functions are the Gaussian function and the Lorens function. Although the Lorens function is often more suitable the Gaussian function has been selected because of its mathematical simplicity. If a Gaussian wavefunction is assumed for each of the vibrational bands, then the intensity at any value of the wavenumber (w) is given by the relation:

$$I(w) = \frac{w}{\sqrt{\pi}\,d} \sum_{n=0}^{\infty} I_{on} \exp\left(\frac{w - w_n}{d}\right)^2 \qquad 2.9$$

where d is the bandwidth and w_n is the position of the n^{th} vibrational band in wavenumbers. I_{on} is the intensity of the transition from the o^{th} vibrational level in the groundstate to the n^{th} vibrational level in the excited state and is related to I_{on-1} through the relation:

$$M^2 = \frac{I_{01}}{I_{00}} = 2\frac{I_{02}}{I_{01}} = 3\frac{I_{03}}{I_{02}} = \ldots \qquad 2.10$$

M is a factor derived from the displacement of the equilibrium vibrational position in the excited state with respect to the equilibrium vibrational position in the groundstate and is called the Franck-Condon or displacement parameter.

A computer program was written to fit the measured absorption spectra to equation 2.9 and 2.10 according to the least squares method, with the bandwidth, α, the transition energy to the ground vibrational state of the excited state, w_o, the displacement parameter, M, and the vibrational spacing in the first excited state, v_1, as variables. This program is shown in Appendix 2.

2.4.1 Analysis of the spectrum of caffeine in water.

The absorption spectrum of caffeine in water was obtained by taking the average of the extinction coefficients as a function of wavenumber as obtained from the 1 cm cell readings described later in this chapter.

The following values were found to give the best fit:

$$\alpha = 1044 \text{ cm}^{-1}$$

$$M = 1.23$$

$$w_o = 35{,}255 \text{ cm}^{-1}$$

$$v_1 = 1260 \text{ cm}^{-1}$$

The fit for most points was accurate to within 1.0% which indicates

that the assumptions made are basically correct. There is some evidence of a very low intensity band around 35,000 cm^{-1} which causes a slight distortion in the fit at the high energy end of the range. Absorption due to the low energy tail of transition III causes the discrepancy between the fitted and measured values in the 39,000-40,000 cm^{-1} region. The resulting fit is shown in Fig. 2.2.

2.4.2 Analysis of spectrum of caffeine in cyclohexane.

Cyclohexane, 500 ml, (spectroscopic quality) was obtained from Drug Houses of Australia. A small quantity of caffeine was dissolved in cyclohexane, 20 ml, and diluted to give an optical density reading of approximately .6, in a 1 cm cell at 36,600 cm^{-1}. The spectrum of this solution was run against air on the SP700 spectrophotometer. The run was then repeated with the solvent only and the spectra were subtracted. The resulting optical density was then fitted to equations 2.9 and 2.10.

The best fit was obtained for the following values of the variables:

$$\alpha = 874 \text{ cm}^{-1}$$

$$M = 1.23$$

$$w_0 = 34{,}970 \text{ cm}^{-1}$$

$$v_1 = 1300 \text{ cm}^{-1}$$

The fit is rather insensitive to small changes in v_1 and reasonable fits can be obtained in the range 1250-1300 cm^{-1}. The bandwidth has decreased

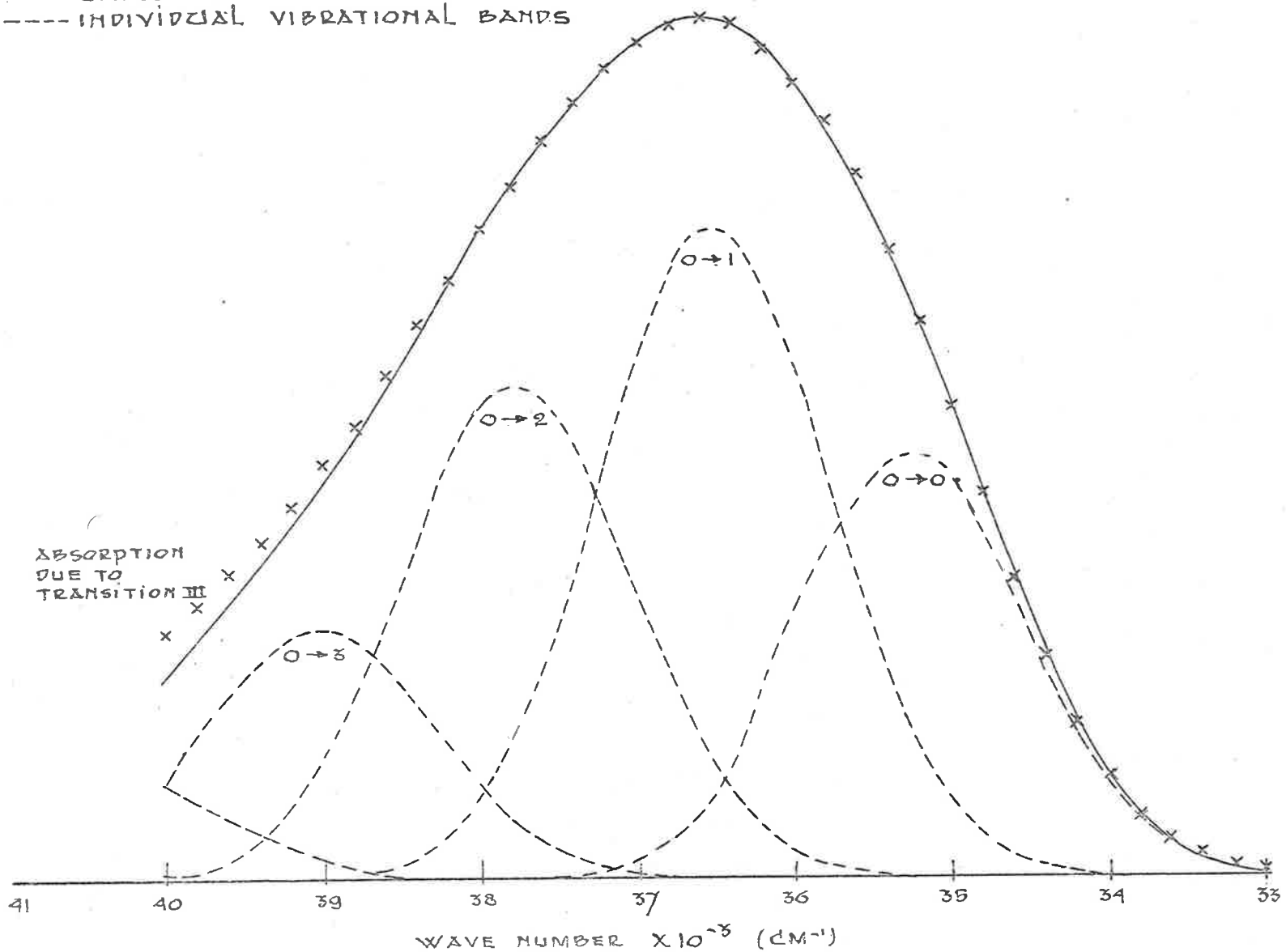
× EXPERIMENTAL POINTS
—— GAUSSIAN FIT
---- INDIVIDUAL VIBRATIONAL BANDS
ABSORPTION DUE TO TRANSITION III
0→3
0→2
0→1
0→0
41
40
39
38
37
36
35
34
33
WAVE NUMBER X10^-3 (CM^-1)

FIG. 2.2.

in the organic solvent, with a shift to the red of about 300 cm^{-1}. This shift is also evident in PVA films. The fit is not as good as in the case of water and a shoulder which cannot be fitted by the given model has appeared at 34,800 cm^{-1}. The shoulder causes a distortion of the fitted curve. The resulting fit is shown in Fig. 2.3. The shoulder could be due to the presence of the $\pi^* \leftarrow n$ transition which might be enhanced in non-aqueous solution, or due to the breakdown of the assumption that only the symmetric mode of vibration is observed. When the 35,400-34,400 region was illiminated from consideration a better overall fit was obtained, although fitting errors were still relatively large.

2.4.3 Conclusions.

The vibrational spacing of the caffeine molecule in the first excited state is 1280 cm^{-1} ± 20 cm^{-1} while the displacement parameter M was calculated as 1.23 ± .03. The value of 1280 cm^{-1} for the vibrational spacing of the first excited state fits in well with the value of 1300 as given by Drobnik and Augenstein (1966A) for purine. These values will be used later in the theoretical calculation of the dimer spectrum.

2.5 MATHEMATICAL MODEL FOR THE AGGREGATING SYSTEM

The following model is proposed to describe the aggregation of caffeine in aqueous solution:

GAUSSIAN FIT FOR ABSORPTION DUE TO TRANSITION II OF CAFFEINE IN CYCLOHEXANE.

× EXPERIMENTAL POINTS
—— GAUSSIAN FIT
--- INDIVIDUAL VIBRATIONAL BANDS

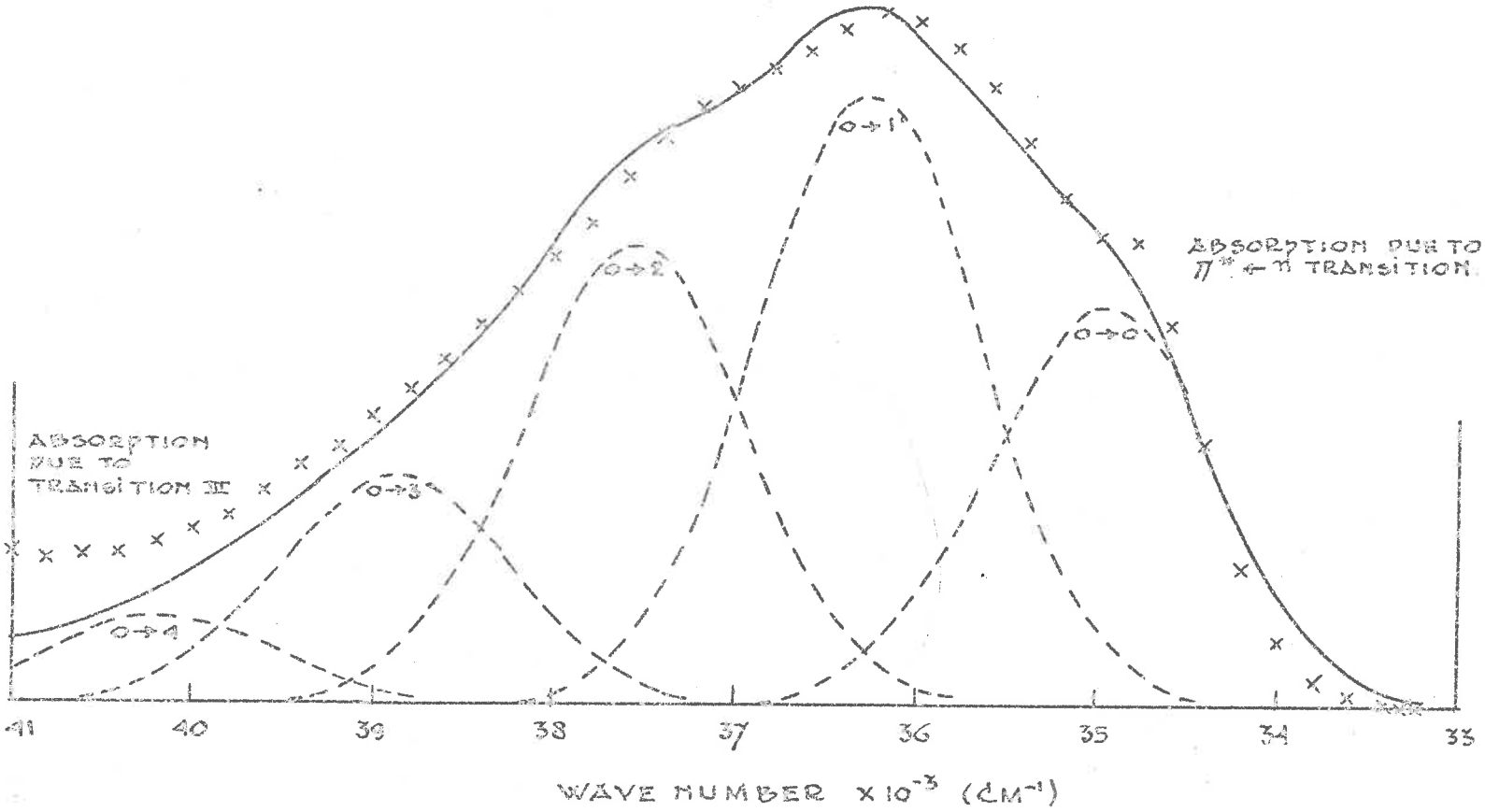

FIG. 2.3

$$A_1 + A_1 \rightleftharpoons A_2 \qquad k_2 = A_2/A_1^2$$
$$A_1 + A_2 \rightleftharpoons A_3 \qquad k_3 = A_3/A_2A_1$$
$$A_1 + A_3 \rightleftharpoons A_4 \qquad k_4 = A_4/A_3A_1$$
$$A_1 + A_{i-1} \rightleftharpoons A_i \qquad k_i = A_i/A_{i-1}A_1$$

$$K_n = \prod_1^n k_i = \frac{c_n}{c_1^{\,n}} \qquad 2.11$$

where c_i is the concentration of the i^{th} species.

An allowance has to be made for equilibria of the type:

$$A_{n-j} + A_j \rightleftharpoons A_n$$

These equilibria do not affect the validity of equation 2.11, although they do change the value of K_n. If c is the total concentration of the aggregating molecule:

$$c = c_1 + 2c_2 + 3c_3 + \dots + nc_n$$
$$\text{i.e. } c = \sum_s ic_i \qquad 2.12$$

where $\sum_s$ denotes a summation over all species present in the solution.

Substituting 2.11 into 2.12:

$$c = \sum_s ic_1^{\,i}K_i \quad \text{where } K_1 = 1 \qquad 2.13$$

The optical density of the solution is given by:

$$\varepsilon_t c = \varepsilon_1 c_1 + \varepsilon_2 c_2 + \dots + \varepsilon_n c_n \qquad 2.14$$

The apparent extinction of the solution is obtained by dividing the optical density by the concentration. It should be realised that

the measured absorption is due to monomer-dimer-trimer etc. species, so that the extinction is a linear combination of the coefficients of these species. To distinguish between the measured extinction and the true extinction coefficient due to a given singular molecule, the measured extinction will be referred to as the apparent extinction ($_t$).

$$\varepsilon_t = \sum_s^1 \varepsilon_i \left(\frac{c_i}{c}\right) \qquad 2.14a$$

By solving equation 2.13 for given values of K_1, K_2, ..., K_n, values for c_1, c_2, ..., c_n, can be obtained. These concentrations can be expressed in the form of the fraction of the compound in the i^{th} aggregate:

$$P_i = \frac{ic_i}{c} = \frac{iK_i c_i^i}{\quad} \qquad 2.15$$

and hence equation 3.14 can be written in the form:

$$\varepsilon_t = \varepsilon_1 P_1 + \frac{\varepsilon_2 P_2}{2} + \ldots + \frac{\varepsilon_n P_n}{\quad}$$

$$\varepsilon_t = \sum_s^1 \bar{\varepsilon}_i P_i \qquad 2.16$$

where $\bar{\varepsilon}_i$ is the extinction of the i^{th} species per monomer unit. This equation applies to all solutions. If there are m solutions, then the set of m equations can be written in matrix form as:

$$\varepsilon_{tj} = \sum_s^1 P_{ij}\, \bar{\varepsilon}_i \qquad 2.17$$

where $\underline{\varepsilon}_t$ is a column vector, $\underline{P}$ is an mxm matrix.

No exact solution to equation 2.17 is possible since the apparent extinction coefficients are experimental values and include experimental errors. The most suitable criterion for a solution to the equation

is to find values for the extinction coefficients such that:

$$\sum_{s} \Delta \varepsilon_j = \sum_{s} (\varepsilon_{tj} - \sum_{s} \bar{\varepsilon}_i P_{ij})^2 \qquad 2.18$$

is a minimum. This means that a least squares fit is carried out.

Equation 2.17 is more suitable for the least squares solution than equation 2.14 since the left hand side of equation 2.17 will be of the same order for all concentrations while if equation 2.14 were solved, weighting factors would have to be included in the calculations.

To solve equation 2.17, values for K_1, K_2, ..., K_n, $\bar{\varepsilon}_1$, $\bar{\varepsilon}_2$, ..., $\bar{\varepsilon}_n$, have to be found such that the sum of the squares of the deviations is a minimum. This however is impractical since it would give rise to a large number of variables. The simplifying assumption that the constants for each consecutive step are equal, has been used frequently (T'so, 1963, 1964A; Kankare, 1970). This reduces the number of variables from 2n to n+1. Substituting $K_i = k^i$ into equation 2.13 gives:

$$c = \sum_{s} i c k^{i-1}$$

or

$$ck - \sum_{s} i(c_1 k)^{i=0} \qquad 2.19$$

Equation 3.19 is a simple polynomial which can be solved by the Newton-Raphson method (Fröberg).

The mathematical treatment of the results can be reduced to five steps:

1) The equilibrium constant is defined (e.g. k = 13).

2) With the total concentration (c) of the aggregating species known,

c_1k can be calculated. Equation 2.19 can then be set up as a polynomial in c_1k. For a monomer-dimer-tetramer system, for instance, the equation becomes:

$$4(c_1k)^4 + 2(c_1k)^2 + (c_1k) - ck = 0$$

This is an equation of the type:

$$4X^2 + 2X^2 + X - a_o = 0$$

This equation can be solved to give a unique solution for c_1k and subsequently for c_1.

3) Once c_1 has been found c_2, c_3, c_4, etc. are calculated using equation 3.11 and from these the percentage of caffeine in the monomer (P_1), dimer (P_2), trimer (P_3), etc., form are calculated.

4) For each solution (j) an equation of the type:

$$\epsilon_{tj} = \bar{\epsilon}_1 P_{1j} + \bar{\epsilon}_2 P_{2j} + \bar{\epsilon}_3 P_{3j} + \cdots$$

can be set up. Each equation containing the unknowns $\bar{\epsilon}_1$, $\bar{\epsilon}_2$, $\bar{\epsilon}_3$, ... being the extinction coefficients per monomer unit for the monomer, dimer, trimer, etc., respectively. A large set of these simultaneous equations are available however (eighty or more). This set of m simultaneous equations is solved by the least squares method to give $\bar{\epsilon}_1$, $\bar{\epsilon}_2$, $\bar{\epsilon}_3$, etc.

5) The sum of the squares of the deviations for the best fit for the k value set is determined and compared with the sum calculated for other values of the equilibrium constant. The value of the equilibrium constant giving the best fit is then selected by inspection.

The computer program for the calculations is shown in Appendix 3.

For a monomer-dimer system there can be set up a much simpler mathematical equation, which can be solved by a least squares linear fit. The mathematics of this method are shown in Appendix 4.

2.6 EXPERIMENTAL

2.6.1 Instrumental.

All absorption readings were taken on a Unicam SP700 recording spectrophotometer, situated in an air-conditioned instrument room maintained at 22°C ± .2°C. The instrument was allowed a minimum warm-up period of 30 minutes. The zero transmission and zero optical density were adjusted at 36,600 cm^{-1} and were checked frequently while readings were taken, although generally no adjustment was found to be necessary. The spectra were recorded at scan speed 3 (2,200 cm^{-1}/min), chart speed 120 inch/hour, and resolution 2, over the range 46,000-30,000 cm^{-1}.

2.6.2 Cells.

The cells used in the absorption measurements were of three types covering a range in pathlength from 40 mm to .012 mm. They were the standard type of quartz silica long pathlength, 40, 10, and 5 mm cells; the two silica plates type, .3 and .1 mm; and the R.I.I.C. (Research and Industrial Instrument Company, London, England) UV-01 short pathlength ultraviolet cell, which can be used over a range from 2 mm to .012 mm by inserting teflon spacers.

Each cell was calibrated using freshly prepared alkaline potassium chromate solution (Haupt, 1952) prepared from potassium dichromate (B.D.H., ANALAR, 99.9% pure) in a solution of .10N potassium hydroxide. Potassium dichromate was used in preference to potassium chromate since the former can be obtained in a purer form. The concentration of chromate was selected to give an optical density of .6 ± .02 at 36,600 cm^{-1} in the cell used. The calibrated pathlength was reproduced to better than .5% for the UV-01 cell. The types of cells used together with the calibrated pathlengths (mm) are shown in Table 2.1.

The readings taken with the UV-01 cell were found to be highly reproducible. This could be due to the cell itself being set back in a metal block such that the windows would not be subject to damage or dirt. The reproducibility of the readings with the UV-01 cell was found to be highly sensitive to the method of filling. Good reproducibility was obtained when the solution was sucked in with an even pressure using a 5 ml syringe connected to the Luer lock of the cell. However when the liquid was forced in through the syringe, very poor reproducibility was obtained. Only a small amount of solution was required for rinsing and 5 ml or less was ample for several readings.

2.6.3 Calibration of the linearity of the SP700 spectrophotometer.

Ten alkaline dichromate solutions were prepared and their optical densities measured at 36,600 cm^{-1} in the UV-01 cell, using a .1 mm spacer, against a .10N potassium hydroxide blank. The short pathlength

TABLE 2.1

CELL TYPE	CELL LENGTH	CAL_1	CAL_2	$CAL_{AV.}$
QS	40	-	-	-
QS	10	10.03	10.01	10.02
QS	5	5.04	5.00	5.02
PLATES	.3	.3227	.3213	.322
PLATES	.2	.2148	.2156	.215
PLATES	.1	.1000	.1004	.1002
UV-01	2	1.79_4	1.78_6	1.79_0
UV-01	1	1.03_2	1.04_0	1.03_6
UV-01	.5	.520	.522	.521
UV-01	.2	$.204_2$	$.204_2$	$.204_2$
UV-01	.1	$.100_8$	$.101_2$	$.101_0$
UV-01	.05	.0505	.0505	.0505
UV-01	.025	$.0257_8$	$.0258_3$	$.0258_0$
UV-01	.012	$.0133_4$	$.0133_4$	$.0133_4$

cell was used because optical densities can be measured more accurately using this cell. A graph of optical density versus concentration seems to obey Beer's Law, but when the measured optical density of the solution was converted to the measured pathlength of the cell $l = (O.D/\varepsilon \cdot c)$, a small non-linearity was observed. This is shown in Fig. 2.4.

If it is assumed that the readings obtained at the low optical density end of the scale are correct, then the readings of .8 optical density are approximately .5% too high. Since all cell calibrations are done at .6 optical density all corrections should be made with respect to this value and subsequently corrections will range from -.25% at the low optical density end of the scale to +.25% for the highest values used for optical densities around .8. These corrections are of the order of the experimental error.

2.6.4 Preparation of solutions.

Sets of aqueous solutions of caffeine were prepared in the range 12 gm/litre (6×10^{-2}M) to .02 gm/litre (1×10^{-4}M). Each set, containing approximately ten solutions, was prepared on the same day as the spectra were recorded and covered a range of optical densities from .7 to .35 in the cell used. In this range of optical densities, only a small correction for the non-linearity of the SP700 spectrophotometer was necessary.

The most concentrated solution of each set was prepared by dissolving

OF THE CHROMATE SOLUTION USED.

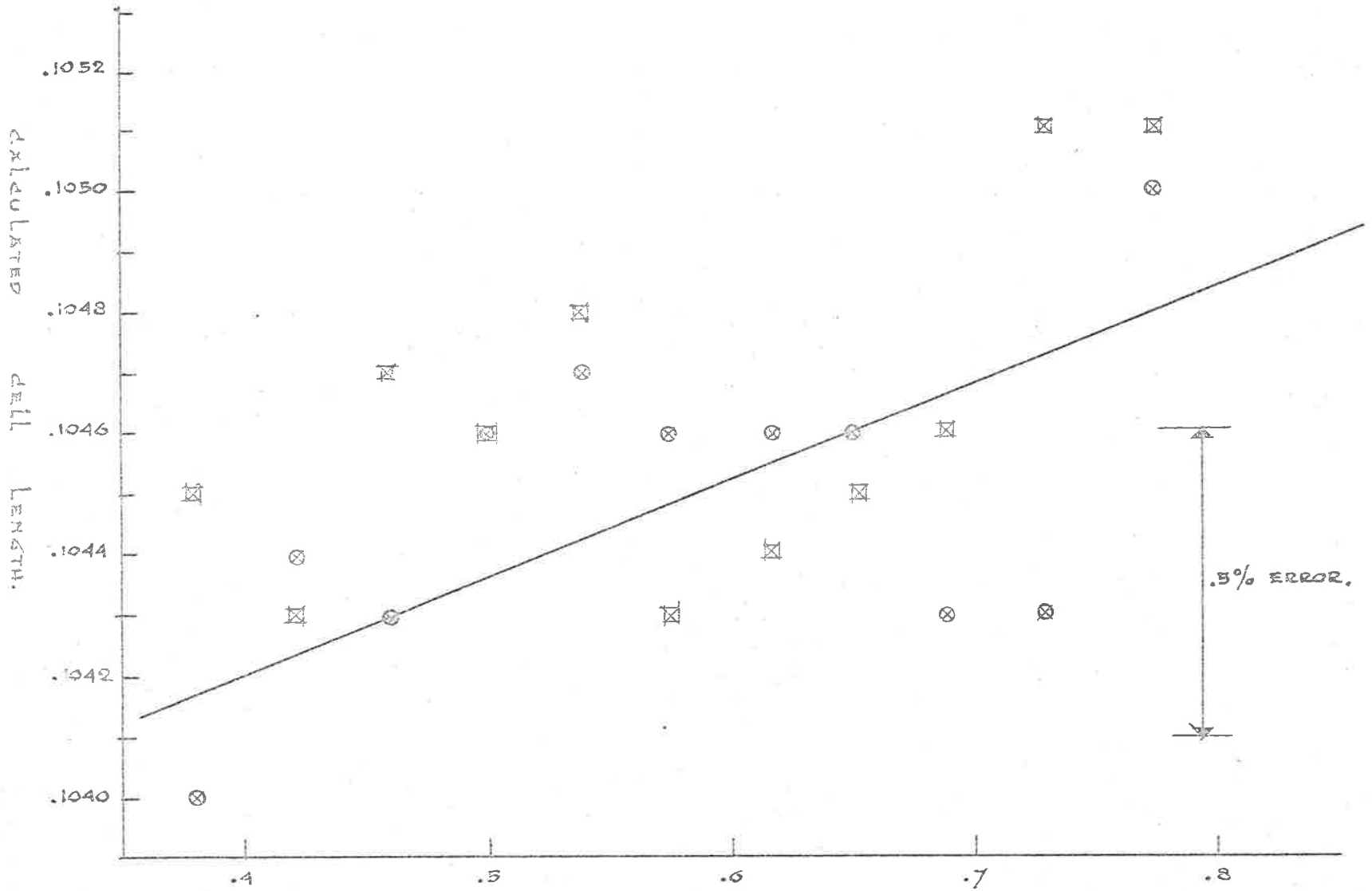

FIG. 2.4.

dried caffeine in water contained in a volumetric flask. All other solutions of the set were prepared from this solution by diluting a known weight of it with a known weight of water. The ratio of the original weight to the final weight of the solution gives the dilution factor. A very small error is introduced because the densities of the solution and the water are not the same, and hence the ratio of the weights is not equal to the ratio of the volumes. The error introduced in the concentration in this way is less than .1% for the most concentrated and effectively non-existent for the more dilute solutions.

2.6.5 Spectroscopic measurements.

All absorption spectra were measured on the Unicam SP700 recording spectrophotometer using scan speed 3 (2,200 cm^{-1}/min), chart speed 120 inch/hour, resolution 1, and with damping on 2.

To ensure complete equilibration at room temperature (22.0°C ± .2°C), the caffeine solutions were left in the instrument room for at least one hour prior to measurement. If the UV-01 adjustable pathlength cell was used, the cell was calibrated within four hours of commencement of the readings. The zero transmission and optical density settings of the spectrophotometer were adjusted prior to commencement and checked at frequent intervals during the measurements. Care was taken that the cells were always placed in the same position in the cell holder.

First two blanks (water) were run against air over the range

46,000 cm^{-1} to 30,000 cm^{-1}. The cells were then rinsed and filled with solution and the optical density was determined against air at the absorption maximum. The cells were then refilled and the optical density was determined again. If the optical density agreed within .001, the spectrum was run from 46,000 to 30,000 cm^{-1}.

The spectra for all solutions belonging to a given set were run one after the other without a break, to keep the systematic errors within the set to a minimum.

For the spectra determined in the UV-01 cell, optical densities were read from the chart from 46,000 cm^{-1} to 35,000 cm^{-1}, at 1000 cm^{-1} intervals and at the absorption maximum (36,600 cm^{-1}), while for the silica fixed pathlength cells, only the optical density at the maximum was determined. The average of the optical densities of the blanks was then subtracted after which a small baseline correction was made. The baseline correction was made by comparing the optical densities of the solution and the blanks in the non-absorption region (33,000-30,000 cm^{-1}). A correction for the non-linearity of the spectrophotometer was made for the readings taken at the absorption maximum, but not for those taken at the other points.

2.7 RESULTS

2.7.1 The determination of the extinction coefficients of caffeine species with a floating k value.

The apparent extinction at the absorption maximum was fitted by

the method described, to monomer-dimer, (1-2), monomer-dimer-trimer, (1-2-3), monomer-dimer-trimer-tetramer, (1-2-3-4), and monomer-dimer-tetramer, (1-2-4), models. The resulting fits are shown in Table 2.2.

TABLE 2.2

MODEL	1-2	1-2-3	1-2-3-4(3=4)	1-2-4
k_{min}	4.6	7.8	7.8	9.2
ε_1	9750	9780	9781	9788
ε_2	4856	6718	6979	6755
ε_3	-	5968	6364	-
ε_4	-	-	6364	4938
$\sum\Delta\varepsilon^2$	157820	119454	119408	112594

If a 1-2-3-4 model is assumed, the values for the extinction coefficient per monomer unit for the tetramer varying from -200 to +1800 for k values in the range 6 to 13 are obtained, while no significant reduction in the sum of the squares of the deviations is obtained ($\sum\Delta\varepsilon^2$ = 118973). Because of the large number of variables used in the fit and the small concentration of the tetramer involved, there is a large uncertainty in the calculated value of the extinction coefficient for this species.

A more realistic approach is to assume that the extinction coefficient per monomer unit for the tetramer is the same as that for

the trimer. This changes equation 2.17 to:

$$\epsilon_{tj} = \bar{\epsilon}_1 P_{1j} + \bar{\epsilon}_2 P_{2j} + \bar{\epsilon}_3 (P_{3j} + P_{4j}) \qquad 2.20$$

which can be solved as before. The results obtained from this are those shown in Table 2.2.

An alternative method of eliminating $\bar{\epsilon}_4$ from the fit is to assume a fixed value for this coefficient which reduces equation 2.17 to:

$$\epsilon_{tj} - \bar{\epsilon}_4 P_{4j} = \bar{\epsilon}_1 P_{1j} + \bar{\epsilon}_2 P_{2j} + \bar{\epsilon}_3 P_{3j} \qquad 2.21$$

in which case the left hand side of the equation is known for each concentration.

The 1-2-4 model gives a fit that is approximately 6% better than the other models. Fig. 2.5 and 2.6 show the measured extinction coefficients for the 1-2-3 and the 1-2-4 models respectively, as a function of the equilibrium constant, together with the sums of the squares of the deviations. The sum of the squares in each case varies only slightly as a function of the equilibrium constant. For the 1-2-4 model for instance, the minimum of 112594 is found for an equilibrium constant of 9.2. For a k value of 10.5, the sum of the squares is 112782. The method does not seem to be sensitive to changes in the value of the equilibrium constant used in the calculations. This results in a very large uncertainty in the value for this constant.

It should be realised that if the sum of the squares of the deviations is 112594, the majority of this is due to deviations of the experimental values from the ideal fit. Even if the correct model

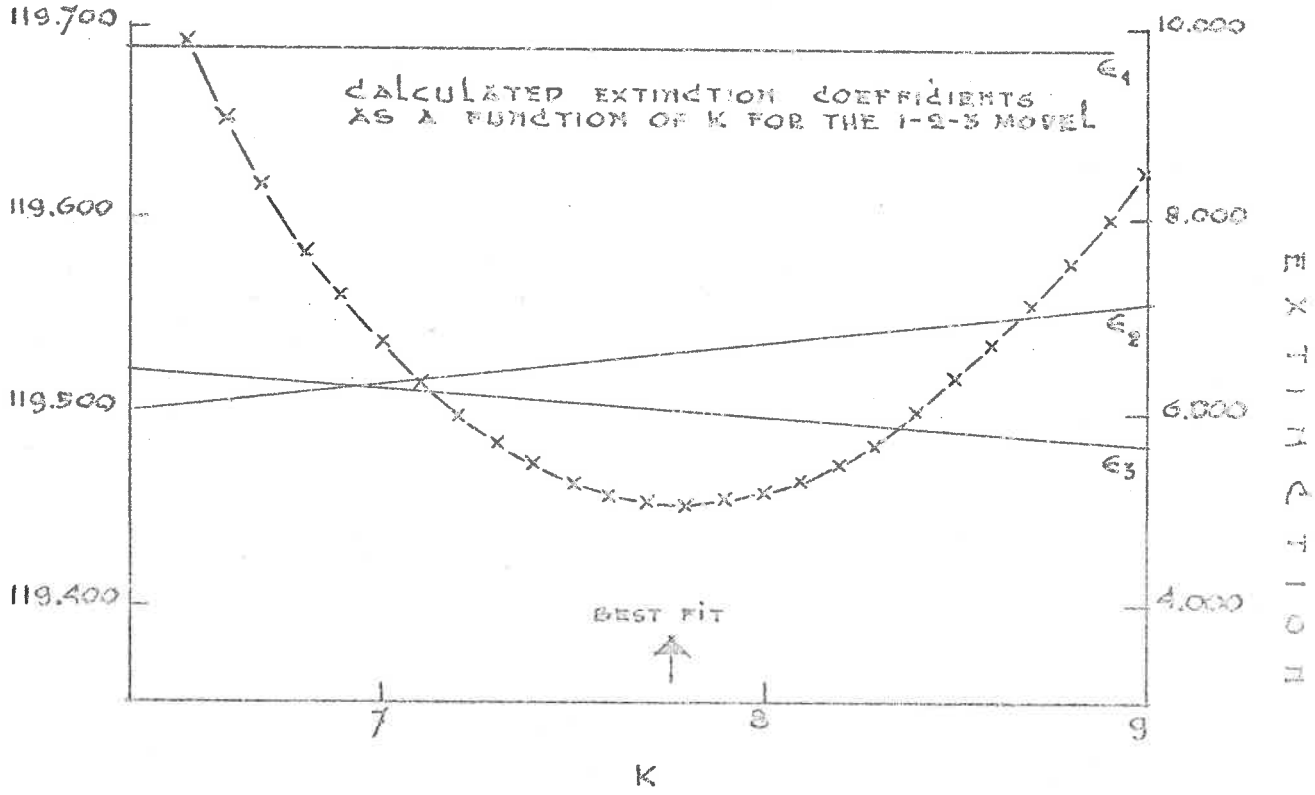
CALCULATED EXTINCTION COEFFICIENTS AS A FUNCTION OF K FOR THE 1-2-3 MODEL
119.700
119.600
119.500
119.400
10.000
8.000
6.000
4.000
ϵ_1
ϵ_2
ϵ_3
BEST FIT
7
8
9
K
SUM OF THE SQUARES OF THE DEVIATIONS ($\Sigma\Delta\epsilon^2$).
MOLECULAR EXTINCTION

FIG. 2.5

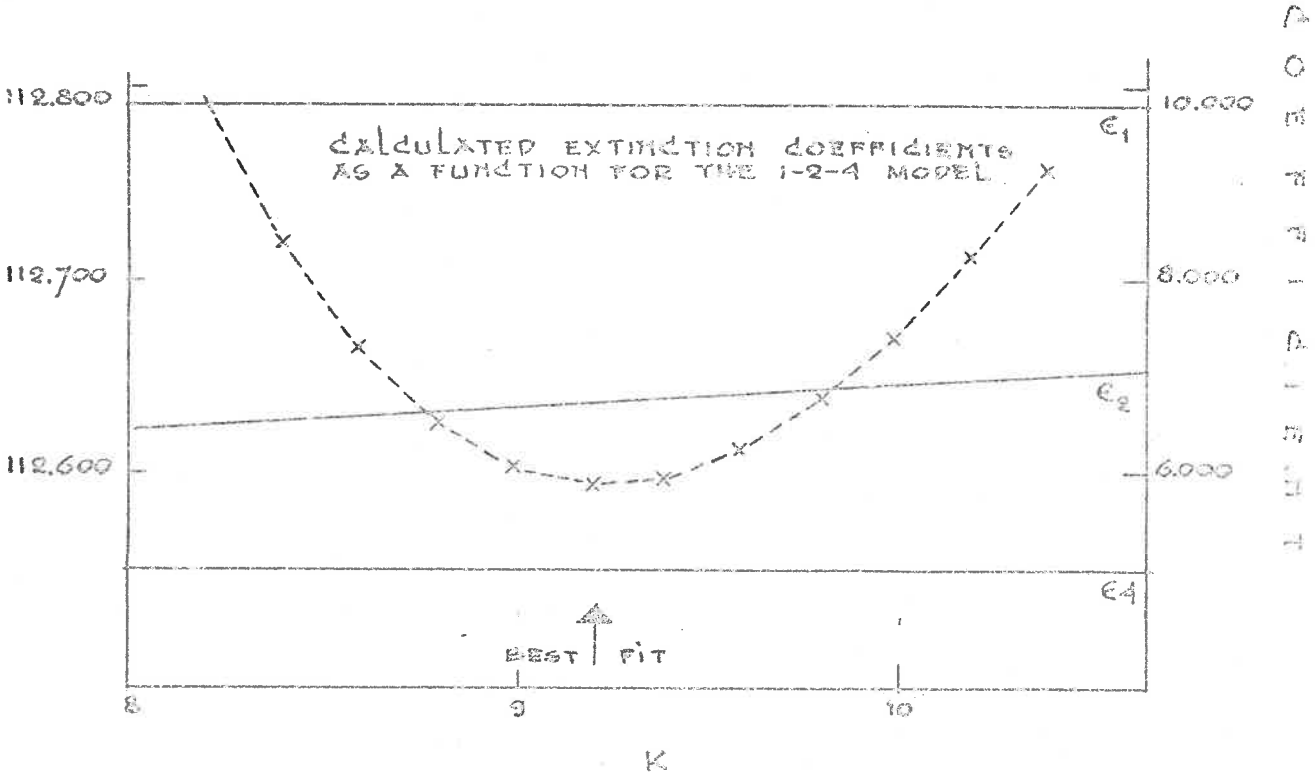
CALCULATED EXTINCTION COEFFICIENTS AS A FUNCTION FOR THE 1-2-4 MODEL
112.800
112.700
112.600
10.000
8.000
6.000
ϵ_1
ϵ_2
ϵ_4
BEST FIT
8
9
10
K
MOLECULAR EXTINCTION

FIG. 2.6

were assumed, and if the exact extinction coefficients were known and if these were used in the fit, the sum of the squares of the deviations would still be considerable and most probably well above 100,000. In this case an improvement from 119000 to 112000 must represent a considerable improvement in the fit. From this it can be concluded that a 1-2-4 aggregation model is most likely. This is in agreement with the results obtained by Guttman and Higuchi (1957), who, using a two phase equilibrium system, concluded that caffeine was likely to associate in the 1-2-4 form and obtained measured equilibrium constants for temperatures in the range $0^{\circ}C$ to $40^{\circ}C$ which on interpolation give an equilibrium value of k = 13.2 litre/M at $22^{\circ}C$. Guttman and Higuchi's value of the equilibrium constant is in good agreement with the value that can be calculated from the osmotic coefficient (.650 at $20^{\circ}C$) given by T'so, Melvin and Olson (1963) for caffeine. If a 1-2-4 equilibrium is assumed the given osmotic coefficient would correspond to a constant of 13.2 litre/M at $20^{\circ}C$. The work of T'so, and Guttman and Higuchi especially, leaves very little doubt that an equilibrium value of the order of 13 is correct. Guttman and Higuchi calculated an equilibrium constant for the formation of the tetramer in caffeine which is approximately the cube of the constant for the dimerisation which justifies the assumption which is made in the calculations that all steps in the aggregation are equally probable.

Thakkar et al (1970) derive an equilibrium constant of 8.6 ± 1 litre/M

from fitting the relative NMR shifts of the caffeine protons on aggregation. The accuracy of this constant is extremely doubtful since no tetramers were included in the calculation. At the highest concentration used (.1M) in these measurements over 20% of the monomer units would be in the tetramer form. The value for the constant was determined by fitting the experimental values which are limited to less than twenty points for each calculation to a least squares fit. The uncertainty in the equilibrium constant quoted in this work would be many times larger than the value given by the authors.

The direction and relative magnitudes of the proton shifts can be explained, according to Thakkar, by a configuration referred to in group-symmetric terms as a C_2 configuration, although other card stacked configurations could also account for the observed shifts.

2.7.2 The determination of the spectra of caffeine species for fixed k.

The extinction values calculated for the solutions used in the UV-01 cell show a much smaller scatter (Fig. 2.7) and subsequently only these data were used to calculate the extinction coefficients at wavenumbers other than the absorption maximum. These solutions give 80 experimental values to be fitted by k, $\varepsilon_1(w)$, $\varepsilon_2(w)$, and $\varepsilon_{3or4}(w)$. The data was fitted at wavenumbers from 46,000 cm^{-1} to 35,000 cm^{-1} at 1000 cm^{-1} intervals and the corrected and uncorrected absorption maximum data values. Equilibrium constants ranging from 6 to 16 were obtained

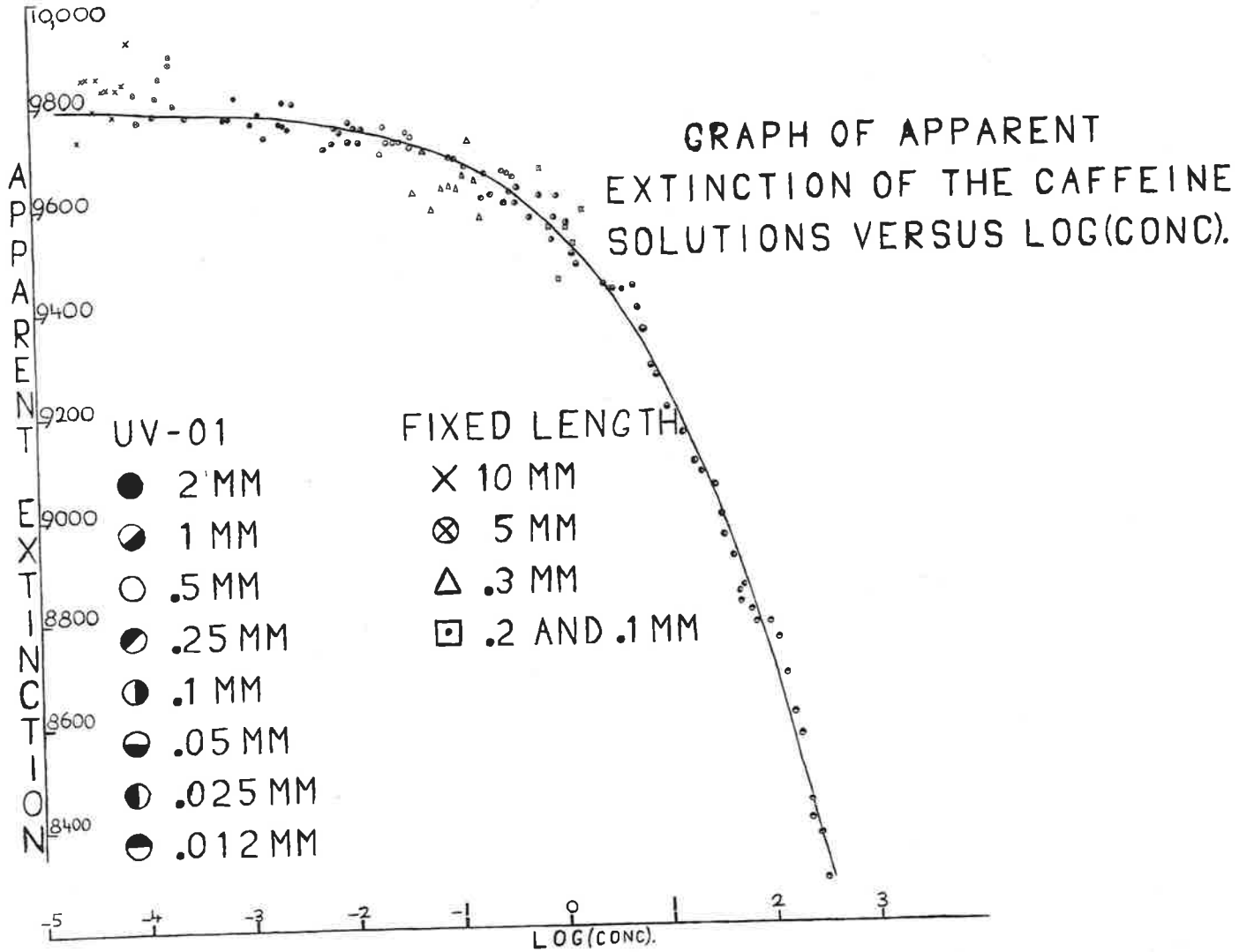
GRAPH OF APPARENT EXTINCTION OF THE CAFFEINE SOLUTIONS VERSUS LOG(CONC).
APPARENT EXTINCTION
10000
9800
9600
9400
9200
9000
8800
8600
8400
UV-01
2 MM
1 MM
.5 MM
.25 MM
.1 MM
.05 MM
.025 MM
.012 MM
FIXED LENGTH
X 10 MM
⊗ 5 MM
△ .3 MM
⊡ .2 AND .1 MM
-5
-4
-3
-2
-1
0
1
2
3
LOG(CONC).

FIG 2.7.

from the best fit criterion depending on the wavelength used.

The calculated extinction coefficients vary strongly with the value of the equilibrium constant used. If a complete spectrum is required then it becomes necessary to fix the equilibrium constant and to calculate the spectrum accordingly.

With the equilibrium constant assumed to be equal to 13 litre/M the values for the monomer, dimer, and tetramer extinction coefficients were calculated for the monomer-dimer-tetramer and the monomer-dimer-trimer models using the eighty UV-01 cell solutions for wavelengths from 35,000 to 46,000 cm^{-1} at 1000 cm^{-1} intervals. The extinction coefficients for the maximum were also calculated for the data corrected for the non-linearity of the spectrophotometer, and for the uncorrected data. The resulting extinction coefficients are shown in Tables 2.3 and 2.4.

The extinction coefficients calculated from the measured apparent extinction for the 1-2-3 and 1-2-4 models are shown as a function of wavelength in Fig. 2.8. Neither model gives a consistently lower sum of the squares of the deviations over the range studied.

2.7.3 The interpretation of the spectra of aggregates of caffeine.

Because of the similarities in the spectra obtained using the 1-2-4 and the 1-2-3 models, the following observations can be made independently of the model that is selected to correspond to caffeine aggregation.

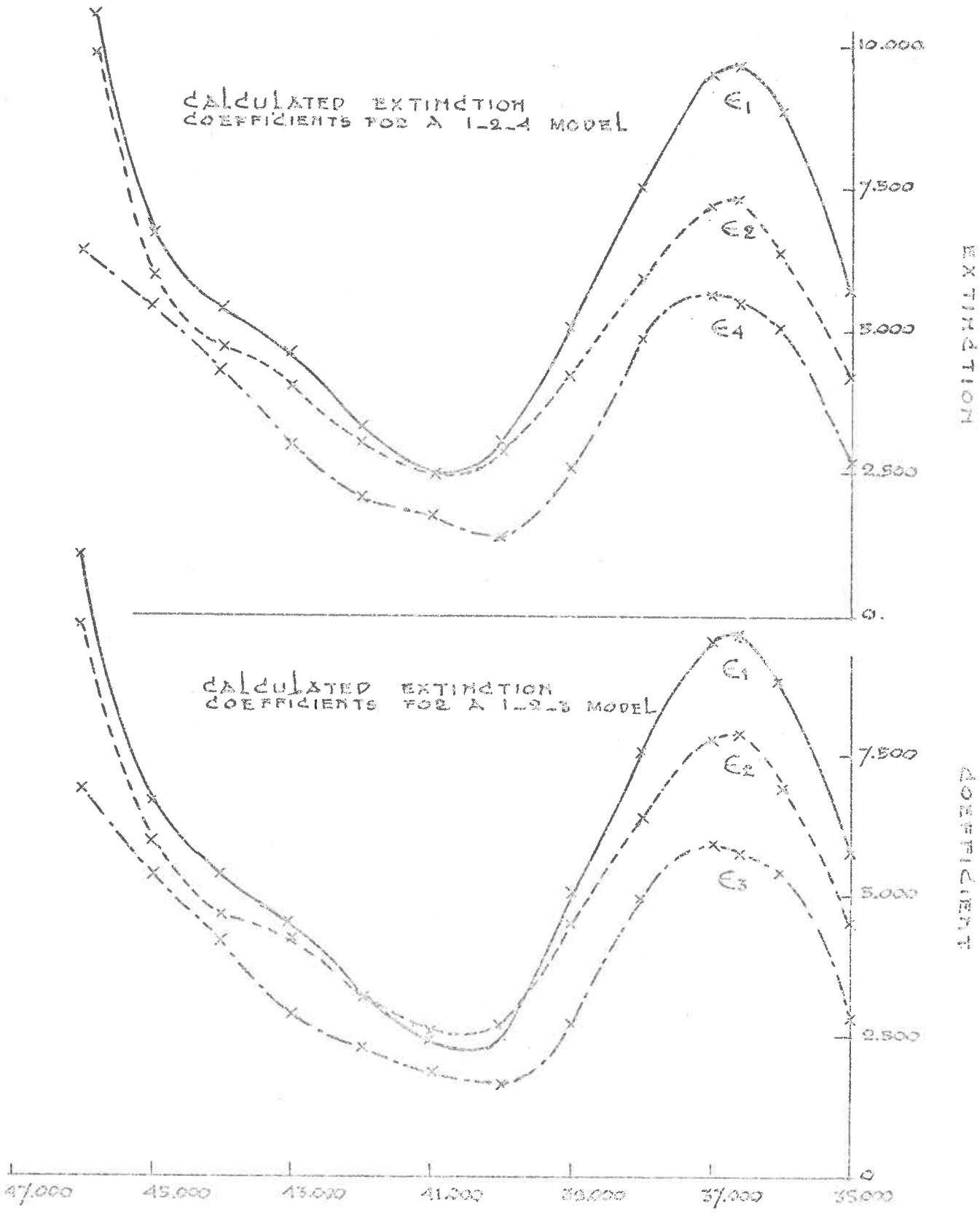
CALCULATED EXTINCTION COEFFICIENTS FOR A 1-2-4 MODEL
ϵ_1
ϵ_2
ϵ_4
10.000
7.500
5.000
2.500
0.
EXTINCTION COEFFICIENT
CALCULATED EXTINCTION COEFFICIENTS FOR A 1-2-3 MODEL
ϵ_1
ϵ_2
ϵ_3
7.500
5.000
2.500
0
47.000
45.000
43.000
41.000
39.000
37.000
35.000
WAVE NUMBER (cM^{-1}).

FIG. 2.8.

TABLE 2.3

CALCULATED EXTINCTION COEFFICIENTS FOR 1-2-4 MODEL

WAVE-NUMBER	ε_1	$\Delta\varepsilon_1$	ε_2	$\Delta\varepsilon_2$	ε_4	$\Delta\varepsilon_4$
35,000	5079	15	4252	124	2770	591
36,000	8899	14	6524	116	5316	554
36,600	9763	11	7407	94	5566	450
$36{,}600_{cor}$	9794	9	7502	73	5030	348
37,000	9610	14	7377	118	5731	562
38,000	7662	14	6043	115	4945	547
39,000	5129	10	4256	83	2644	397
40,000	3094	7	2546	62	1463	383
41,000	2501	7	2546	62	1803	294
42,000	3352	12	3134	97	2181	462
43,000	4672	15	4072	123	3007	589
44,000	5446	13	4556	105	4411	501
45,000	6783	15	5830	123	5630	587
46,000	11097	26	9202	214	6565	1020

TABLE 2.4

CALCULATED EXTINCTION COEFFICIENTS FOR 1-2-3 MODEL

WAVE-NUMBER	ϵ_1	$\Delta\epsilon_1$	ϵ_2	$\Delta\epsilon_2$	ϵ_3	$\Delta\epsilon_3$
35,000	5066	18	4636	226	2830	516
36,000	8886	17	6997	219	5406	498
36,600	9748	14	7944	183	5836	416
$36{,}600_{cor}$	9775	11	8155	136	5327	309
37,000	9597	18	7858	229	5996	521
38,000	7651	17	6414	217	5035	494
39,000	5117	12	4636	152	2793	345
40,000	3086	12	3238	150	1692	343
41,000	2497	9	2658	116	1908	263
42,000	3346	14	3307	182	2318	415
43,000	4662	18	4383	226	2969	514
44,000	5440	15	4733	195	4286	445
45,000	6776	18	6073	229	5478	521
46,000	11079	32	9829	401	6910	914

There is an overall decrease in the extinction coefficient per monomer unit on aggregation. This change in extinction can be correlated to the increase in the extinction of DNA on going from the native state to the denatured state. The extinction at the maximum was found to have increased by a factor of 1.43 by Falk (1964) when a DNA film was denatured by high humidity. Falk regarded the increase in intensity as due to the change in the environment of the nucleotides from one in which each is in a close stacked arrangement, to one in which each has become hydrated. This is the inverse process to that which takes place when the monomer units aggregate. For dimerisation one would expect the change in intensity to be approximately half of the change observed in DNA since the monomer units go from an environment in which they are fully hydrated to one in which they are hydrated on one side and stacked with another monomer unit on the other side. Table 2.5 shows the calculated changes in the extinction of caffeine.

TABLE 2.5

MODEL	ε_1	ε_2	$\varepsilon_1/\varepsilon_2$
$1\text{-}2\text{-}4_{cor}$	9794	7502	1.30
1-2-4	9763	7407	1.32
$1\text{-}2\text{-}3_{cor}$	9775	8155	1.20
1-2-3	9748	7944	1.22
DNA	denatured	native	1.43

For the 1-2-4 model the calculated value for ϵ_2 is greater than the value calculated for ϵ_1 at 41,000 cm^{-1}, but even then the difference between the values is well within the calculated variance, so that the order of the two coefficients may actually be reversed. This could be due to an increase in the intensity of transition III in the dimer.

One of the basic rules in absorption spectroscopy studies of interacting molecules is that the total integrated intensity of the absorption spectrum for the interacting system should remain constant with respect to the non-interacting system. This means that the interactions responsible for the decrease in the intensity of transition II are most probably associated with interactions of bands in the region above 47,000 cm^{-1}. The coupling in the dimer between transition II of the first molecule and transition II of the second molecule seems to be weak, since little change is observed in the band corresponding to transition II in the dimer spectrum. Although no large splitting or shifts are observed, the band does seem to be slightly broadened with a possible shift to the blue of 50-100 cm^{-1}. These effects seem to be much stronger in the tetramer (or trimer) spectrum, although the large uncertainty in these spectra leaves some doubt about any conclusions drawn from them.

Interaction between transitions II and III would be weak due to the low oscillator strength of transition III, although the relative intensity of transition III in the dimer seems to have increased.

3. POLARIZED ABSORPTION SPECTROSCOPY

3.1 INTRODUCTION

To calculate the exciton interaction in the caffeine dimer, knowledge of both the magnitude and direction of the transition moments are essential. Unfortunately, molecular orbital calculations at this stage cannot accurately predict the magnitude of the transition moments, while theoretical calculations of the direction of the transition moments have not led to any useful results at all. For purine, for instance, the transition moment direction for transition II changes by approximately 90° when configuration interaction is included in SCF-MO calculations (Pullman, 1968).

Experimentally, the magnitude of the transition dipole, usually referred to as the oscillator strength, can be obtained relatively easily from integrating the extinction of the corresponding vibronic band in the absorption spectrum (see section 4.5). The direction of the transition moment can be determined experimentally by a variety of methods including polarised absorption of single crystals, polarised secular reflection of single crystals (Stewart and Davidson, 1963), polarised fluorescence (Jablonski, 1935), and polarised absorption of partially oriented molecules. For the first three techniques extensive instrumentation and highly specialised skills are required, especially for the crystal methods. Although a fluorimeter was available, it was still in the experimental stage and not ready for polarized fluorescence studies.

The polarized absorption of partially oriented films method is restricted to planar molecules and in-plane transition moment directions. The magnitudes of the angles of the transition moments are obtained with respect to the longitudinal axis of the molecule, without indicating whether these are positive or negative angles. Often the ambiguity in the angle determination can be resolved by studying a derivative of the compound which has a different orientational axis.

The most convenient method of orienting the molecules is by the method developed by Fraser (1953, 1958, 1960) and modified by Tanizaki (1959, 1965). Molecules which are dissolved in a polyvinyl alcohol (PVA) sheet will tend to orient if the sheet is stretched along an axis. Both Tanizaki and Fraser developed a method of correlating the measured dichroic ratio and the amount of stretching of the sheet with the angle of the transition moment. The Tanizaki method was based on a mathematical model in which an imaginary sphere of the PVA film was deformed into an ellipsoid of equal volume. The stretch ratio was defined as the ratio of the major and minor axes of the ellipsoid. A set of complex mathematical equations was derived relating the stretch and the dichroic ratio with the transition moment angle. Experimentally the stretch is determined by putting four equally spaced dots on the film defining the X and Y axes of the film. On stretching the X axis will become the major axis while the Y axis becomes the minor axis. The stretch ratio is determined from the ratio of the distance between the dots on the major axis and those on the minor axis.

Fraser's model is much simpler. The stretch ratio is defined as the ratio of the original length of the film and length of the film after stretching. The relationship between the stretch and the degree of orientation was assumed to follow the one derived by Kratky (1933) for the distribution of rod-like crystals in an isotropic matrix.

Both theories fail to include the molecular shape in the calculations. This means that for a given stretch chlorobenzene would be expected to be oriented to the same degree as anthracene. A better theory would be one that includes an allowance for the molecular shape (e.g. ratio of minor to major axis of the molecule). Recently Thulstrup et al (1968, 1970) introduced a highly complex model in which the shape of the molecule is taken into consideration.

Stretch ratios calculated by the Tanisaki method are approximately related to the ones calculated by Fraser's method by the relation:

$$S_f^{3/2} = S_t \qquad 3.1$$

The results obtained with the two methods for a given film were found to be very similar. Because of its greater simplicity, Fraser's method was selected for the interpretation of the results in this work.

3.2 THEORY

The properties of a light beam are specified by three perpendicular vectors; $\underline{c}$, $\underline{E}$, $\underline{M}$, representing the velocity, the electrical and the magnetic vectors respectively. Interaction between the electrical vector

of the light and the oscillating dipole of the molecule gives rise to transitions whose probabilities (P_{ab}) are proportional to the square of the interaction between the electrical vectors and the transition moments ($\underline{M}_{ab}$) (Fraser, 1958).

$$P_{ab} \propto (\underline{M}_{ab} \cdot \underline{E})^2 \qquad 3.2$$

When ordinary light passes through a solution of the absorbing compound, both the molecules and the electrical vectors are randomly oriented. If however, plain polarized light is used, and the molecules are oriented by setting them in a PVA film, then:

$$P_{ab} \propto |\underline{M}_{ab}|^2 |\underline{E}|^2 \cos^2\theta \qquad 3.3$$

where θ is the angle between the plane of polarisation and the transition moment. It follows that the extinction coefficient (ε) is related to the angle between the plane of polarisation and the transition moment by:

$$\varepsilon = K \cos^2\theta \qquad 3.4$$

where K is a proportionality constant.

Fraser introduced the following model. Consider a molecule oriented with its long axis along the OC axis of a three-dimensional cartesian set of coordinates, OABC (Fig. 3.1). Because the molecule can take up any position about the OC axis, the possible orientations of the transition moment vector, $\underline{M}_{ab}$, form a circular cone of semi-angle α about the OC axis, where α is the angle between the transition moment vector and the long axis of the molecule.

With the light travelling along the OA axis the electrical vector

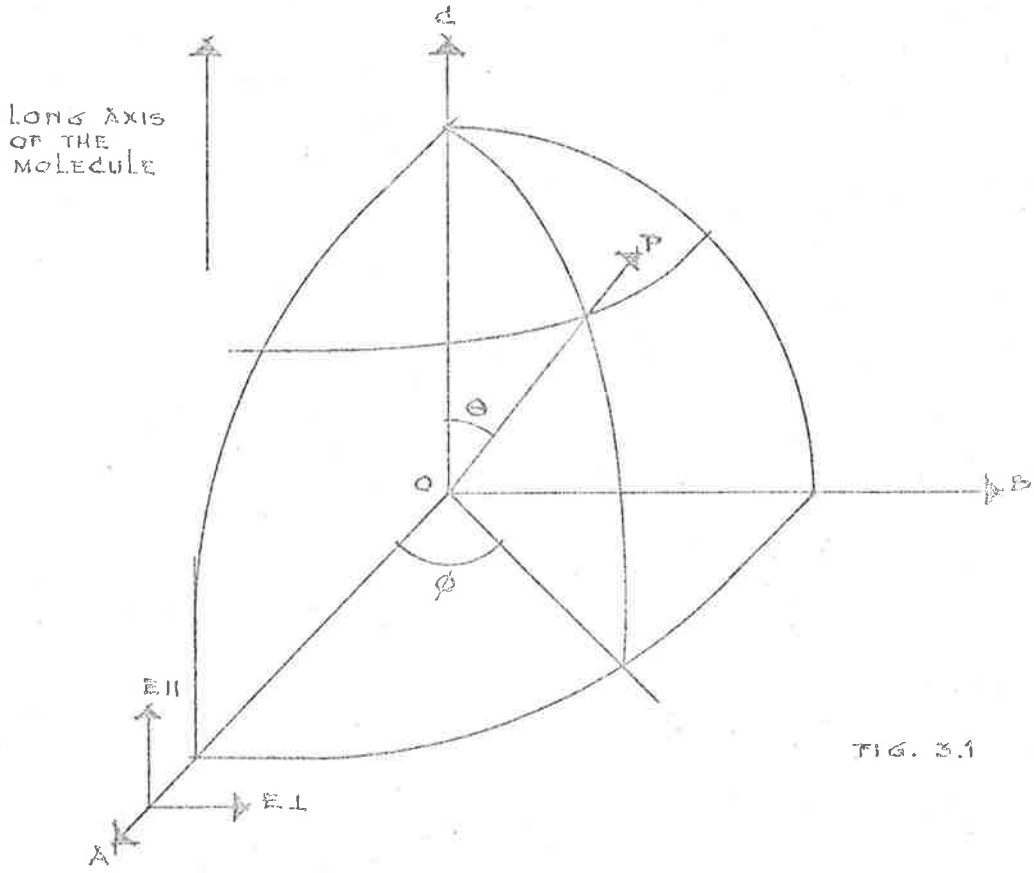
LONG AXIS OF THE MOLECULE
Z
C
P
θ
O
B
φ
E II
E⊥
A

FIG. 3.1

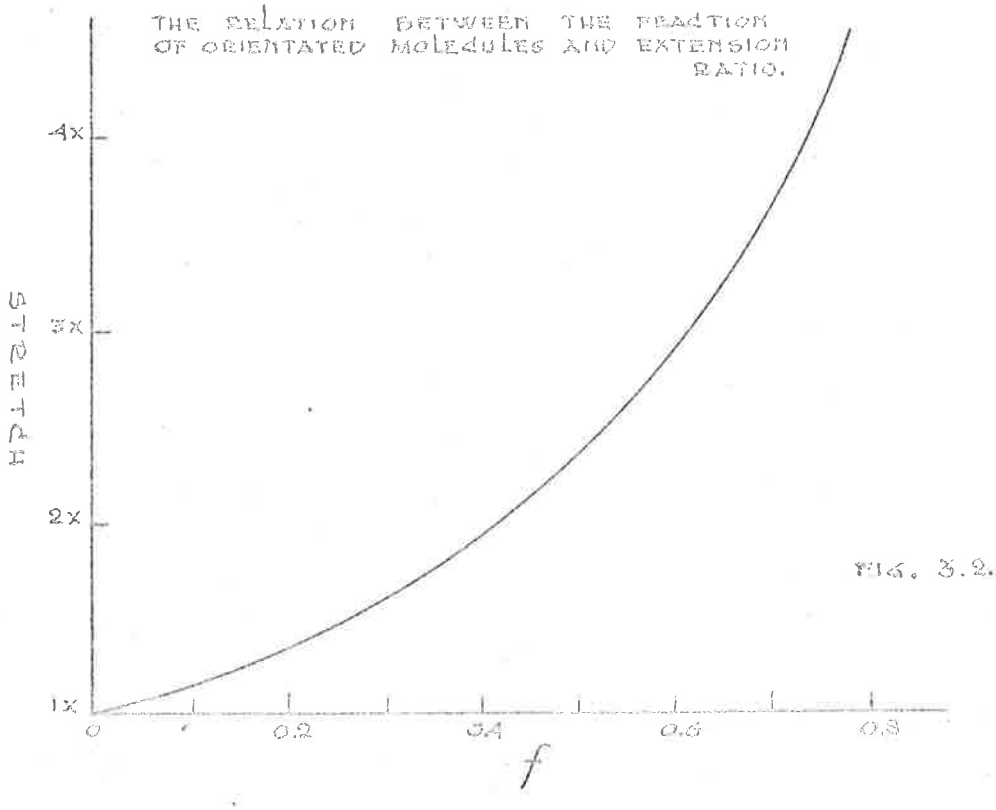
THE RELATION BETWEEN THE FRACTION OF ORIENTATED MOLECULES AND EXTENSION RATIO.
STRETCH
4x
3x
2x
1x
0
0.2
0.4
0.6
0.8
f

FIG. 3.2.

is polarized either in the OC direction (parallel to the axis of orientation) or the OB direction (perpendicular). If the light is polarised parallel to the OC axis the angle between the electrical vector and the transition moment is equal to α. The extinction is given by:

$$\varepsilon_{/\!/} = K \cos^2\alpha \qquad 3.5$$

For light polarised parallel to the OB axis the projection of the transition moment on the electrical vector is given by the relation:

$$\underline{M}_{ab} \cdot \underline{E} = |\underline{M}_{ab}| \; |\underline{E}| \sin\alpha \sin\phi \qquad 3.6$$

where ϕ is the angle the plane of the molecule makes with the OA axis. The experimental extinction however, is the measured averaged extinction of a large number of molecules distributed over all possible orientations about the OC axis. The extinction is in this case obtained from integrating over all possible orientations ($0 \leq \phi \leq 2\pi$).

$$\varepsilon_1 = \frac{K}{2\pi} \int_0^{2\pi} \sin^2\alpha \sin^2\phi \, d\phi \qquad 3.7$$

The dichroic ratio for perfect alignment is defined as:

$$R_o = \frac{\varepsilon_{/\!/}}{\varepsilon_\perp} = 2\cot^2\alpha \qquad 3.8$$

For a perfectly aligned sample, equation 3.8 gives the angle of the transition moment vector with respect to the long axis of the molecule. In practice however, perfect alignment is impossible and only partial alignment of the sample occurs, resulting in a lower dichroic ratio than would have been expected in the ideal case. The simplest model allowing for non-ideality, introduced by Fraser, (1953), assumes that

a fraction (f) of the molecules is oriented while the remainder of the molecules is randomly distributed. For partial orientations equations 3.5, 3.7, and 3.8 combine to give:

$$R = \frac{1 + \frac{1}{3}(R_o - 1)(1 + 2f)}{1 + \frac{1}{3}(R_o - 1)(1 - f)} \qquad 3.9$$

where R is the dichroic ratio for partial orientation. Substituting $f = 1$ in 3.9 gives $R = R_o$.

Fraser (1958) found that the most plausible relation between the fraction of oriented molecules and the extension ratio (S) of the film was derived by Kratky (1933) for the distribution of rod-like crystals embedded in an isotropic matrix. Fig. 3.2 shows the relation between the fraction of oriented molecules and the extension ratio S.

3.3 EXPERIMENTAL

3.3.1 Preparation of PVA films.

A 5% solution of polyvinyl alcohol (J.T. Baker Chemical Company, Baker grade, 99-100% hydrolyzed) in 1:5 ethanol-water was prepared. Of this solution 15 ml was poured into a perspex tray (3" x 4") floating on mercury, and left to set. After 74 hours the PVA film was removed from the tray and the edges, which were slightly uneven, were trimmed. The remainder of the film was cut into four equal rectangles and stored between filter papers, under a light weight, until used.

3.3.2 Preparation of oriented films.

A square glass plate (20 cm x 20 cm) was thoroughly cleaned with distilled alcohol and a thin layer of caffeine solution (.2 gm/litre) was poured onto it. A piece of PVA film was placed on top, and a few millilitres of the solution was then poured on top and left to soak in for 30 seconds, after which the solution was poured off. To remove crinkles from the film it was rolled flat with a ¼ inch glass rod while excess solution around the edge of the film was absorbed with filter paper.

Because of its high plasticity when wet, the PVA film was dried in a dessicator for 3 hours prior to transferring it to the stretcher. During drying the corners of the film were stuck down with Dymo tape to stop it from curling.

The stretcher, based on a design by Tsunoda and Yamaoka (1965), is illustrated in Fig. 3.3. The film was clamped on by means of two brass plates which were screwed onto the fixed and the movable arms of the stretcher.

The stretching of a PVA film can be aided in two ways. At high temperatures the film can be stretched to many times its original length in a very short period of time, but stretching by this method would be uneven and lead to unreproducible results. The other method consists of stretching the film in an atmosphere of high humidity. As the film absorbs moisture from the atmosphere it can be stretched relatively easily. Enclosing the stretcher with film in a container with several

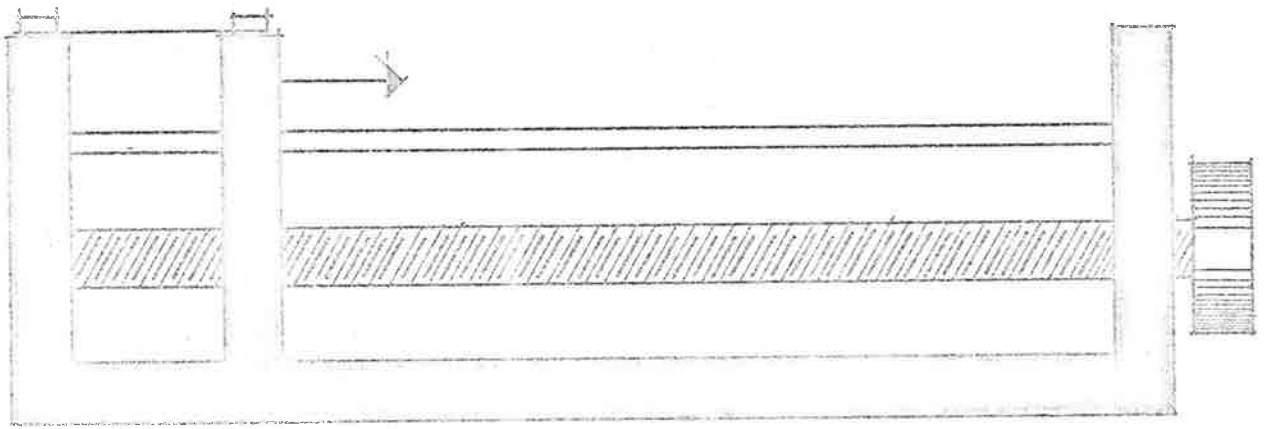

FIG. 3.3 STRETCHING DEVICE.

crystallizing dishes filled with water at approximately 60°C allows the film to be stretched to three times its original length in one hour.

It was necessary to dry the films after they had been stretched to overcome relaxation effects, and hence stop the film from contracting after it was removed from the stretcher. A stream of hot air from a hairdryer was found to be the most convenient method.

3.3.3 Preparation for spectroscopic measurements.

For the spectroscopic measurements in the ultraviolet, the PVA films were put on a blackened machined block (4.3 cm x 1.2 cm x .9 cm) through which an elliptical hole (3.0 cm x .7 cm) had been drilled. A small frame with a rubber gasket was screwed onto the block to prevent the film from contracting. The film hence forms a window in the brass block.

In between spectroscopic measurements the films were stored in a blackened desiccator over silica gel.

3.3.4 Correction to the spectra.

Most of the work on oriented films up to now has been done in the infrared region of the spectrum. In this region, scattering corrections can be conveniently made by extrapolating from the region where no scattering occurs. Since scattering depends on the fourth power of the frequency (equation 2.4) a plot of log(optical density of scatter) versus log(wavenumber) should have a gradient of 4. From this the

optical density due to the scattering in the absorption region, in theory, can be predicted.

This method was however found to be unsatisfactory for use in this work for at least two reasons. Firstly; because of the high quality of the films used, the intensity losses due to scatter were small, much smaller than the losses due to reflection which do not depend on the fourth power of the wavelength. Secondly; for corrections to measurements in the ultraviolet, where the hydrogen lamp is used, the extrapolation has to be done from the visible region, where a tungsten lamp is used. The difference in the optical density measured at 30,000 cm^{-1} (the change-over point), using the two lamps, make it extremely difficult to make an accurate correction.

It was found to be more convenient to prepare a blank PVA film from the same batch of films with approximately the same amount of stretch. Fig. 3.4 shows the scattering and reflection as a function of wavelength as obtained from the blank, together with the unpolarised spectrum of a caffeine-PVA film. It can be seen that the light losses due to scatter are nearly negligible for all values of the wavenumber but the 45,000-46,000 cm^{-1} region, where the high absorption of caffeine reduces the errors, introduced due to inadequate correction. The use of a blank PVA film compensated for most scatter and reflection so that only a small base line correction was needed to allow for small variations in thickness and quality of the film.

SPECTRUM OF CAFFEINE_P.V.A. FILM AND BLANK.

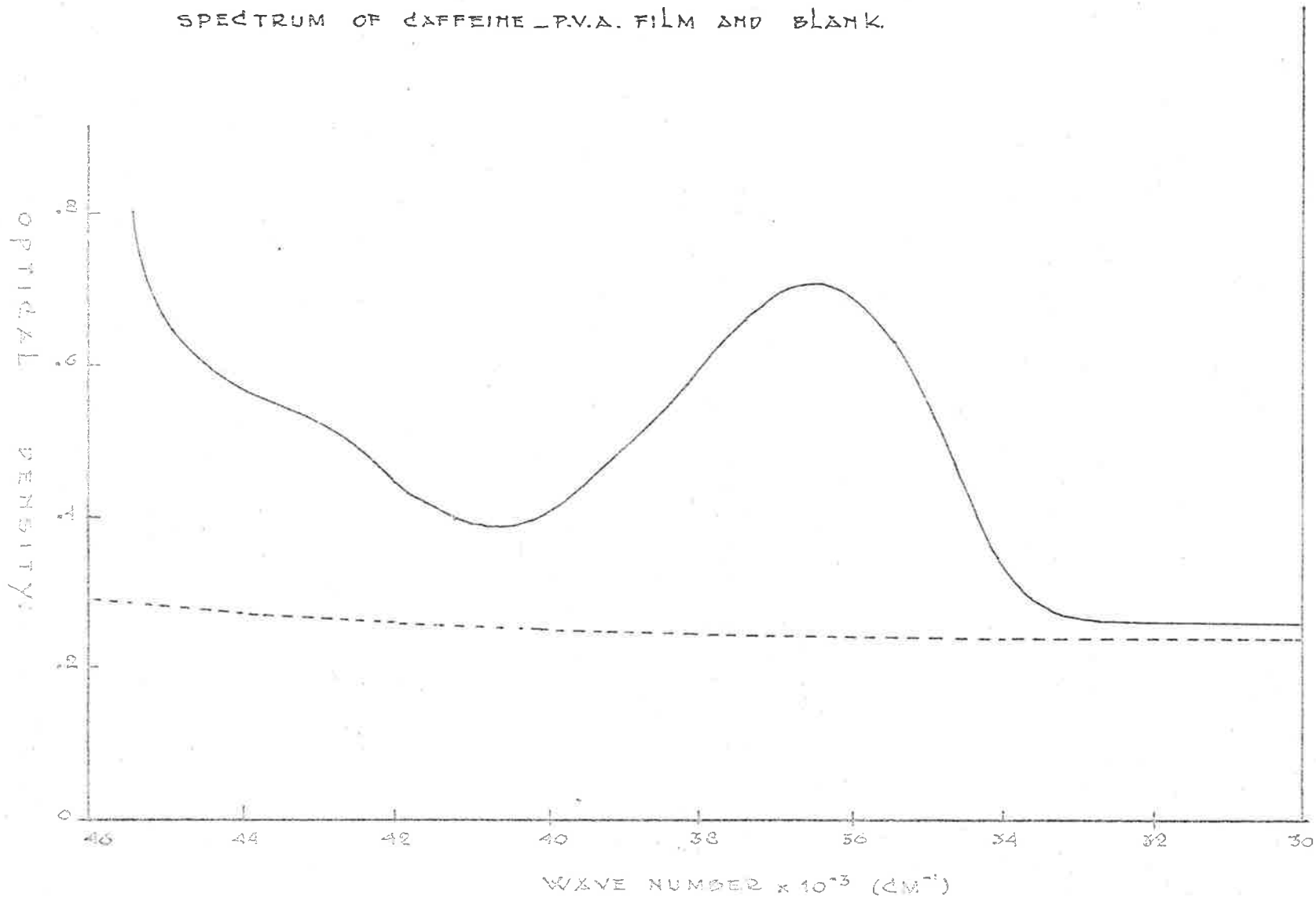

FIG. 3.4

The ratio of the corrected optical density at the absorption maximum, 36,600 cm^{-1}, to the optical density at the absorption minimum, 40,800 cm^{-1}, for the spectrum shown in Fig. 3.4, were found to be within 4% of the similar ratio calculated from the solution absorption spectrum.

3.3.5 Spectroscopic readings.

All readings were taken using the Unicam SP700 double beam recording spectrophotometer. Calcite polarising prisms (Archard-Taylor modification of a Glan Foucault polariser) were placed in both the reference and the sample compartment. The incident radiation was polarised parallel and perpendicular to the direction of stretching of the film by rotating the prisms. All readings were taken according to the following procedure.

A minimum warm up period of 30 minutes was allowed after which the zero transmission and optical density settings of the spectrophotometer were adjusted at 36,600 cm^{-1}. The prisms were placed near the front of the sample and reference compartments, always facing the same direction, while the films were placed near the back of the sample compartment, to reduce scattering losses. The readings were taken in the following sequence:

1) Prisms //, blank

2) Prisms //, film

3) Prisms ⊥, film

4) Prisms ⊥, blank

When the blank and the film were interchanged, the complete cell holder was interchanged to ensure a reproducible positioning of the film in the cell holder. All readings were taken at scan speed 3 and resolution 1. Since caffeine does not absorb in the 33,000-30,000 cm^{-1} region the difference in absorption between the sample and the blank was used to correct for small differences in film thickness and reflection.

3.4 THE DETERMINATION OF THE AXIS OF ALIGNMENT OF THE MOLECULE

3.4.1 Introduction.

To accurately determine which way a given molecule will align in a stretched PVA film, a highly complex model would be required. It would have to include allowances for the energy of distortion of the PVA strands when the molecule is included in the film, the free space between the PVA strands, and the molecular shape and size. Since the use of such a model is not possible, two independent methods have been developed, both of which give comparable results.

3.4.2 The plastic bag method.

A model of the molecule is stretched in a plastic bag and the angle of orientation of the molecule is observed. The plastic bag simulates the environment around the molecule in the stretched film. A photograph of the alignment of caffeine in the bag is shown in

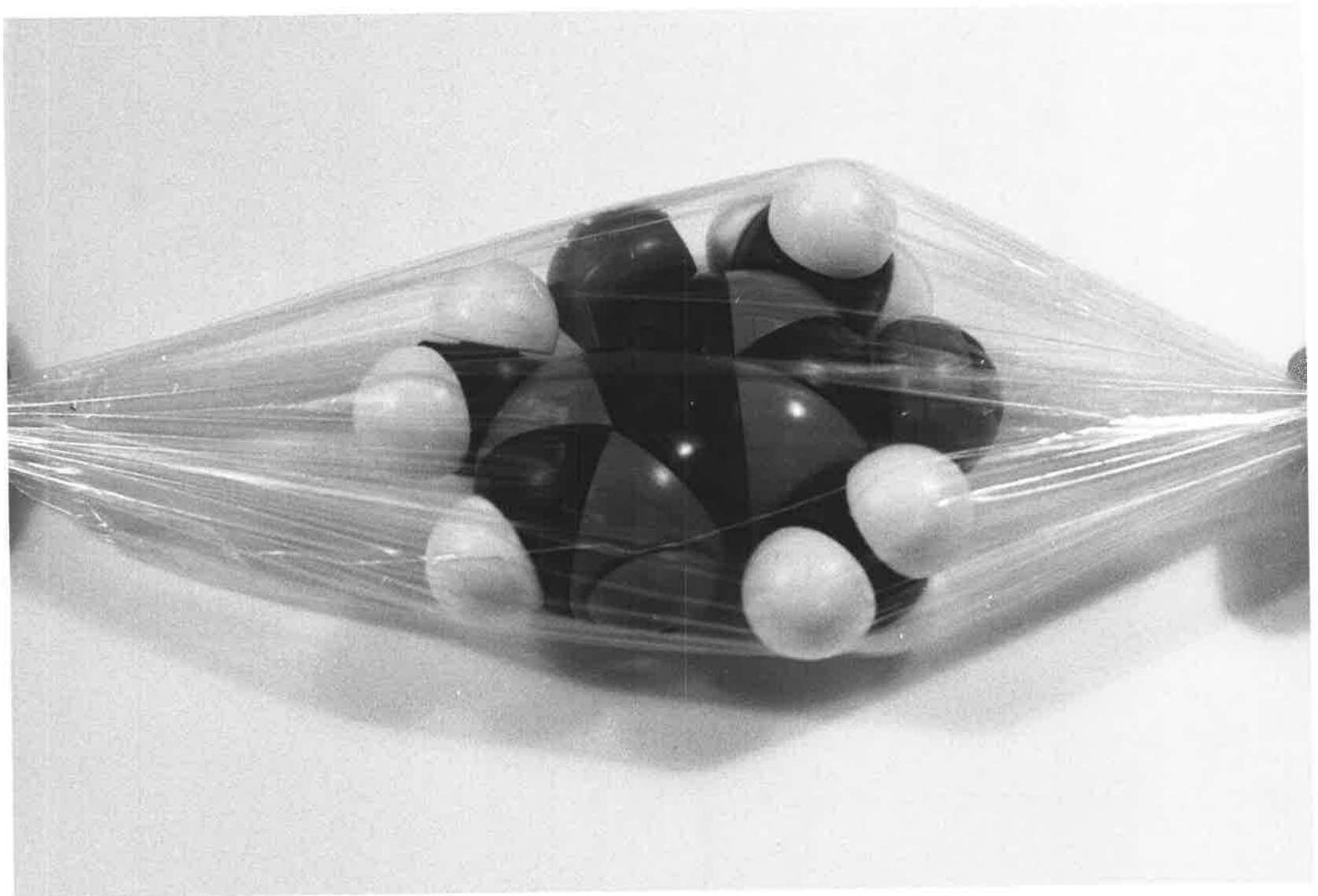

FIG 3.5.

Fig. 3.5. The angle of orientation is estimated at approximately 30° with respect to the perpendicular to the C_4—C_5 axis.

3.4.3 The major axis method.

From the two-dimensional shape of the planar molecule the major and minor axes are calculated.

The molecular shape was defined by the coordinates and the atomic radius (Haylward and Findlay) of the atoms in the molecule. A two-dimensional density matrix was set up in which the density was set equal to unity for a point inside the molecule and equal to zero for a point outside the molecule. The centre of gyration and the major and minor axes of the molecule were calculated accordingly. Because of the three-dimensional distribution of the atoms in a methyl group, this group was approximated by a single atomic radius of 1.20 Å centred at the carbon atom. Other atomic radii used were .73 Å for nitrogen, .77 Å for carbon, .73 Å for oxygen and .37 Å for hydrogen.

The computer program for the major axis calculation based on the above model is shown in Appendix 4. For caffeine the angle between the perpendicular to the C_4—C_5 axis and the axis of alignment was calculated as -25° (approximately the C_2= O bond direction), while for parent molecule xanthine the corresponding angle was calculated as -9°. Fig. 3.6 shows the molecular shape as defined by the model, together with the major axis as calculated.

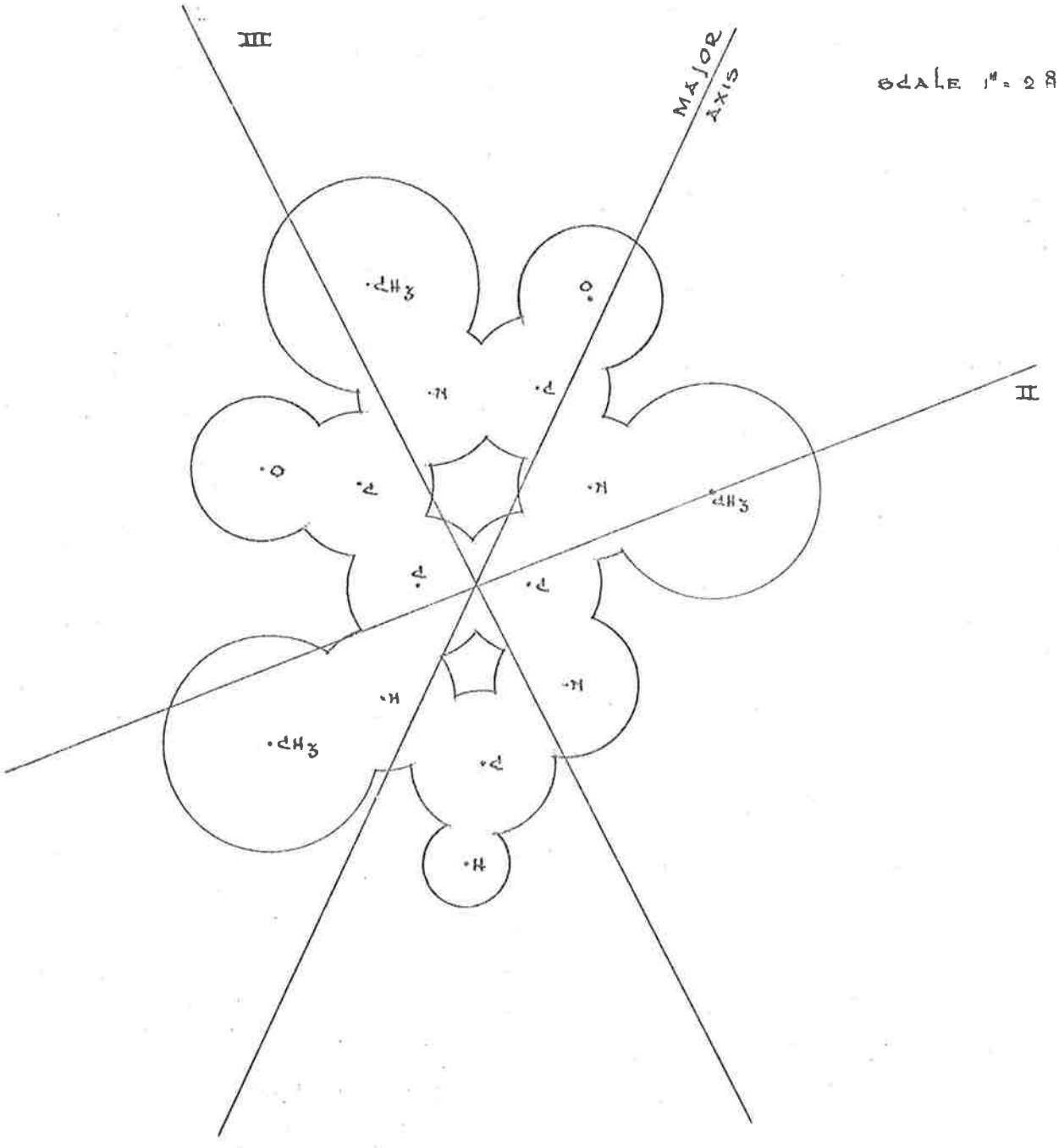

THE SHAPE OF THE CAFFEINE MOLECULE WITH THE MAJOR AXIS AND THE PROPOSED TRANSITION MOMENT DIRECTIONS FOR TRANSITIONS II AND III.

FIG. 3.6

3.5 THE DICHROIC SPECTRUM OF CAFFEINE

The dichroic ratio can be related through equation 3.8 to the angle between the transition dipole and the long axis of the molecule. Subsequently when the dichroic ratio is measured as a function of wavenumber, it will remain constant throughout the region where one transition dominates the spectrum. The dichroic ratio will thus give an indication where one transition finishes and another starts.

A nitrogen $\pi^* \leftarrow n$ transition by its very nature has a transition dipole perpendicular to the plane of the molecule, and as such, perpendicular to the long axis of the molecule. For complete orientation, the dichroic ratio for a nitrogen $\pi^* \leftarrow n$ transition must be equal to zero, while for partial orientation the dichroic ratio would still be considerably less than one.

The maximum of transition II was found to have shifted from 36,600 cm^{-1} for caffeine in aqueous solution to 36,300 cm^{-1} for caffeine in the PVA film.

Fig. 3.7 shows the dichroic ratio as a function of wavelength together with the parallel and perpendicular polarised spectra for 2x stretch. There is no indication of the presence of a nitrogen $\pi^* \leftarrow n$ transition in the 33,000-34,000 cm^{-1} region although other workers (Kelly, 1970; Drobnik and Augenstein, 1966A,B, 1967; Clark and Tinoco, 1965) have reported the presence of this band in purine and substituted purines. The presence of a low intensity $\pi^* \leftarrow n$ transition could account for the non-fluorescence of caffeine in organic solvents.

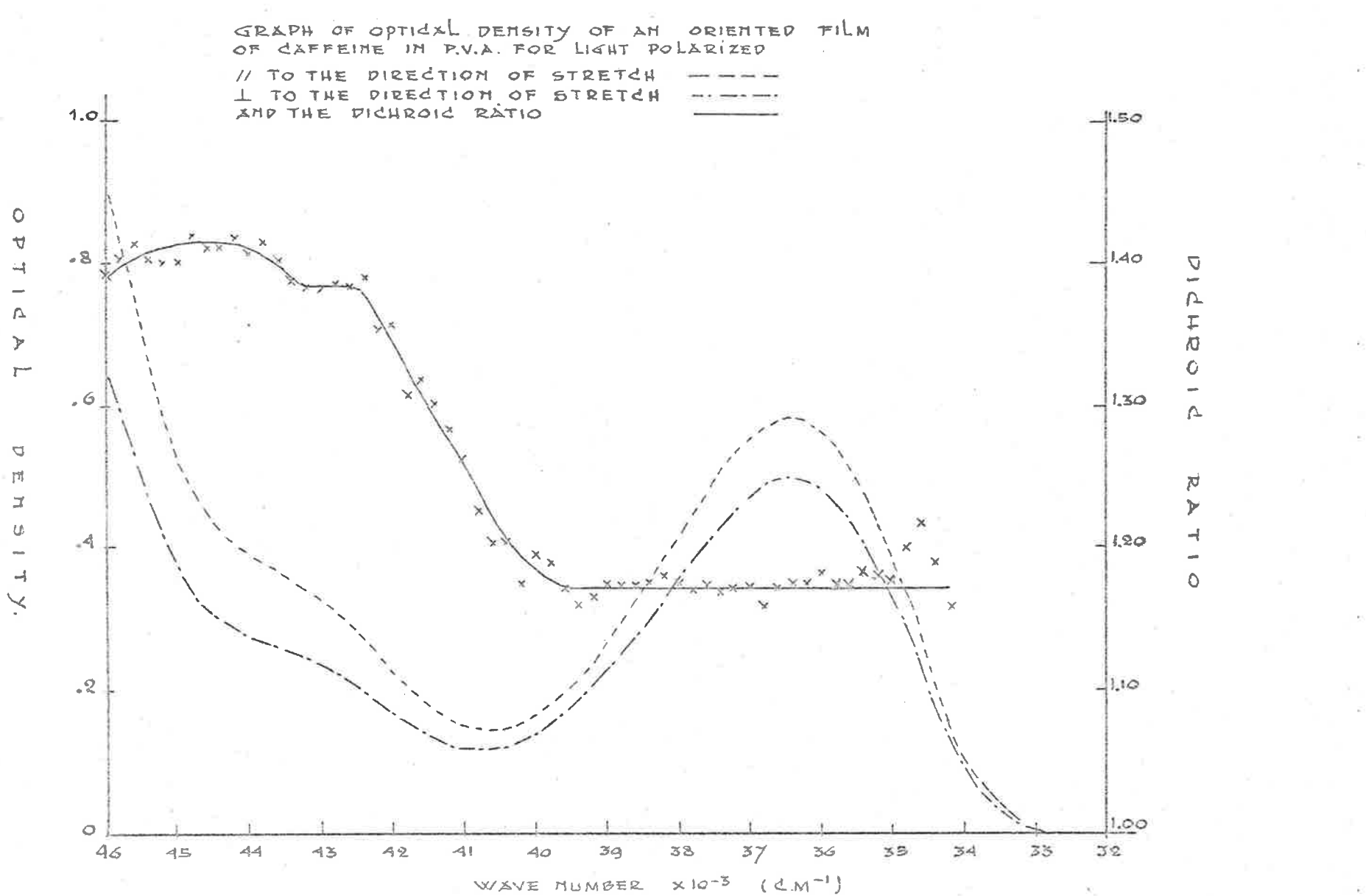
GRAPH OF OPTICAL DENSITY OF AN ORIENTED FILM OF CAFFEINE IN P.V.A. FOR LIGHT POLARIZED
// TO THE DIRECTION OF STRETCH
⊥ TO THE DIRECTION OF STRETCH
AND THE DICHROIC RATIO
OPTICAL DENSITY.
1.0
.8
.6
.4
.2
0
DICHROIC RATIO
1.50
1.40
1.30
1.20
1.10
1.00
46 45 44 43 42 41 40 39 38 37 36 35 34 33 32
WAVE NUMBER x10⁻³ (c.M⁻¹)

FIG. 3.7

The dichroic ratio was found to be constant over the range 34,000-40,000 cm^{-1} which shows that only transition II contributes to the spectrum in this region. In the 40,000-42,000 cm^{-1} range the dichroic ratio increases and remains approximately constant from 42,000 to 46,000 cm^{-1}, although in the 45,000 to 46,000 cm^{-1} region there must be a considerable contribution from transition IV. Since the dichroic ratio is greater than one for the range studied and since all transitions have high extinctions, it can be concluded that transitions II, III and IV are all $\pi^* \leftarrow \pi$ transitions.

The dichroic ratio over the region 35,000-38000 cm^{-1} was averaged and plotted as a function of stretch as shown in Fig. 3.8 together with the predicted dichroic ratio curves. These predicted dichroic ratio curves were derived by combining equation 3.8 (for R_o equal to 1.40 and 1.50) with Kratky's (1933) stretch-orientation function. These limiting cases could correspond to transition moments at 50° and 49° respectively with respect to the longitudinal axis of the molecule. Transition II can then be assigned a transition dipole direction of $50^\circ \pm 1^\circ$. Transitions III and IV can be assigned approximate transition moment angles of 44° and 43° respectively, if the dichroic ratio for the 2x stretch (Fig. 3.7) is extrapolated to infinite stretch.

3.6 THE INTERPRETATION OF THE DICHROIC SPECTRUM OF CAFFEINE

To determine the absolute orientation of the transition moment vectors in caffeine, films of xanthine and 3-methyl-xanthine in PVA were prepared. The dichroic spectrum of xanthine is shown in Fig. 3.9.

THE MEASURED DICHROIC RATIO AS A FUNCTION OF STRETCH FOR ORIENTED CAFFEINE IN P.V.A. TOGETHER WITH THE THEORETICAL FUNCTION FOR $R_0 = 1.40$ AND $R_0 = 1.50$.

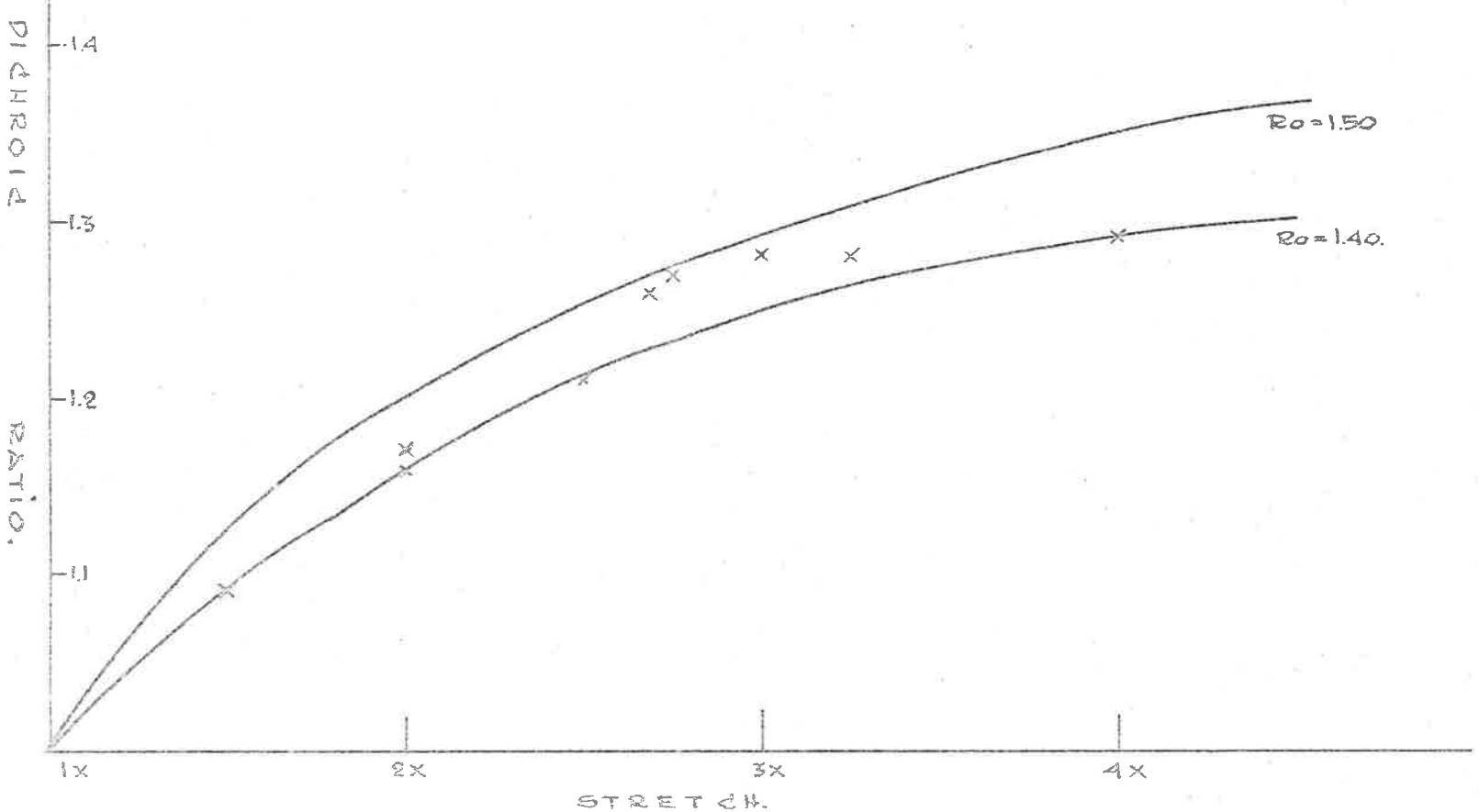

FIG. 3.8.

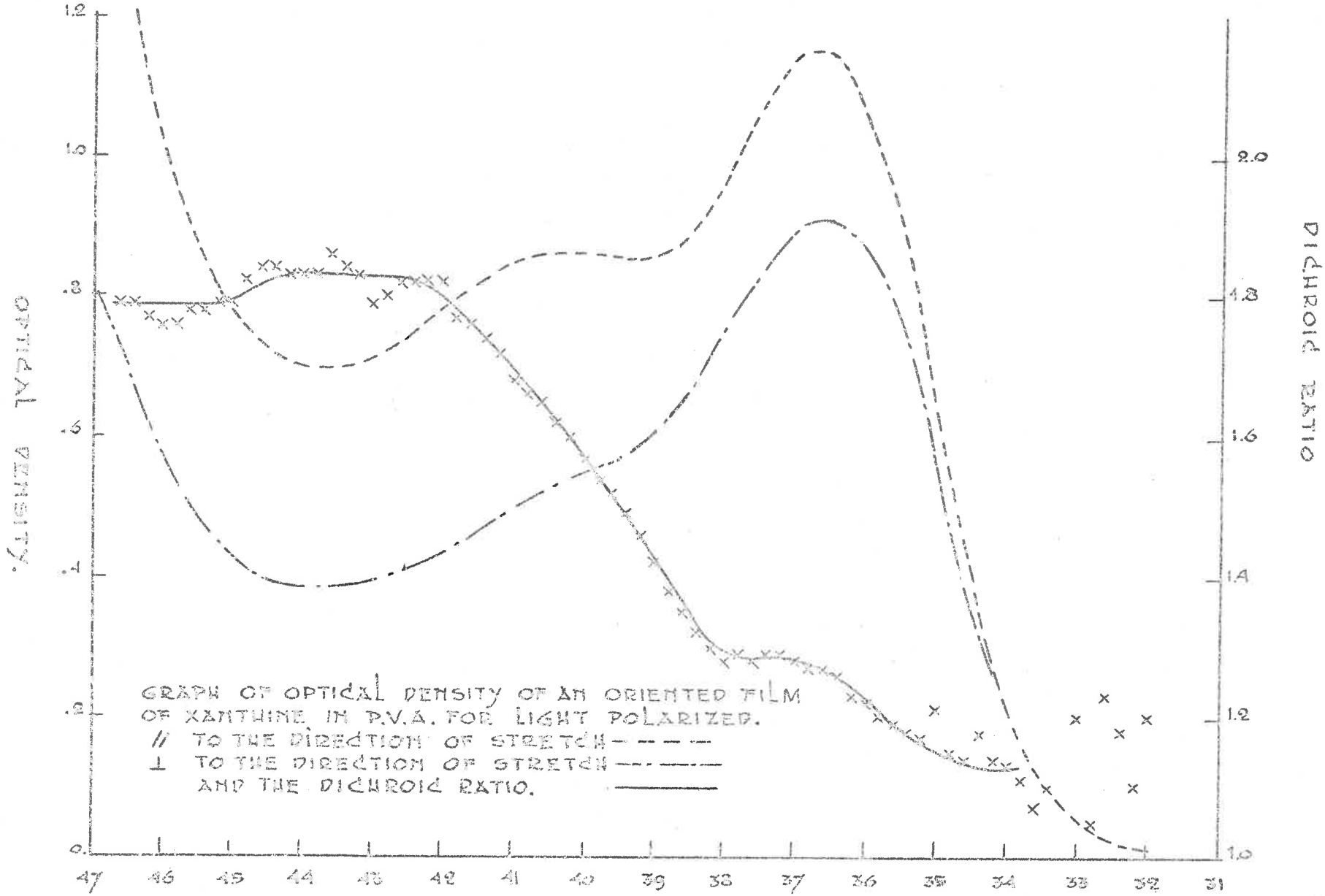
OPTICAL DENSITY
DICHROIC RATIO
1.2
1.0
.8
.6
.4
.2
0
2.0
1.8
1.6
1.4
1.2
1.0
47 46 45 44 43 42 41 40 39 38 37 36 35 34 33 32 31
WAVE NUMBER x 10⁻³ (CM⁻¹)
GRAPH OF OPTICAL DENSITY OF AN ORIENTED FILM OF XANTHINE IN P.V.A. FOR LIGHT POLARIZED.
// TO THE DIRECTION OF STRETCH
⊥ TO THE DIRECTION OF STRETCH
AND THE DICHROIC RATIO.

FIG. 3.9.

The angle of the axis of alignment for xanthine was calculated as -9° with respect to the perpendicular to the $C_4—C_5$ axis, while the corresponding angle for caffeine was calculated as -25°. If the transition moment directions are not strongly affected by the substitution of the three methyl groups on the xanthine molecule, the measured transition moment angles would be expected to shift by approximately 16°. The direction of the shift could be used to determine the absolute angles of the transition moments.

No major changes in the transition moment angles with respect to the axis of alignment was observed. The transition moment angles were calculated as 49°, 45° and 44° for transitions II, III and IV respectively. Transition moment angles for 3-methyl-xanthine were also found to be the same. Table 3.1 gives some of the transition moment directions determined from oriented PVA studies by other authors.

All transition moment directions fall into the range 42°-51°. The substitution of methyl groups of xanthine or adenine does not seem to affect the axis of alignment. Either the effect of substituting one or more methyl groups on the axis of alignment has been highly over-estimated in the models used, or some types of forces other than mechanical forces were responsible for the alignment of the molecules in the PVA lattice. Thulstrup (1970B) and Smirnov (1957) suggested that orientation may be due to electrostatic forces.

To test the possibility of forces other than mechanical forces being responsible for the alignment of the molecules in the film, a film of

TABLE 3.1

EXPERIMENTAL TRANSITION MOMENT DIRECTIONS FOR PURINE AND PYRIMIDINE BASES

MOLECULE	TRANSITION II	TRANSITION III	TRANSITION IV	AUTHOR
caffeine	50	44	43	present work
xanthine	49	45	44	"
3-m-xanthine	48	45	43	"
6-m-purine	46	49	49	Kelly, (1970)
adenine	46	-	49	Fueslero, (1969)
9-m-adenine	44	-	51	"
adenosine	45	-	50	"
uracil	47	-	50	"
uridine	46	-	50	"
thymine	49	-	47	"
cytosine	46	44	49	"
cytidine	45	46	49	"
guanine	51	42	44	"
guanosine	49	46	45	"

caffeine in polyethylene was prepared by soaking a piece of polyethylene (household type) in a warm solution of caffeine (5%) in carbon tetrachloride for 30 seconds. The film was stretched to 3.5 times its original length.

The dichroic spectrum of caffeine in polyethylene is shown in Fig. 3.10. A shoulder has appeared in the spectrum at 34,600 cm^{-1}. This seems to be the same shoulder that is observed in the absorption spectrum of caffeine in cyclohexane. This band is not observed in PVA since $\pi^* \leftarrow n$ transitions are, in general, less intense and shift to higher energies in polar media.

The band has a dichroic ratio greater than unity. The band cannot be a nitrogen $\pi^* \leftarrow n$ band since these transitions are, by definition, perpendicular to the plane of the molecule, and as such have a dichroic ratio of less than one. Carbonyl $\pi^* \leftarrow n$ transitions can have a dichroic ratio greater than one and can be found at wavenumbers as low as 30,000 cm^{-1} (Murrell). It can thus be concluded that the 34,600 cm^{-1} band corresponds to a carbonyl $\pi^* \leftarrow n$ transition.

The measured dichroic ratio for the film of caffeine in polyethylene for transition II can be estimated at 1.04, while the ratio for transitions III and IV can be estimated as 1.13 and 1.20 respectively. These dichroic ratios combine with the estimated degree of orientation f = .64 (for 3.5 x stretch) and equation 3.9 to give transition moment angles of 54°, 53° and 52°.

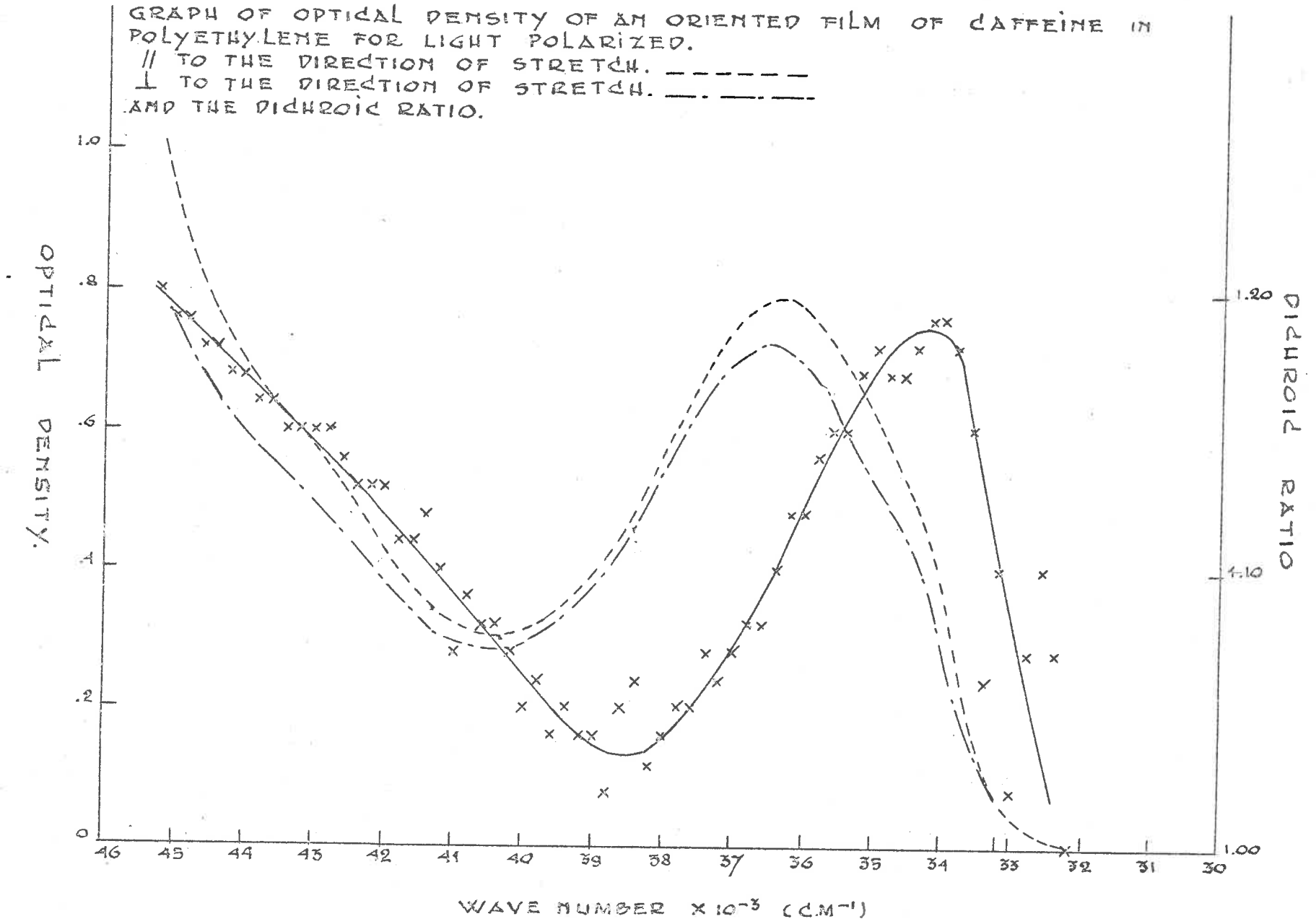
GRAPH OF OPTICAL DENSITY OF AN ORIENTED FILM OF CAFFEINE IN POLYETHYLENE FOR LIGHT POLARIZED.
// TO THE DIRECTION OF STRETCH. – – – – – –
⊥ TO THE DIRECTION OF STRETCH. —. —. —.
AND THE DICHROIC RATIO.
OPTICAL DENSITY.
1.0
.8
.6
.4
.2
0
DICHROIC RATIO
1.20
1.10
1.00
46 45 44 43 42 41 40 39 38 37 36 35 34 33 32 31 30
WAVE NUMBER × 10⁻³ (C.M⁻¹)

FIG. 3.10

The transition moment angles all seem to have shifted to higher values by angles ranging from 3° to 10°. Since all three transition moments have not shifted by the same amount, it seems likely that the degree of orientation of the caffeine in polyethylene of unknown history is not the same as that for a similarly stretched PVA film. Thulstrup et al (1970A) found that the degree of orientation of molecules in stretched polyethylene films is, in general, less than expected.

If a degree of orientation of $f = .15$ is assumed, transition moment directions of 50°, 45° and 42° are obtained. This is in good agreement with the results obtained for caffeine in PVA (50°, 44°, 43°).

It can be concluded that the axis of orientation of caffeine in polyethylene is the same as the axis of orientation in PVA. Since the axis of alignment seems to be independent of the medium, it seems likely that the forces responsible for the orientation of the alignment of the molecule are mechanical in nature. The reason why the substitution of methyl groups on the basic purine skeleton does not seem to affect the axis of alignment cannot be explained at this stage, although it can be speculated that this axis is a property of the basic purine skeleton only.

An attempt now has to be made to assign absolute transition moment directions for caffeine. No concrete evidence is available to aid the assignment of absolute moment directions, but there are some theoretical considerations and experimental observations that can be used to determine this assignment. It can be noted that if transitions II and III are

presumed to be on opposite sides of the axis of alignment, the angle between the two transition moment directions is $95^{\circ} \pm 2^{\circ}$ for all compounds listed in Table 3.1. The same applies for the angle between transitions II and IV. Although it is not conclusive evidence it could be considered as an indication that transitions II and III have approximately the same direction and are at approximately 95° to transition II. Other indications to support this assignment are:

1) Transitions II and III can be considered to have arisen from perturbation of the benzene B_{2u} and B_{1u} bands (Clark and Tinoco, 1965) whose polarisation directions are almost perpendicular.

2) Polarised absorption studies of a single crystal of 9-methyl-adenine (Stewart and Davidson, 1963) indicate that transition II is polarized at at least 70° to transition IV. Polarised absorption studies of a single crystal of 1-methyl-thymine (Stewart and Davidson, 1963) and polarised specular reflection studies of a single crystal of thymine (Rosa, 1966) indicates that these bands are polarised at least 75° from one another. Photoselection studies of guanine, guanisine and 9-ethyl-guanine (Callis, Rosa and Simpson, 1964 and Borrensen, 1967) show that transitions II and III are not parallel.

The only case in which evidence was found that the proposed assignment of transition moment angles does not apply to all purine and pyrimidine bases was found for cytosine and 1-methyl-cytosine (Callis, 1966) where polarised specular reflection studies indicate that bands II and III are parallel.

Chen and Clark (1969) studied polarised reflection spectra of purine and found an angle of 48° of the first $\pi^* \leftarrow \pi$ transition with respect to the $C_4 - C_5$ axis but the assignment of the other band was somewhat indefinite.

If the calculated axis of alignment is assumed to be correct, only the assignment of the sign of the angle of transition II with this axis is required to produce an absolute assignment of the transition moment directions. Perturbation theory applied to the benzene system (Clark and Tinsley, 1965) predicts that transition II is likely to be polarised along the line of the two keto groups, while transition III would be polarised perpendicular to this line. If these directions are assumed to be approximately correct the transition moment directions as shown in Fig. 3.6 and Fig. 4.1 can be derived.

The transition moment directions assigned to caffeine and xanthine are in close agreement to the directions assigned in uracil by Fucaloro (1969) using correlations with crystal data, and is also in good agreement with the transition moment directions calculated from π electron only self-consistent field molecular orbital calculations with configuration interaction (see Section 4.2).

4. THEORETICAL CALCULATIONS

4.1 INTRODUCTION

Theoretical evaluation of ground and excited state molecular interactions requires an accurate knowledge of ground and excited state electron distributions and energy levels. These properties can be obtained from all valence electron Self Consistent Field (SCF) calculations with configuration interactions. Some success has been obtained recently in these types of calculations (e.g. Klopman and O'Leary, 1970).

At this stage in the development of the theory, satisfactory results can be obtained for ground state molecular properties of complex systems, but extensions to include excited states of π electron systems (Del Bene and Jaffe, 1968) offer little advantage over the much simpler SCF-MO π electron calculations. For this reason, two separate sets of calculations were performed, one for the molecular ground state and one for the excited states.

All valence electron SCF calculations, without configuration interactions, were used to calculate ground state electron distributions and dipole moments. These results were then used to estimate the magnitude of the Van der Waals' interactions between the molecules.

The π electron SCF-MO calculations, with configuration interactions, were used for the purpose of interpreting dimer spectra in terms of exciton interactions.

4.2 TOTAL ELECTRON CNDO CALCULATIONS

4.2.1 Introduction.

The Complete Neglect of Differential Overlap method (CNDO) was first introduced by Pople, Santry and Segal (1965). In this method, which is discussed in detail by Pople and Beveridge (1970), and by Klopman and O'Leary (1970), only valence electrons are treated explicitly, the inner shells being treated as part of a rigid core. The zero-differential overlap approximation is used for all products of different atomic orbitals ($S_{uv} = \int \phi_u \phi_v \, dr = 0$). The two electron integrals are assumed to depend only on the nature of the atoms on which the two orbitals involved are centred. This way γ_{AB} is the average electrostatic repulsion between any electron on atom A and any electron on atom B.

Further assumptions include the neglect of monatomic differential overlap in the interaction integrals involving cores of other atoms ($\langle u|V_B|v\rangle = \delta_{uv} V_{AB}$), and the taking of diatomic off-diagonal core matrix elements to be proportional to the corresponding overlap integrals. This last assumption takes the bonding capacity of the overlap to be dependent on the extent of the overlap.

$$H_{uv} = \beta_{uv} = \beta^{\circ}_{AB} S_{uv} \qquad 4.1$$

where β is the resonance integral.

This reduces the Fock Hamiltonian for the diagonal element to:

$$F_{uu} = U_{uu} + (P_{AA} - \tfrac{1}{2}P_{uu})\gamma_{AA} + \sum_{B(\neq A)}' (-P_B \gamma_{AB} + (Z_B \gamma_{AB} - V_{AB})) \qquad 4.2$$

while the non-diagonal Hamiltonian becomes:

$$F_{uv} = \beta^{\circ}_{AB} S_{uv} - \tfrac{1}{2} P_{uv} \gamma_{AB} \qquad ,u \neq v \qquad 4.3$$

where all terms have their usual quantum chemical meaning.

4.2.2 Integral evaluation.

In the version of CNDO used (CNDO/2) the integrals β°_{AB}, $U_{uu} = U_u$, V_{AB}, are evaluated by the following approximations:

$$\tfrac{1}{2}(I_u - A_u) = U_u + Z_A - \tfrac{1}{2}\gamma_{AA} \qquad 4.4$$

$$\beta^{\circ}_{AB} = \tfrac{1}{2}K(\beta^{\circ}_{A} + \beta^{\circ}_{B}) \qquad 4.5$$

where K is a known constant (usually 1).

$$V_{AB} = Z_B \gamma_{AB} \qquad 4.6$$

4.2.3 Calculations.

The computer program of Pople and Beveridge (1970) was used with minor modifications on the University of Adelaide CDC 6400 computer to calculate both σ and π ground state charge distributions in caffeine.

4.2.4 Results.

The calculated σ, π, and total electron densities for the ground states of caffeine and xanthine are compared with those calculated by Pullman (1968) for xanthine, in Table 4.1. There are no marked variations in the electron density for the different methods used.

TABLE 4.1

XANTHINE AND CHARGE DISTRIBUTIONS FROM ALL VALENCE ELECTRONS CALCULATIONS

ATOM NO.	ATOM SYMBOL	X COORD.	Y COORD.	σ PULLMAN	σ CNDO	π PULLMAN	π CNDO	TOTAL PULLMAN	TOTAL CNDO
1	N	-2.37	-0.61	-.441	-.491	.234	.236	-.207	-.255
2	C	-2.43	0.81	.286	.252	.190	.201	.476	.453
3	N	-1.21	1.40	-.434	-.450	.254	.219	-.180	-.231
4	C	0.00	0.66	.257	.168	-.033	.064	.224	.232
5	C	0.00	-0.66	.148	.160	-.145	-.263	.003	-.103
6	C	-1.25	-1.38	.191	.074	.187	.191	.378	.265
7	N	1.35	-1.08	-.444	-.497	.392	.423	-.052	-.074
8	C	2.02	0.06	.186	.132	.075	.069	.261	.201
9	N	1.22	1.13	-.285	.030	-.306	-.274	-.591	-.244
10	O	-3.46	1.41	-.053	.081	-.441	-.446	-.494	-.365
11	O	-1.39	2.59	-.065	.050	-.406	-.419	-.471	-.369
12	CH_3	-3.71	-1.24	.195	.139			.195	.139
13	CH_3	-1.15	2.90	.196	.134			.196	.134
14	CH_3	1.89	-2.45	.195	.138			.195	.138
15	H	3.36	-0.11	.069	-.020			.069	-.020

4.3 SEMI-EMPIRICAL (PPP-SCF-MO-CI) π ELECTRON CALCULATION

4.3.1 Introduction.

The Pariser-Pople-Parr (Parr, 1963) semi-empirical SCF-MO method for π electron systems has been used successfully for interpretation and prediction of the absorption spectra for aromatic molecules. The parameters required are usually obtained by comparison of the calculated singlet transition energies with the experimental spectrum of a test molecule. These parameters are then used to calculate the spectra of a series of related molecules. The present calculations are based on the method described by Bailey (1969).

In this method, the core parameter has been evaluated using the Goeppert-Mayer and Sklar (1938) approximation:

$$U_{uu} = I_u \qquad 4.7$$

where I_u is the valence state ionisation potential for the isolated atom. The one centre repulsion integral (γ parameter) has been approximated by the formula given by Pariser and Parr (Parr, 1963):

$$\gamma_{uu} = I_u - A_u \qquad 4.8$$

where A_u is the valence state electron affinity.

The two centre repulsion integrals (γ_{uv}) are calculated by the Nishimoto-Mataga (1965, 1966) approximation:

$$\gamma_{uv} = e^2/(R_{uv} + a_{uv}), \quad a_{uv} = 2e^2/(\gamma_{uu} + \gamma_{vv}) \qquad 4.9$$

where R_{uv} is the distance between atoms. The two centre core integrals U_{uv} are calculated from the gradient of the overlap integrals

(Lindenberg, 1967).

For atoms contributing two electrons to the π system, the γ parameter can be calculated by a method analogous to the one used for the single electron centre. The neutral atom is replaced by the positive ion in which the second and first ionisation potentials are used instead of the valence state ionisation potential and electron affinity. This method, however, is unsatisfactory for the calculation of the core parameter, in which case the approximation discussed by Kwiatkowski (1966) was used. The ionisation potential for these systems is written:

$$I_u = E(X \longrightarrow X^{+}) + \gamma_{uu} \qquad 4.10$$

where X stands for the doubly-charged core atom in the appropriate valence state.

Bailey (1970) introduces three different nitrogen core parameters for nitrogen atoms contributing two electrons. These are the amino-nitrogen, the pyrrolic-nitrogen and the lactamic-nitrogen. These are illustrated in Fig. 4.1.

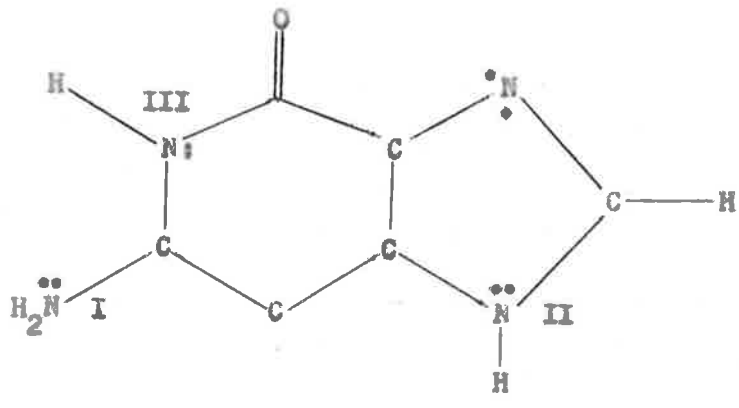

Fig. 4.1 The amino-nitrogen (I), the pyrrolic-nitrogen (II), and the lactamic-nitrogen (III).

The experimental ionisation potentials used by Bailey for these core parameters were those of methyl amine for the amine-nitrogen, dimethyl amine for the pyrrolic-nitrogen, and N-methyl acetamide for the lactamic-nitrogen. Although the use of the ionisation potentials of methyl amine and dimethyl amine for the amino- and pyrrolic- nitrogens seems reasonable, the use of the ionisation potential of N-methyl acetamide for the lactamic-nitrogen does not seem to be justified. The ionisation potential obtained from this molecule is not the ionisation potential of the nitrogen lone pair in an environment of the surrounding atoms, but the ionisation potential of the π electrons of the total nitrogen-carbonyl system. To obtain a pure ionisation potential for the nitrogen lone pair, this part of the molecule would have to be represented by the $H_3C - \ddot{N}H - CH_3$ group. The core parameter to be used in this case is the one for the pyrrolic-nitrogen. Extension of this principle gives an opportunity to include a correction for methylation of the nitrogen atom. Caffeine (1:3:7 trimethyl xanthine) and xanthine are indistinguishable as far as π electron calculations are concerned, yet the first $\pi^* \leftarrow \pi$ transition of caffeine is .07 eV (600 cm^{-1}) to the blue of the corresponding transition in xanthine. If the ionisation potential of trimethyl amine is used in the calculation of the core parameter for the methylated nitrogens in caffeine, the effect of methylation can be included in the calculation. This leads to the definition of three types of nitrogens contributing two electrons; N_{1e}, N_{2e}, and N_{3e}, standing for nitrogens surrounded by one carbon and two hydrogens (amino), two carbons

and one hydrogen (pyrrolic), and by three carbon atoms (methylated pyrrolic). The parameters used in the calculations are shown in Table 4.2.

TABLE 4.2

PARAMETERS USED IN THE CALCULATIONS

	C	N	N_{1e}	N_{2e}	N_{3e}	O
Core (eV)	-11.16	-14.12	-25.73	-25.00	-24.38	-17.70
γ (eV)	11.13	12.34	16.76	16.76	16.76	15.23
S.e.c.*	3.25	3.90	3.90	3.90	3.90	4.55

* Slater effective charge.

The valence state ionisation potentials and electron affinities were taken from Hinze and Jaffe (1962) while the experimental ionisation potentials for the two electron centres were taken from Turner (1966).

4.3.2 Calculations.

Dr. M.L. Bailey and Dr. J.P.M. Bailey kindly consented to the use of their computer program for PPP-SCF-MO calculations and this program was used with minor modifications on the CDC 6400 computer. The coordinates of the atoms in the caffeine molecule were taken from an X-ray crystallographic study by Sutor (1958) in preference to the geometries proposed by Spencer (1959) which are often used for theoretical

calculations. The coordinates for xanthine used in the calculation were assumed to be the same as those for caffeine, so that the effect of methylation on the calculation could be clearly observed. The coordinates for uracil were obtained from Stewart and Jensen (1967) and were used for the calculations on uracil and 1:3-dimethyl uracil. Calculations were carried out using both Slater orbitals and Clementi (1963) Double Zeta-orbitals.

4.3.3 Results: transition energies and oscillator strengths.

Calculations were performed on xanthine, caffeine, uracil and 1:3-dimethyl uracil using both the Bailey nitrogen parameters and the new parameters. The resulting transition energies (in eV) are shown together with the calculated oscillator strengths, in Table 4.3.

The transition energies calculated for caffeine and xanthine using the new parameters seem to be markedly better than those obtained using the Bailey parameters. The reverse applies, however, for uracil and dimethyl uracil where the Bailey parameters seem to produce better agreement with the experimental data.

The relative oscillator strengths of the first two transitions, as calculated using the new parameters, seem to be reversed with respect to the right order of the oscillator strengths.

The introduction of the N_{30} core parameter allows an accurate prediction of the magnitude and direction of the spectral shift of the first $\pi^* \leftarrow \pi$ transition on methylation. This is illustrated in Table 4.4.

TABLE 4.3

MOLECULE	NEW PARAMETERS		BAILEY PARAMETERS		EXPERIMENTAL
	SLATER	D. ZETA	SLATER	D. ZETA	
Xanthine	4.80(.04)	4.76(.04)	5.08(.14)	5.03(.13)	4.62(.18)
	5.49(.10)	5.45(.13)	5.82(.01)	5.77(.01)	
	5.81(.12)	5.81(.15)	6.03(.22)	6.02(.24)	
	5.89(.62)	5.88(.52)	6.27(.35)	6.25(.24)	
	6.21(.10)	6.20(.13)	6.50(.25)	6.49(.28)	
	6.47(.02)	6.48(.03)	7.03(.02)	7.05(.03)	
Caffeine	4.73(.02)	4.69(.02)	as for xanthine		4.54(.18)
	5.39(.14)	5.36(.13)			5.40(.05)
	5.77(.28)	5.76(.32)			} 5.77(.60)
	5.84(.49)	5.85(.37)			
	6.14(.09)	6.14(.12)			
	6.37(.02)	6.39(.02)			6.45(.06)
Uracil	4.58(.07)	4.55(.07)	4.96(.14)		4.81(.20)
	5.43(.16)	5.42(.11)	5.83(.14)		
	5.67(.23)	5.68(.20)	5.96(.22)		6.11(.30)
	6.07(.40)	6.04(.40)	6.58(.34)		6.85
	7.43(.02)	7.41(.02)	7.56(.03)		
	7.93(.17)	7.93(.15)			
1:3-dimethyl uracil	4.49(.06)	4.47(.06)	as for uracil		4.71
	5.34(.15)	5.33(.10)			
	5.62(.24)	5.63(.21)			
	5.97(.42)	5.99(.42)			
	7.40(.02)	7.38(.02)			
	7.89(.02)	7.88(.18)			

TABLE 4.4

ENERGY OF THE FIRST $\pi^* \leftarrow \pi$ TRANSITION (eV)

	XANTHINE	CAFFEINE	SHIFT
calc. (Slater)	4.80	4.73	.07
calc. (D. Zeta)	4.76	4.69	.07
exp.	4.62	4.54	.08
	URACIL	1:3-DIMETHYL URACIL	SHIFT
calc. (Slater)	4.58	4.49	.09
calc. (D. Zeta)	4.55	4.47	.08
exp.	4.81	4.71	.10

In each case methylation produces a red shift of approximately .09 eV (700 cm^{-1}). This red shift can also be reproduced using the Bailey method of parameterisation by using the ionisation potential of acetamide in the calculation of the core parameter.

4.3.4 Results: electron densities and transition moments.

The ground state π electron densities calculated by the SCF-MO method using the various parameters and orbitals are shown in Table 4.5 and can be compared with those calculated by the methods of Pullman (1968), and Pople and Beveridge (1970), as shown in Table 4.1. There seems to be

TABLE 4.5

CALCULATED π CHARGE DISTRIBUTIONS FOR XANTHINE AND CAFFEINE

ATOM NO.	ATOM SYMBOL	TYPE BAILEY	TYPE NEW	BAILEY SLATER XANTHINE	BAILEY CLEMENTI XANTHINE	NEW SLATER XANTHINE	NEW CLEMENTI XANTHINE	NEW SLATER CAFFEINE	NEW CLEMENTI CAFFEINE
1	N	N_{21}	N_{3e}	.260	.265	.354	.359	.380	.385
2	C	C	C	.218	.216	.162	.160	.146	.145
3	N	N_{21}	N_{3e}	.242	.248	.332	.338	.357	.363
4	C	C	C	.026	.025	.005	.003	-.003	-.004
5	C	C	C	-.191	-.193	-.190	-.192	-.198	-.201
6	C	C	C	.236	.234	.196	.195	.185	.183
7	N	N_{2p}	N_{3e}	.490	.494	.490	.493	.519	.523
8	C	C	C	.036	.031	.037	.032	.022	.018
9	N	N	N	-.336	-.334	-.342	-.341	-.348	-.346
10	O	O	O	-.489	-.493	-.524	-.527	-.532	-.537
11	O	O	O	-.492	-.492	-.519	-.519	-.528	-.528

no marked difference in the electron densities calculated using the various methods.

Table 4.6 shows the calculated ground state dipole and the transition dipoles for the first five $\pi^* \leftarrow \pi$ transitions in the caffeine spectrum. The calculated transition moment directions for the first three transitions are shown in Fig. 4.2 together with the directions derived from the experimental results on oriented films.

The experimentally derived transition moment directions are in reasonable agreement with the directions calculated using the new parameters, but when the Bailey parameters were used, different transition moment directions were obtained.

While calculated transition moment directions are in good agreement with the directions predicted from perturbation theory and the directions derived experimentally, the agreement may be due to coincidence.

The polarised film studies only give the absolute value of the angle of the transition moment direction with respect to the molecular axis, which has been estimated from a molecular model. Both the direction of this axis and the assignment of the sign of the angle between this axis and the transition moment can not be assumed to be certain.

There is also some uncertainty associated with the results of π electron theoretical calculations on molecules of relative high complexity.

PROPOSED TRANSITION MOMENT DIRECTIONS FOR CAFFEINE AND XANTHINE

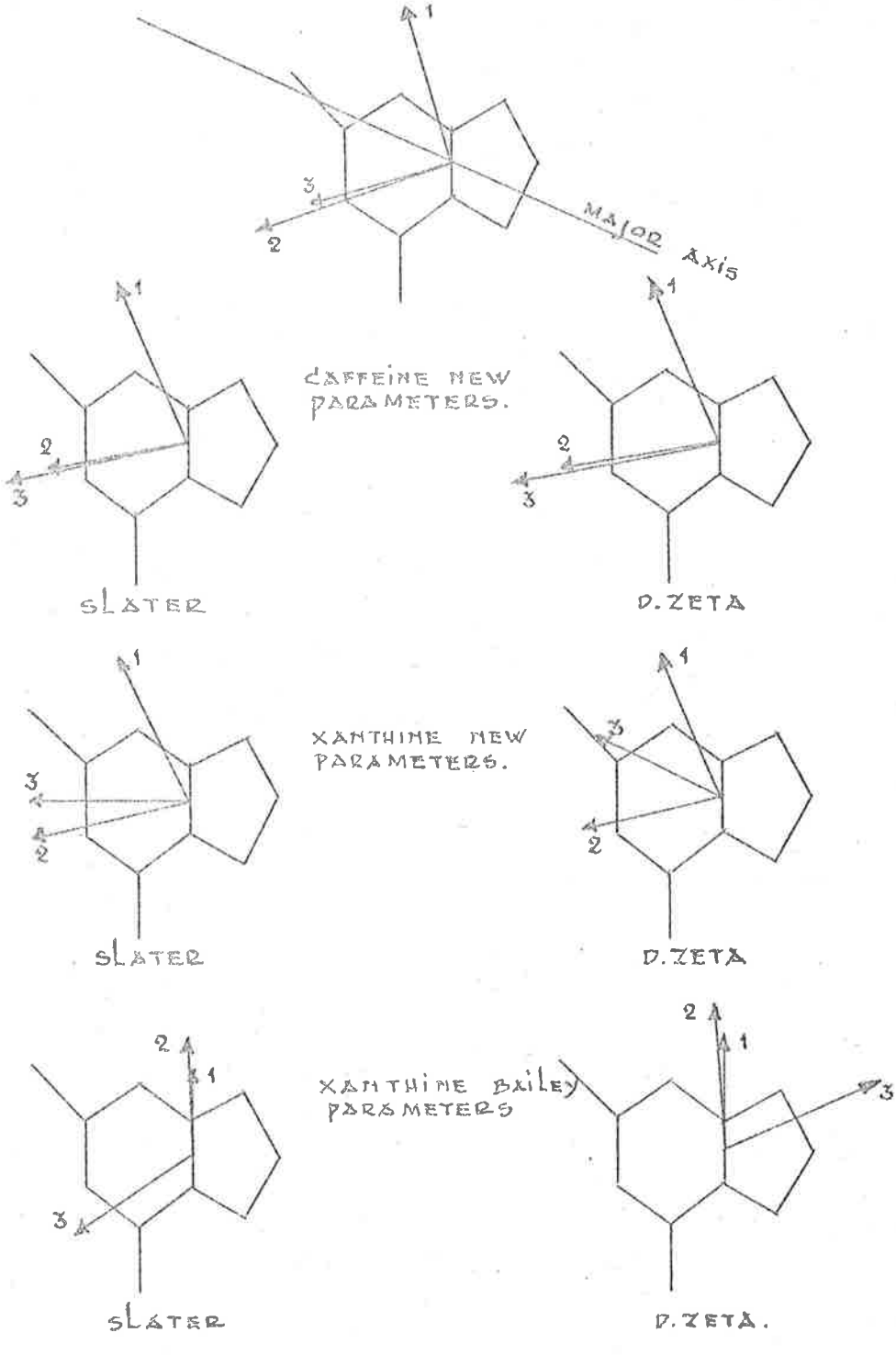

$\pi \rightarrow \pi^*$ TRANSITION MOMENT DIRECTIONS CALCULATED BY THE SCF-MO (BAILEY) METHOD FOR XANTHINE AND CAFFEINE.

FIG. 4.2.

TABLE 4.6

CALCULATED GROUND AND EXCITED STATE DIPOLES AND TRANSITION MOMENTS FOR XANTHINE AND CAFFEINE

STATE n	EXCITED STATE DIPOLES MX	MY	M	TRANSITION MOMENTS ΔMX	ΔMY	ΔM	TRANSITION MOMENT ANGLE θ
CAFFEINE, NEW PARAMETERS, SLATER ORBITALS							
0	4.695	-0.357	4.709	ground state			
1	2.486	4.172	4.856	-2.209	4.529	5.039	116
2	1.303	-0.813	1.536	-3.392	-0.456	3.422	-172
3	0.623	-0.776	0.995	-4.072	-0.419	4.093	-174
4	8.076	2.842	8.562	3.381	3.199	4.654	43
5	0.475	0.287	0.555	-4.220	0.644	4.267	171
CAFFEINE, NEW PARAMETERS, DOUBLE ZETA ORBITALS							
0	4.688	-0.371	4.703	ground state			
1	2.597	4.073	4.830	-2.091	4.444	4.908	115
2	1.618	-0.841	1.824	-3.070	-0.470	3.106	-171
3	0.055	-1.103	1.104	-4.633	-0.732	4.690	-171
4	8.109	2.800	8.579	3.421	3.171	4.664	43
5	1.036	0.790	1.303	-3.652	1.161	3.833	162
XANTHINE, NEW PARAMETERS, SLATER ORBITALS							
0	4.659	-0.330	4.670	ground state			
1	2.488	4.383	5.040	-2.171	4.713	5.189	115
2	1.314	-1.116	1.724	-3.345	-0.786	3.436	-167
3	3.108	0.722	3.190	-1.551	1.052	1.873	146
4	5.676	1.371	5.839	1.017	1.701	1.982	31
5	1.338	0.693	1.507	-3.321	1.023	3.475	163

(contd.)

TABLE 4.6 (contd.)

STATE n	EXCITED STATE DIPOLES MX	MY	M	TRANSITION MOMENTS ΔMX	ΔMY	ΔM	TRANSITION MOMENT ANGLE °
XANTHINE, NEW PARAMETERS, DOUBLE ZETA ORBITALS							
0	4.654	-0.344	4.667	ground state			
1	2.596	4.268	4.996	-2.058	4.612	5.050	114
2	1.688	-1.154	2.045	-2.966	3.662	4.713	-165
3	1.686	-0.169	1.694	-2.968	0.175	2.973	176
4	6.365	1.912	6.838	1.911	2.256	2.956	50
5	1.784	1.137	2.116	-2.870	1.481	3.228	153
CAFFEINE AND XANTHINE, BAILEY PARAMETERS, SLATER ORBITALS							
0	4.639	-0.710	4.693	ground state			
1	4.480	3.636	5.770	-0.159	4.346	4.348	92
2	4.867	2.133	5.314	0.228	2.843	2.851	85
3	3.974	-1.173	4.144	-0.665	-0.463	0.810	-145
4	4.479	-0.983	4.586	-0.160	-0.273	0.316	-120
5	3.075	0.286	3.089	-1.564	0.996	1.854	148
CAFFEINE AND XANTHINE, BAILEY PARAMETERS, DOUBLE ZETA ORBITALS							
0	4.642	-0.721	4.698	ground state			
1	4.430	3.604	5.711	-0.212	4.325	4.330	93
2	4.438	0.821	4.514	-0.204	1.542	1.555	98
3	5.720	-0.310	5.728	1.078	0.411	1.153	21
4	3.180	-0.833	3.288	-1.462	-0.112	1.466	-176
5	3.152	0.528	3.196	-1.490	1.249	1.944	140

4.3.5 Calculation of the ground state molecular interactions by the monopole-monopole approximation.

4.3.5.1 Introduction.

The interaction between base pairs in nucleic acids has been calculated by Pullman et al for both hydrogen bonded pairs (1966A) and for stacked base pairs in aqueous solution in the DNA helix and in single stranded polyribonucleotides, using the monopole approximation. The monopole approximation is usually preferred to the dipole approximation, although the latter has been used to investigate the interaction between complementary base pairs in nucleic acids.

The Van der Waals' forces responsible for these interactions can be divided into three groups, the monopole interaction, the monopole induced dipole and the dispersion of London interaction. For parallel stacked monomer units in a dimer only the monopole-monopole interactions are strongly dependent on the angle between the monomer units. The angular dependence of the Van der Waals' interaction are thus governed by the angular dependence of the monopole-monopole interaction. The calculations by Pullman on vertically stacked base pairs (1966B) showed that the monopole-induced dipole and the dispersion interactions are almost independent of the angle between the monomer units.

The π charge distributions shown for xanthine in Table 4.5 can be combined with Pullman's σ charge distributions shown in Table 4.1 to calculate the most stable configuration of the caffeine dimer.

While the ground state interactions depend on the sum of the

monopole-monopole, the monopole-induced dipole and the dispersion interactions, the exciton interaction for a given transition depends to a first approximation only on the interaction between the transition monopoles (or the transition dipoles in the dipole approximation).

The transition monopoles obtained from the SCF-π electron calculation can be used to estimate the exciton interaction, but because of the large errors involved in these calculations, no reasonable results were obtained. The transition monopole-transition monopole exciton interaction is a delicate balance between large attractive and repulsive forces, while the transition monopoles used in the calculations are small numbers defined as the difference between two larger numbers.

The dipole approximation has the advantage in exciton interaction calculations that no theoretically calculated transition dipoles are required, since the experimentally determined oscillator strength can be used in conjunction with experimentally determined transition moment directions.

The dipole-dipole approximation is used in Section 4.5 to estimate the angle between the transition dipoles.

4.3.5.2 Monopole-monopole interaction in the dimer.

The monopole-monopole interaction was calculated using the calculated ground state charge distributions for:

a) Two vertically stacked parallel monomer units, one of which is rotated about the centre of the $C_4 - C_5$ axis.

b) Two vertically stacked monomer units, one of which is rotated 180° about the axis perpendicular to the C_4—C_5 axis, after which it is rotated about the centre of the C_4—C_5 axis.

The calculations were performed for intermolecular distances of 3.4 Å and 4.2 Å. These calculations were then repeated for a rotation about a point .2 Å displaced along the perpendicular bisector of the C_4—C_5 axis towards the C_1—C_2 axis, which would approximately correspond to the centre of the molecule. The angular dependence of the interaction energy is shown in Fig. 4.3 for an intermolecular distance of 3.4 Å and in Fig. 4.4 for an intermolecular distance of 4.2 Å. From these graphs it can be seen that the two most stable configurations are the C_2 configuration (Fig. 1.2) which corresponds to rotation of one unit through 180° about the perpendicular to the C_4—C_5 axis, and the configuration obtained by rotation of 180° about the perpendicular to the C_4—C_5 axis followed by a rotation of 220° about the centre of the C_4—C_5 axis. The latter configuration is the most stable configuration which is in reasonable agreement with the most stable configuration obtained by Pullman et al (1966B) for base pairs. This configuration is shown together with the rotational axis in Fig. 4.5. The configuration in which both molecules are aligned the same way (C_s configuration) is shown to be energetically highly unfavourable.

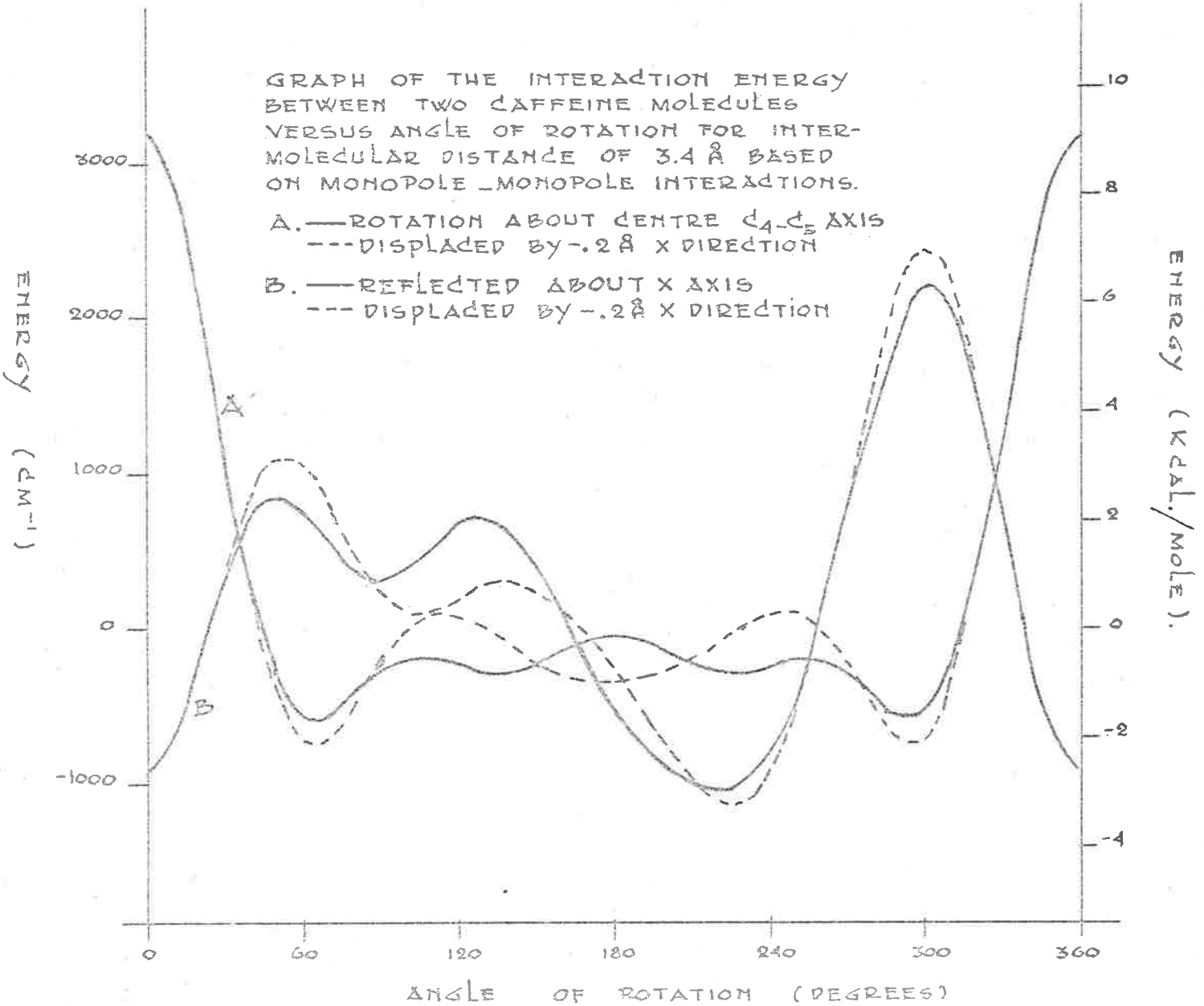
GRAPH OF THE INTERACTION ENERGY BETWEEN TWO CAFFEINE MOLECULES VERSUS ANGLE OF ROTATION FOR INTER-MOLECULAR DISTANCE OF 3.4 Å BASED ON MONOPOLE _MONOPOLE INTERACTIONS.
A. ——ROTATION ABOUT CENTRE C_4-C_5 AXIS
--- DISPLACED BY -.2 Å X DIRECTION
B. ——REFLECTED ABOUT X AXIS
--- DISPLACED BY -.2 Å X DIRECTION
ENERGY (CM⁻¹)
ENERGY (KCAL./MOLE).
3000
2000
1000
0
-1000
10
8
6
4
2
0
-2
-4
A
B
0
60
120
180
240
300
360
ANGLE OF ROTATION (DEGREES)

FIG. 4,3.

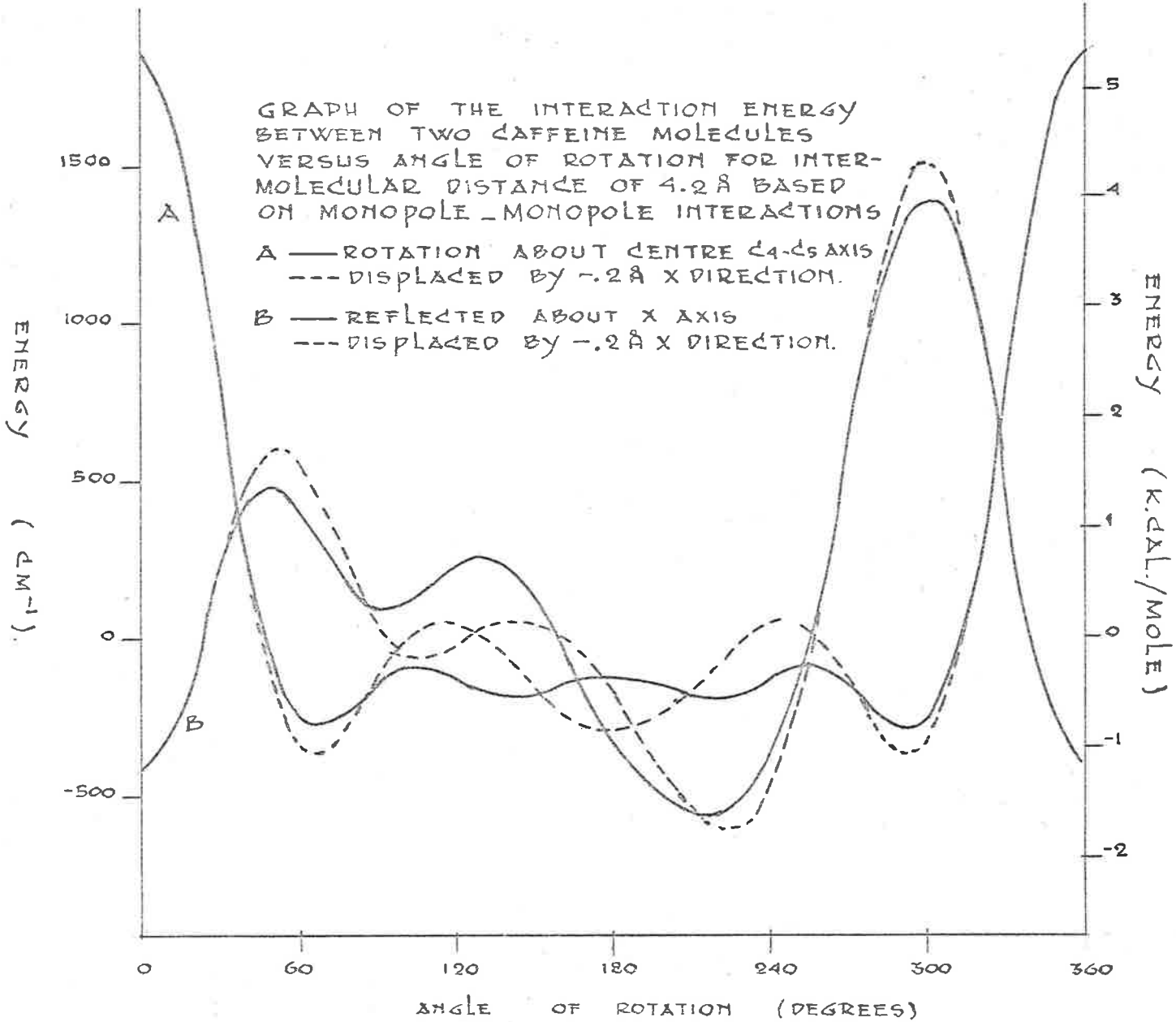
GRAPH OF THE INTERACTION ENERGY BETWEEN TWO CAFFEINE MOLECULES VERSUS ANGLE OF ROTATION FOR INTER-MOLECULAR DISTANCE OF 4.2 Å BASED ON MONOPOLE_MONOPOLE INTERACTIONS
A —— ROTATION ABOUT CENTRE C4-C5 AXIS
--- DISPLACED BY -.2 Å X DIRECTION.
B —— REFLECTED ABOUT X AXIS
--- DISPLACED BY -.2 Å X DIRECTION.
A
B
1500
1000
500
0
-500
ENERGY (CM-1).
5
4
3
2
1
0
-1
-2
ENERGY (K.CAL./MOLE)
0
60
120
180
240
300
360
ANGLE OF ROTATION (DEGREES)

FIG. 4.4.

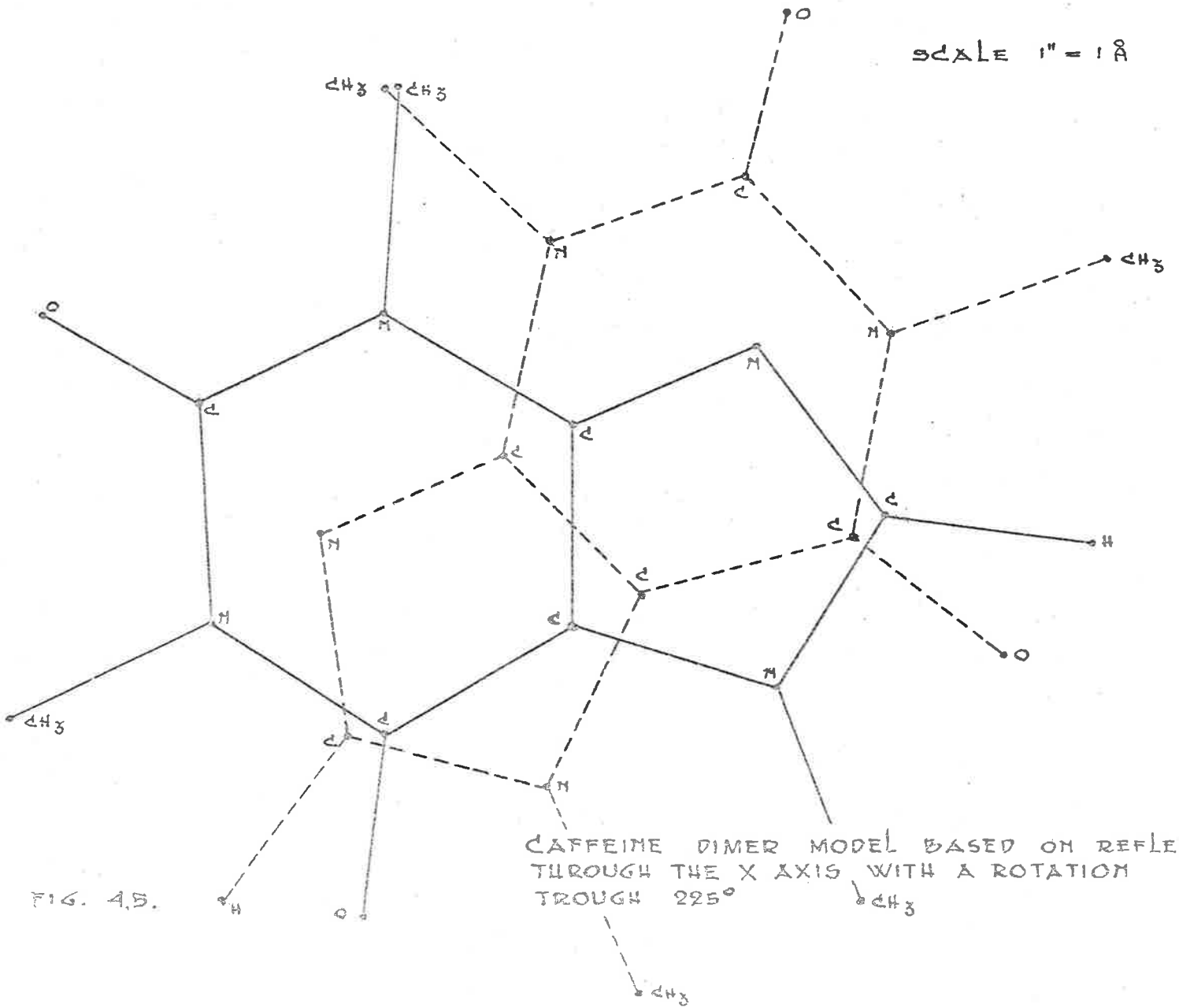

FIG. 4.5.

CAFFEINE DIMER MODEL BASED ON REFLECTION THROUGH THE X AXIS WITH A ROTATION THROUGH 225°

4.4 THEORETICAL CALCULATION OF DIMER SPECTRUM

4.4.1 Introduction.

Since Davydov first introduced the exciton theory of molecular crystals in 1948, a considerable amount of work has been done on the theoretical prediction and interpretation of crystal and polymer spectra. Davydov's theory is based on the Frenkel (1931), or tight binding, exciton model. A rapid transfer of excitational energy is possible within a cluster of identical molecules resulting in a degeneracy of the system equal to the number of molecules. When there is interaction between the excited and ground state molecules, these interactions remove the degeneracy and lead to the development of exciton bands that are the property of the cluster as a whole. The alternative and equivalent interpretation, in view of the Heisenberg uncertainty principle, is that the exciton migrates freely from unit to unit within the cluster.

Early applications of this concept to aggregates and polymers in solution have considered purely electronic wavefunctions. Kasha (1963) gives a comprehensive review of most of the early work on the exciton theory. The interest in this work is mainly focussed on the dimer in which case a simple splitting of the excited state energy levels occurs, corresponding to the wavefunctions:

$$\frac{1}{\sqrt{2}}(\psi_a^*\psi_b + \psi_a\psi_b^*) \text{ and } \frac{1}{\sqrt{2}}(\psi_a^*\psi_b - \psi_a\psi_b^*)$$

The resulting two series of transitions from the ground state will be

denoted as the (+) and (-) series. The relative intensity of the bands corresponding to these transitions is governed by selection rules and depends on the symmetry of the aggregates. If one of the transitions is forbidden either a blue or a red shift can be obtained. This simple theory gives a satisfactory explanation of most of the spectral changes on aggregation.

The main disadvantage of the early applications of the Davydov Theory is that no vibrational interactions are included in the calculations. In the calculation of the intermolecular interaction, integrals involving vibronic wavefunctions should be used instead of purely electronic functions. When molecular vibrations are included each integral must be multiplied by a vibrational overlap factor whose magnitude is not in general equal or even close to unity. Davydov's theory ignores the complex vibrational structure of the electronic bands. The inclusion of the molecular vibrations is thus necessary for either a quantitative or detailed application of the exciton theory to molecular aggregates.

The Born-Oppenheimer separability which applies to a fairly good approximation for molecules cannot be assumed to hold for electronically excited aggregates. Simpson and Peterson (1957) proposed that the Born-Oppenheimer approximation applies in the two limiting cases.

1) Very weak coupling. Perturbation theory applies to the two monomer units.

2) Very strong coupling. Electronic wavefunctions are formed

from the sum of the wavefunctions. Vibrational wavefunctions are formed from combining the individual vibrational wavefunctions. Perturbation theory is then applied to this system to obtain the energy and intensity of the vibrational bands as a function of the interaction energy.

This method was first applied by McRae in a series of articles called "Molecular Vibrations in the Exciton Theory". The main assumptions made are that the Born-Oppenheimer approximation applies in the two limiting cases and that there is only one vibration, which is harmonic. These assumptions have been used in all later theories. McRae's theory has been applied successfully by Kurucsev and Strauss (1970). The main disadvantage of McRae's theory is in the uncertainty about the important intermediate coupling region.

Siebrand (1964) using a variation method obtained a continuous representation of the energy of the vibrational bands as a function of the interaction energy. The wavefunctions obtained for the limiting cases were combined to form a trial function. Eigen values were obtained which behave properly in the limits and join smoothly in the intermediate region.

Merrifield (1963) showed that if it is assumed that the only effect of electronic excitation on the molecular vibration is to produce a change in the equilibrium position without a change in frequency, the vibronic Schroedinger equation for a pair of identical molecules can be solved numerically over the entire range of coupling strengths. This has been

applied by Fulton and Gouterman (1961, 1964), who derived solutions to the dimer problem in terms of the coupling coefficient (ε) and the nuclear displacement parameter (λ). The Fulton-Gouterman method has been applied by Chandross, Ferguson and McRae (1966) to the analysis of the spectra of anthracene dimers and has been applied in this work to the calculation of the dimer spectrum of caffeine.

4.4.2 Calculations.

The Hamiltonian for the system is set up and then split into two commuting operators H' and $H^{\pm}$ after transformation to normal coordinates (Merrifield, 1963) leading to two functions:

$$\phi'_{\mu} = \sum_{\rho} b_{\mu\rho}\phi_{\rho} \qquad 4.11$$

$$\phi^{\pm}_{\nu} = \sum_{\sigma} c^{\pm}_{\nu\sigma}\phi_{\sigma} \qquad 4.12$$

applying for both the (+) and (-) functions where ϕ's are the unperturbed oscillator functions. The coefficients $b_{\mu\rho}$ are simple overlap integrals. For absorption or emission, one of the states involved is the ground state and we only need:

$$(b_{no})^2 = (b_{on})^2 = (2^n n!)^{-1}\lambda^{2n}\exp(-\tfrac{1}{2}\lambda^2) \qquad 4.13$$

The expansion coefficient $c^{\pm}_{\nu\sigma}$ are obtained by the variation principle. This results in a system of linear difference equations for the expansion coefficients which can be solved numerically.

$$a_{\sigma}c_{\nu\sigma-1} + (d^{\pm}_{\sigma} - E^{\pm}_{\nu})c_{\nu\sigma} + a_{\sigma+1} = 0 \qquad 4.14$$

where $$a_\sigma = \lambda\left(\tfrac{1}{2}\sigma\right)^{\sigma} \qquad 4.15$$

$$d_\sigma^{\pm} = \sigma + \tfrac{1}{2}^{\pm}(-1)^{\sigma}\varepsilon \qquad 4.16$$

In the matrix form, equation 4.14 becomes:

$$\begin{bmatrix} (d_0^{\pm} - E_\nu^{\pm}) & a_1 & & \\ a_1 & (d_1^{\pm} - E_\nu^{\pm}) & a_2 & \\ & a_2 & (d_2^{\pm} - E_\nu^{\pm}) & a_3 \\ & & a_3 & \end{bmatrix} \begin{bmatrix} C_{1\nu} \\ C_{2\nu} \\ C_{3\nu} \\ \end{bmatrix} = 0 \qquad 4.17$$

This is a simple Eigen value problem of the type $(C-E)X=0$ where C is now a symmetric tridiagonal matrix. This matrix equation can be solved by Given's method for tridiagonal matrices, or any other standard Eigen value-Eigen function methods.

Solutions to equation 4.17 were obtained from a finite matrix sufficiently large such that the solutions of interest were not sensitive to truncation. A matrix twice the size of the number of solutions required was found to be sufficient. Only the Eigen values $E_\nu^{\pm}$ and the corresponding first term of the Eigen vector $C_{o\nu}$ are of interest, since we are dealing with absorption.

The energy of the excited aggregate with one molecule in the vibrational level ν and the other in vibrational level μ is given by:

$$E^{\pm} = \mu + E_\nu^{\pm} - \tfrac{1}{2}(1 + \lambda^2) + \text{constant} \qquad 4.18$$

while the intensity of the corresponding band is given by:

$$R_{\mu\nu}^{\pm} = \frac{1}{\sqrt{2}}\, b_{\mu o}\, c_{\nu o}^{\pm}(M_a \pm M_b) \qquad 4.19$$

where $\underline{M}_a$ and $\underline{M}_b$ are the usual transition dipoles between electronic states.

For purine aggregation, parallel stacking of the monomer units seems likely. This is in agreement with the results found by T'so (1964B, 1965, 1967) from N.M.R. and theoretical calculations by Pullman et al (1965). In this case, if the transition dipoles are parallel, the (-) series vanishes and a blue shift is observed, while if the transition dipoles are anti-parallel the (+) series vanishes and a red shift is observed. If the transition dipoles are not aligned in the dimer, the spectrum will have contributions from both the (+) and (-) series. For a given angle θ between the transition dipoles, the relative contributions of the (+) and (-) series to the dimer spectrum is given by $M\cos\frac{\theta}{2}$ and $M\sin\frac{\theta}{2}$ respectively.

The computer program for the theoretical calculation of the dimer spectrum is shown in Appendix 7. Solutions are found for given ε and λ. The vibrational spacing and the bandwidth in the aqueous solution are included in the program to produce a complete dimer spectrum for both the (+) and (-) series.

4.4.3 Results.

The experimentally determined dimer spectrum shows little or no splitting of the band corresponding to transition II, but shows a possible shift of the absorption maximum to the blue of 50-100 cm^{-1}. This implies that the angle between the transition moment directions of the two units

of the dimer for transition II is between 0° (parallel) and 90° (perpendicular). Angles greater than 90° are unlikely since this would produce a red shift in the dimer spectrum.

The theoretical dimer spectrum for the band corresponding to transition II was calculated by the method described using the bandwidth (1044 cm^{-1}) and the vibrational spacing (1300 cm^{-1}) obtained from the monomer spectrum (Section 2.3), for the case of parallel dipoles ($\theta = 0$, $M_+ = 1$, $M_- = 0$) and perpendicular transition dipoles ($\theta = 0$, $M_+ = M_-$). The vibrational spacing in the ground state is, as part of the theory, assumed to be equal to the vibrational spacing in the excited state in which case the displacement parameter (λ) is equal to the M (1.23) calculated in Section 2.3. The theoretical dimer spectrum for the two limiting cases is shown as a function of the coupling coefficient in Fig. 4.6 and Fig. 4.7.

In the case of parallel dipoles a strong blue shift is observed for interaction coefficients greater than .25. In the experimental dimer spectrum a blue shift of approximately 100 cm^{-1} is observed. The theoretically calculated blue shift is in general over-estimated since no coulombic interactions are taken into account. These coulombic interactions tend to produce a red shift which reduces the observed blue shift, although this red shift is seldom greater than 400 cm^{-1}. It thus seems unlikely that a coupling coefficient any greater than .25 can account for the experimentally determined dimer spectrum in this case.

THEORETICALLY PREDICTED CAFFEINE DIMER SPECTRA (TRANSITION II) ASSUMING CONTRIBUTIONS FROM THE (+) SERIES ONLY AS A FUNCTION OF THE INTERACTION COEFICIENT (ϵ).

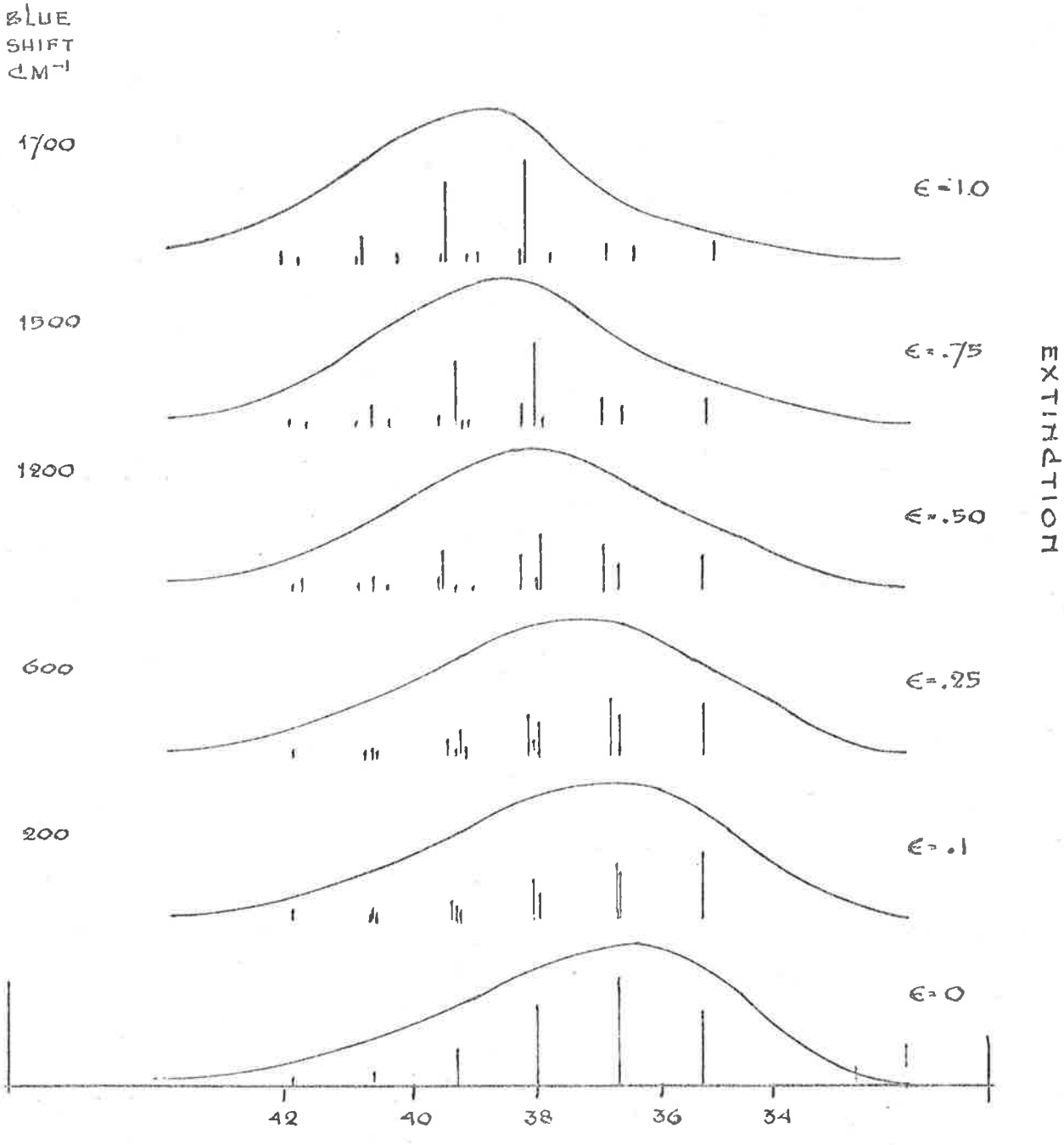

FIG. 4.6

THEORETICALLY PREDICTED CAFFEINE DIMER SPECTRA. (TRANSITION II) ASSUMING EQUAL CONTRIBUTION FROM (+) AND (−) SERIES AS A FUNCTION OF THE INTERACTION COEFFICIENT (ϵ).

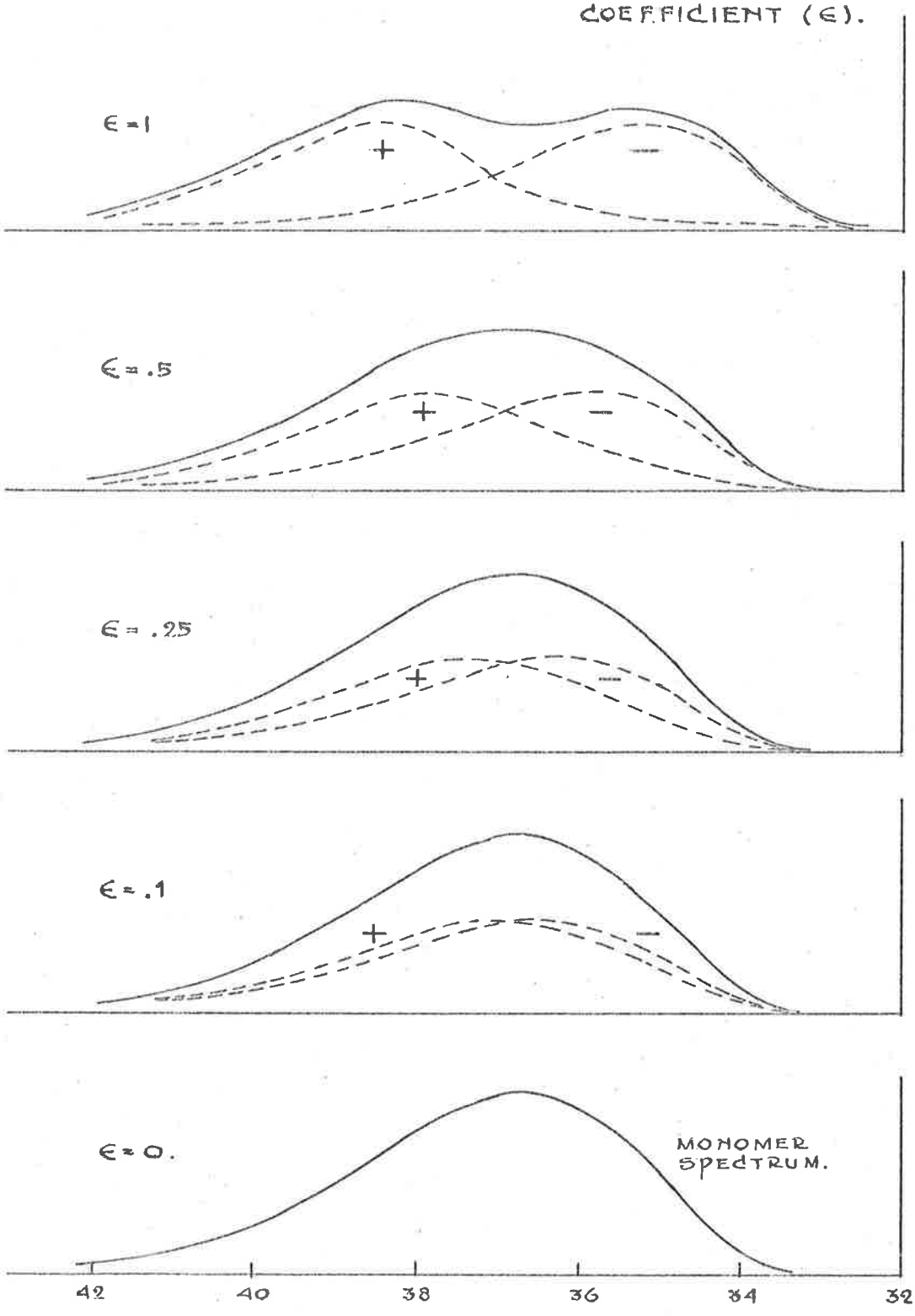

FIG. 4.7.

A comparison is made between the theoretically calculated dimer spectrum and the dimer spectrum calculated from absorption measurements for $\varepsilon = .1$, $.25$, and $.5$ in Fig. 4.8. In each case it was found to be necessary to reduce the blue shift by a small amount, allegedly due to coulombic interactions. For wavenumbers greater than 38,000 cm^{-1} a poor fit is obtained between the theoretical and experimental dimer spectra because the theoretically calculated dimer spectrum only takes account of transition II and ignores the contribution due to transition III. This contribution was estimated from the Gaussian fit for the monomer and subtracted from the experimental dimer spectrum resulting in an experimental estimate of transition II over the range 39,000-41,000 cm^{-1}. A very good fit was obtained for $\varepsilon = .1$ using a coulombic shift of 100 cm^{-1}.

If perpendicular transition dipoles are assumed, a reasonable comparison between the experimental and calculated dimer spectra can be obtained for both $\varepsilon = .1$ and $\varepsilon = .25$. The interaction between the transition dipoles produces a separation of the (+) and (-) series resulting in a broad spectral band. The observed dimer spectrum cannot account for a coupling coefficient greater than .25. The theoretical curve for $\varepsilon = .1$, $.25$, and $.5$ and the experimentally observed curve are shown in Fig. 4.9.

In both of the cases it is unlikely that the experimental dimer spectrum can be accounted for by assuming a coupling coefficient any greater than .25. This would also hold in the intermediate range for

A COMPARISON BETWEEN THE THEORETICALLY CALCULATED DIMER SPECTRUM FOR INTERACTION COEFFICIENT $\epsilon = .1, .25$ AND $.5$ FOR PARALLEL DIPOLES AND THE MEASURED DIMER SPECTRUM.

⊙ EXPERIMENTAL POINTS.
X WITH CORRECTION FOR SPECTROPHOTOMETER.
Ⅲ CORRECTED FOR ABSORPTION DUE TO TRANSITION Ⅲ.

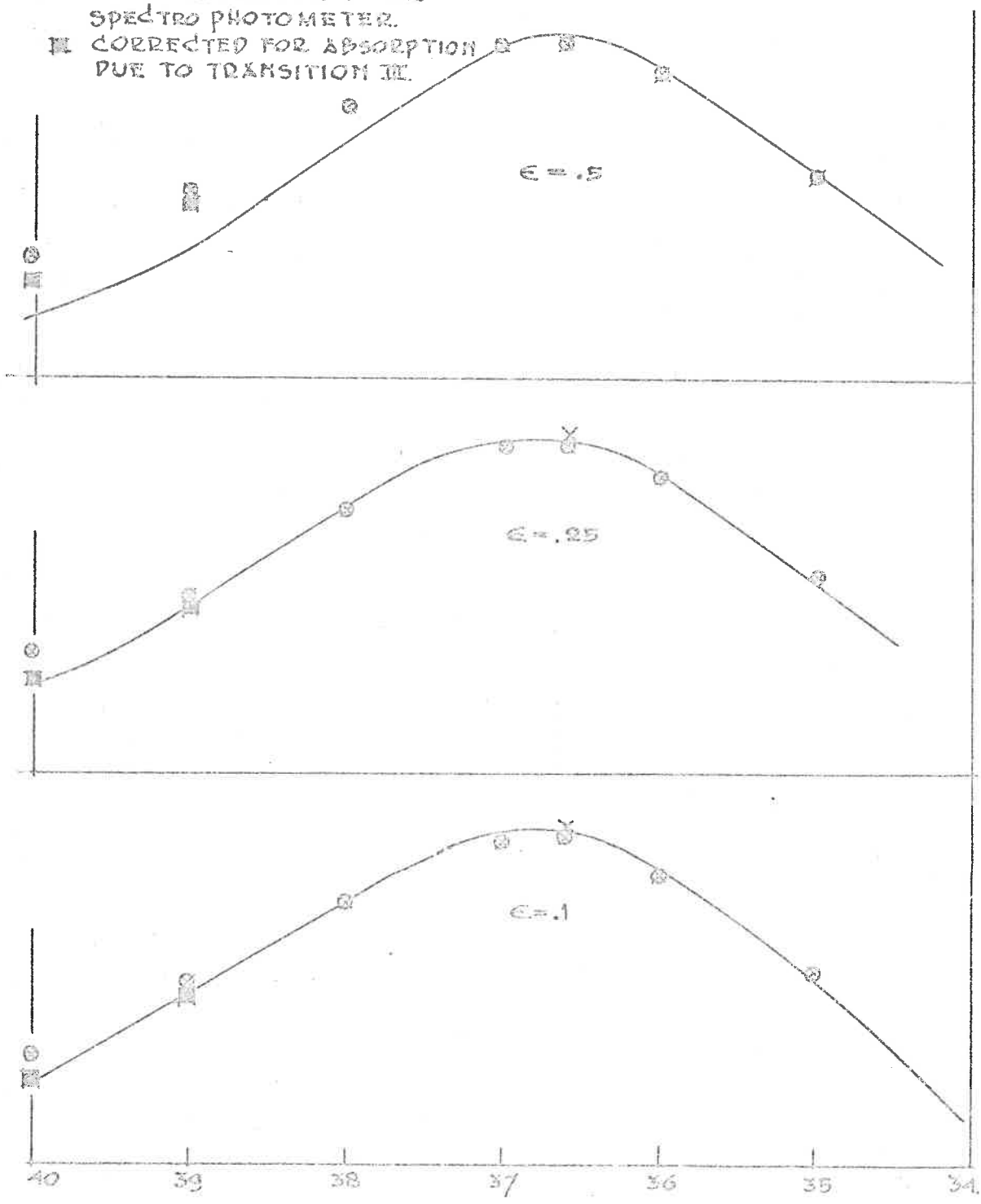

FIG. 4.8.

A COMPARISON BETWEEN THE THEORETICALLY CALCULATED DIMER SPECTRUM FOR INTERACTION COEFFICIENT ϵ=.1, .25, .50 FOR NEAR PERPENDICULAR DIPOLES AND THE MEASURED DIMER SPECTRUM.

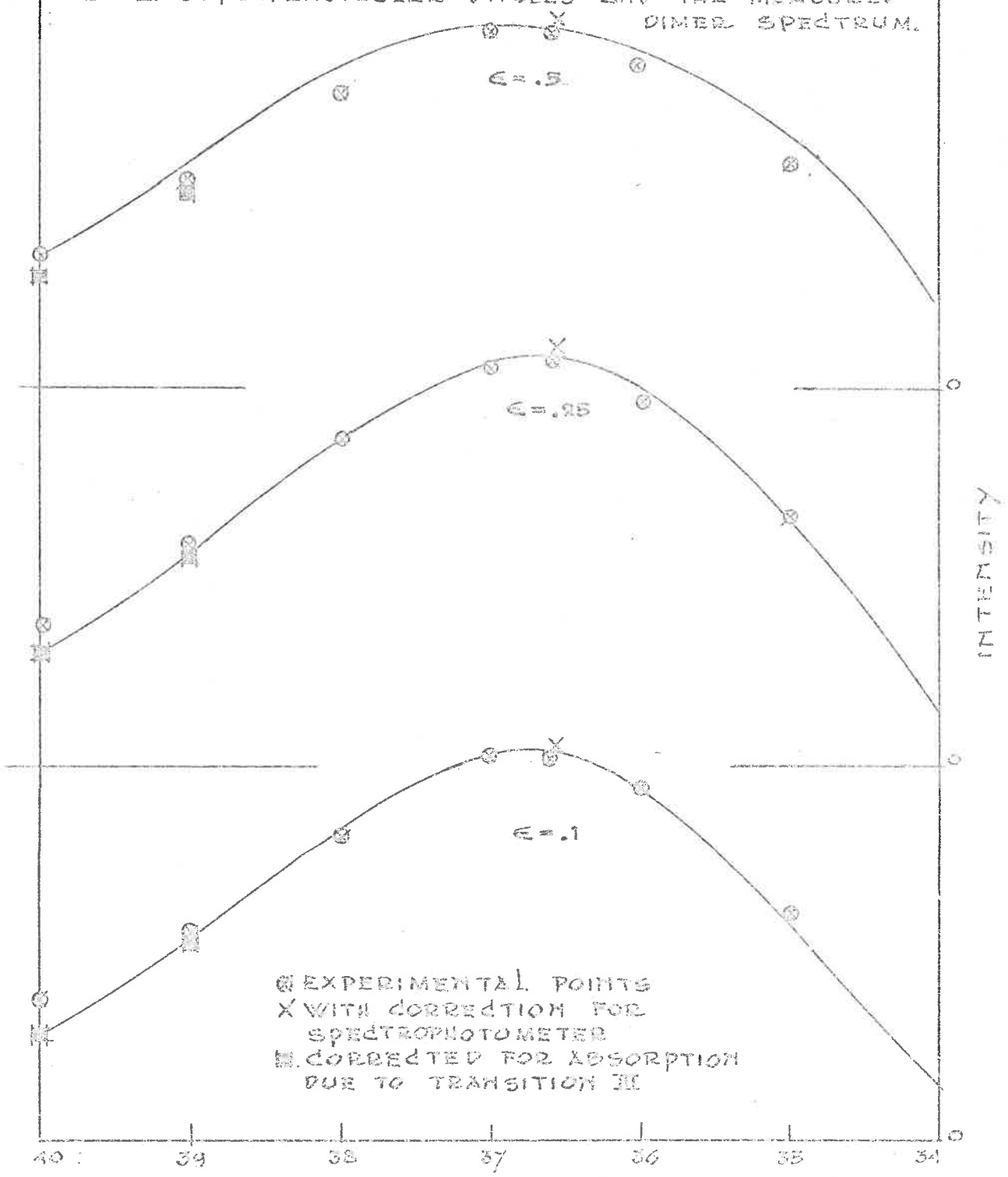

⊗ EXPERIMENTAL POINTS
X WITH CORRECTION FOR SPECTROPHOTOMETER
⊠ CORRECTED FOR ABSORPTION DUE TO TRANSITION III

FIG. 4.9.

$0^\circ < \theta < 90^\circ$. In all further calculations it will thus be assumed $0 < \varepsilon < .25$.

It seems likely that $\varepsilon = .1$ will give a reasonable estimate of the coupling coefficient for the caffeine dimer. This indicates that the weak coupling takes place in the caffeine dimer, and possibly in the dimers of many other purines and substantial purines.

4.5 CALCULATION OF THE EXCITON INTERACTION COEFFICIENT FROM THE DIPOLE-DIPOLE APPROXIMATION

4.5.1 Introduction and theory.

The dipole-dipole approximation can be conveniently used to estimate the magnitude of the exciton interaction energy in the caffeine dimer since the experimentally determined oscillator strength can be used to determine the magnitude of the dipoles.

The energy of interaction between two ideal dipoles is given by Kauzmann (1957) as:

$$\phi_{ab} = \frac{1}{r_{ab}^3}\left(\mu_a \mu_b - 3(\mu_a \cdot r_{ab})(\mu_b \cdot r_{ab})/r_{ab}^2\right) \qquad 4.20$$

This equation would hold also for interaction between transition dipoles. For dimers consisting of parallel stacked units, and an inplane transition, the last term can be neglected so that equation 4.20 reduces to:

$$\phi_{ab} = \frac{1}{r_{ab}^3} \underline{M}_a \underline{M}_b \qquad 4.21$$

where $\underline{M}_a$ and $\underline{M}_b$ are the transition dipoles.

The oscillator strength (f) for a transition is given by Hirschfelder, Curtis and Bird (1964) as:

$$f = \frac{8\pi^2 \nu m_e}{3he^2} M^2 \qquad 4.22$$

where ν is the frequency of the transition, m_e is the mass of an electron, h is Planck's constant and e is the electronic charge.

Substituting 4.22 into 4.21 and converting to reciprocal centimetres gives:

$$\phi_{ab} = \frac{1}{r_{ab}^3} \frac{3e^2}{8\pi^2 e^2 \omega m_e} f \cos\theta \ cm^{-1} \qquad 4.23$$

where θ is the angle between the transition dipoles.

If transition II is considered to be centred at 36,600 cm^{-1} on substitution we obtain:

$$\phi_{ab} = \frac{2.927 \times 10^5}{(r_{ab} \times 10^8)^3} f \cos\theta \ cm^{-1} \qquad 4.24$$

The oscillator strength of transition II can be obtained from numerical integration of the extinction value over the band. Since band II overlaps with band III the fitted Gaussian function was used instead (Section 2.4). The oscillator strength is given by:

$$f = 4.32 \times 10^{-9} \int \varepsilon_{ex}(\omega) \, d\omega \qquad 4.25$$

A value for the oscillator strength f = .182 was found.

4.5.2 Results and interpretation.

If the Van der Waals' separation value of r_{ab} = 3.4 Å is used we obtain:

$$\phi_{ab} = 1355 \cos\theta \text{ cm}^{-1}, \qquad \varepsilon = 1.042 \cos\theta = \frac{\phi_{ab}}{V_1}$$

where ε is related to the interaction energy through the vibrational spacing. The interaction energy estimated from dipole-dipole interaction in general is too high and Kurucsev (1970) found that an intermolecular distance of 4.2 Å (Pullman, 1966, uses 4.0 Å) gave more realistic values for the interaction energy. This results in a value for the interaction energy of:

$$\phi_{ab} = 718 \cos\theta \text{ cm}^{-1}, \qquad \varepsilon = .552 \cos\theta$$

If a coupling coefficient of $\varepsilon = .1$ is assumed, then an angle of 85° is obtained for r_{ab} = 3.4 Å and an angle of 80° is obtained for r_{ab} = 4.2 Å.

For a coupling coefficient of $\varepsilon = .25$, r_{ab} = 3.4 Å gives θ equal to 76° and r_{ab} = 4.2 Å results in an angle of 63°.

From this it can be concluded that the angle between transition dipoles in the caffeine dimer can be estimated as 75° ± 10°.

The calculated angle between the transition moments of the units of the dimer does not fit in with the two configurations which are predicted to be the most stable by the monopole-monopole interaction calculations (Section 4.3.5). In the model bases on reflection about the X axis and rotation through 220°, Fig. 4.5, the proposed transition moments would be nearly anti-parallel. If this were the case strong

interactions and a large red shift would be expected.

For the C_2 model based on reflection about the X axis (Fig. 1.2), the angle between the transition moments is estimated to be between 120° and 150° depending on the angle of orientation of the transition moment in the monomer unit. If the two units in the dimer are slightly twisted with respect to each other an angle of between 75° and 105° could easily occur.

It is interesting to note that the stable configuration based on rotation through 65° without reflection, gives an angle between the transition moments equal to the angle of rotation, independent of the proposed axis of alignment.

It should be realised that the configurations calculated in Section 4.3.5 were derived using theoretically calculated monopoles, and as such would not be very reliable.

The calculated angle between the transition moments of the two units of the dimer of $75^\circ \pm 15^\circ$ is in good agreement with the experimental observation that little or no shift occurs in the 36,600 cm^{-1} absorption maximum on dimerisation.

5. FLUORESCENCE SPECTROSCOPY

5.1 INTRODUCTION

In the study of the excited states of molecules, fluorescence spectroscopy is complementary to absorption spectroscopy. In absorption spectroscopy, the transition from the lowest vibrational level in the ground state to vibrational levels in the excited state are observed. The molecule usually stays in the excited state long enough for the vibrational energy to be lost to the environment, so that fluorescence takes place from the lowest vibrational level of the excited state to vibrational levels in the ground state.

Fluorescence can thus be used to study the vibrational structure of the ground state. In solution at room temperature the vibronic bands remain unresolved, but if the temperature is reduced to -20°C the individual vibrational bands can be clearly observed. Cohen and Goodman (1965) studied the luminescence of purine and adenine in EPA (a 5:5:2 mixture of ether, isopentane and ethanol) and other solvents at 77°K, and found a vibrational spacing of approximately 300 cm^{-1} for the ground state of purine. At this temperature phosphorescence from the lowest triplet state will make a major contribution to the luminescence. The deactivation processes competing with fluorescence are shown in Fig. 5.1.

When the sample is excited with plane polarised light, the molecules whose transition moment directions for absorption coincide with the plane of polarisation of the light, will absorb strongly. On emission, the majority of the fluorescence will be polarised parallel to the

RELATIONSHIP BETWEEN TRANSITIONS GIVING RISE TO ABSORPTION, FLUORESCENCE, PHOSPHORESCENCE, AND QUENCHING PROCESSES.

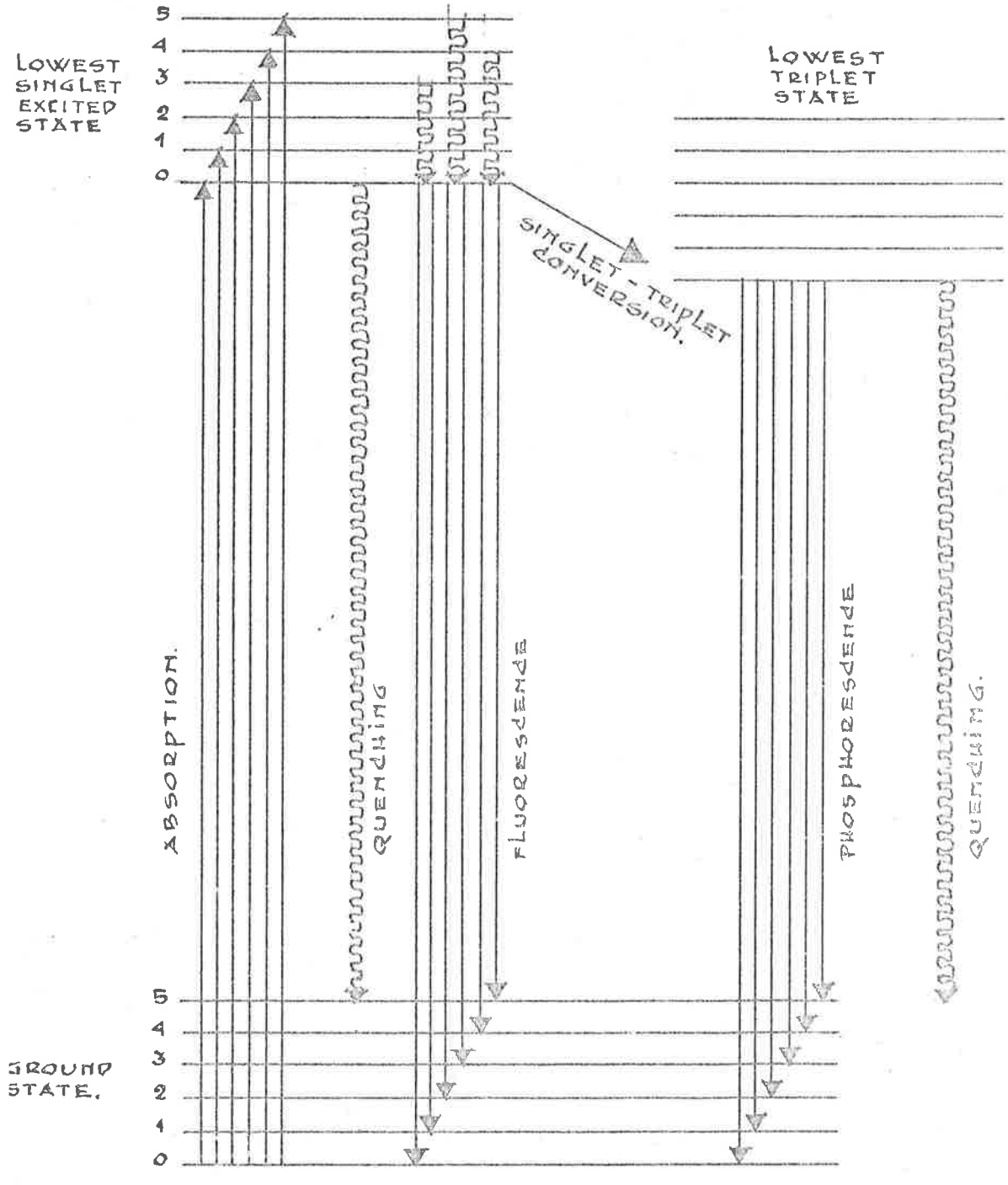

FIG. 5.1

transition moment for the emission. Polarised fluorescence can thus be used to determine the transition moment direction for the transition from the lowest singlet excited state to the ground state.

If the orientation of the molecule changes significantly between absorption and emission, the degree of polarisation of the light emitted will be reduced. For this reason polarised fluorescence studies are usually done on molecules in highly viscous solutions (Hercules).

If emission occurs from the state to which the molecule was originally excited, the transition moment vector for the emission will be the negative of the vector for the corresponding absorption, so that the same angle is obtained experimentally. If an inter-system cross-over occurs to a lower singlet state, the measured transition moment direction for emission will be different from the one measured for absorption. In this way, the presence of low lying $\pi^* \leftarrow n$ states can be observed.

If, on aggregation, a dimer is formed whose quantum efficiency is not equal to the quantum efficiency of the monomer, or if the fluorescence spectrum of the dimer is significantly different from the spectrum for the monomer, the fluorescence spectrum can, like the absorption spectrum, be used to study the aggregation.

A high resolution fluorimeter (Fig. 5.2), based on the one described by Ainsworth and Winter (1964), was designed by Dr. T. Kurucsev of the Department of Physical and Inorganic Chemistry of the University of Adelaide.

This fluorimeter, which includes provisions for polarised and low

THE FLUORIMETER

1. Drive
2. Drive cable - to clutch
3. Fan
4. Exhaust
5. Lamphousing - Xenon arc
6. Powerleads - Xenon arc
7. Prism - monochromator
8. Focussing sleeve
9. Filters
10. Cell holder
11. Cooling rod
12. Cell
13. Filters
14. Slit
15. Grating monochromator
16. Waveguide
17. Prism holder
18. Chopper (140/840 cycles)
19. Shutter - to photomultiplier
20. Power supply
21. Rectifier
22. Rectifier input
23. Rectifier output (140 and 840 cycles)
24. Impedance match
25. AGC
26. XY recorder
27. Photomultiplier power supply
28. Keithly electrometer
29. Backvoltage supply
30. Birefringence apparatus


1
2
3
4
5
6
7
8
9
10
11
12
13
14
15
16
17
18
19
20
21
22
23
24
25
26
27
28
29
30

FIG. 5.2.

temperature (-20°C) fluorescence, is described in detail in the following section. The fluorimeter was tested in detail and an approximate correction curve characteristic of the fluorimeter was determined. The fluorescence spectra of quinine sulphate and caffeine were recorded. Because the fluorimeter is still in the experimental stage, it was not possible to include low temperature and polarised fluorescence studies in this work.

The fluorimeter is shown schematically in Fig. 5.3.

5.2 DESCRIPTION OF THE FLUORIMETER

5.2.1 The source.

The source consists of an Osram XBO/4 450 watt, high stability lamp set in a Schoeffel (Westwood, N.J., U.S.A.) LH 151 lamphousing (5). The lamphousing is set on a swivelling base so that the lamp can be used as a source for both the fluorimeter and the birefringence apparatus (30). The lamphousing features a cooling fan, a spherical reflection mirror and a focussing sleeve. The lamp voltage is obtained from a stabilised 300 volt supply (19) for a range of currents up to 50 amps. A maximum current of 28 amps was used for the spectral measurements. The lamphousing is fitted with an additional blowing fan (3) which further cools the lamphousing by a flow of air. The ozone generated by the lamp is drawn off through a vinyl exhaust tube (4) powered by a suction fan.

The light from the lamp is passed through a Schoeffel model QPM-30

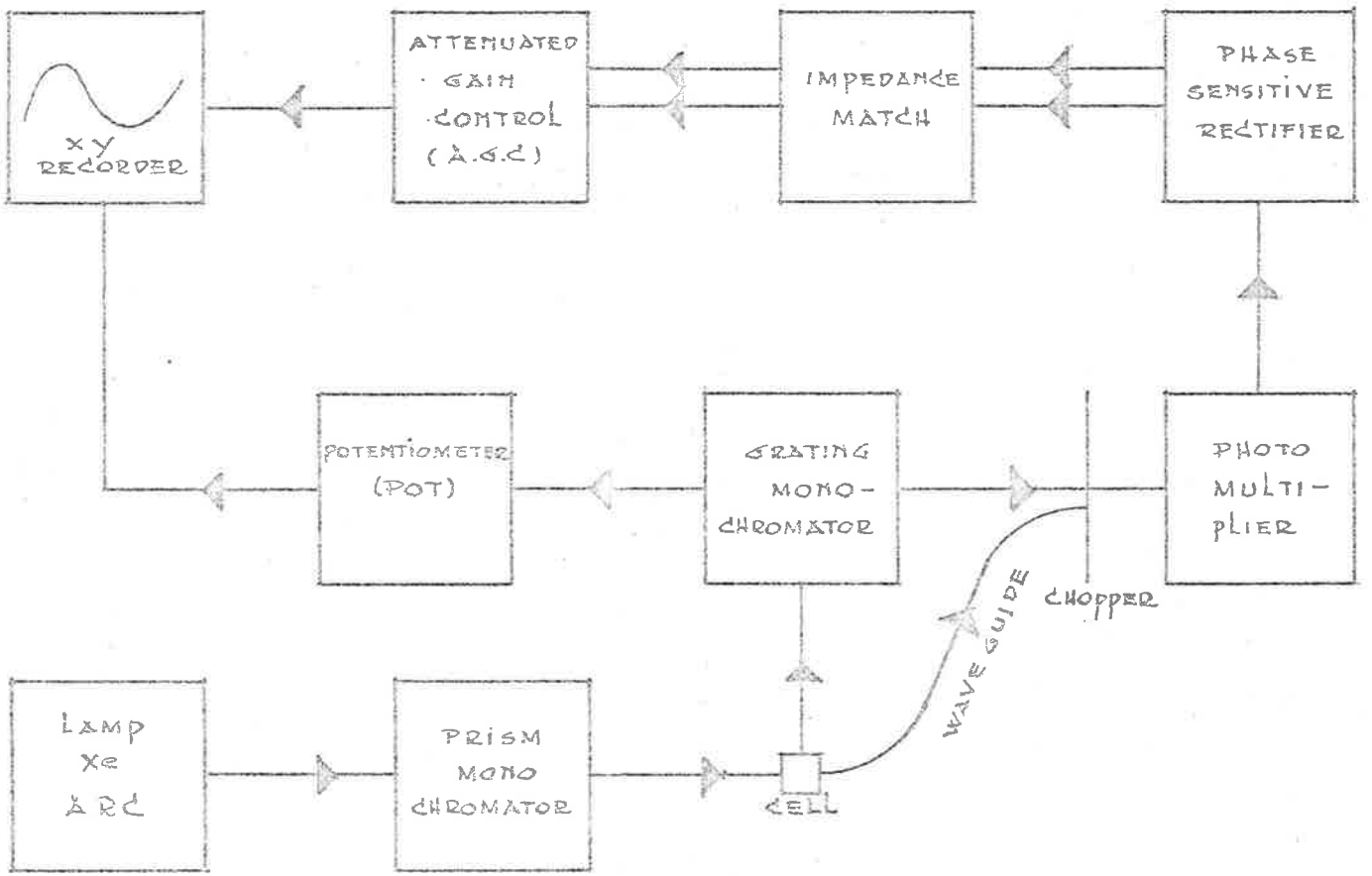

FIG. 5.3 FLUORIMETER BLOCK DIAGRAM.

prism monochromator (7), which is a small dimension monochromator fitting onto the focussing sleeve of the LH 151 lamphousing. The monochromator does not change the direction of the light beam, and so acts like a filter inserted in the light beam. The prism is turned by means of a micrometer. The wavelength (and wavenumber) of the light transmitted by the monochromator is shown as a function of the micrometer setting in Table 5.4. The spectral bandwidth of the light is controlled by means of a slit. The light beam passing through the monochromator can be focussed by means of an attached Schoeffel QPM-31 focussing sleeve (8).

5.2.2 The cell compartment.

A schematic diagram of the cell compartment is shown in Fig. 5.4. The range of the wavelength of the light admitted to the cell compartment can be controlled by means of a filter (9), although no filter was used in the current measurements. The light passes through a focussing lens to the cell holder (10), which consists of a cylindrical blackened brass container with a "red fibre" plate top. Two quarts-silica fluorescence cells are set in a solid brass block. Quarts-silica windows in the cell holder allow a path for the light to pass through and allow observation of the front, fluorescent, cell (12) at right angles. The back cell contains a solution of Rhodamine B (8 gm/litre) in ethylene glycol. The quantity of light transmitted by the fluorescent solution is proportional to the intensity of the excitation beam. This light is absorbed by the

* IF REQUIRED

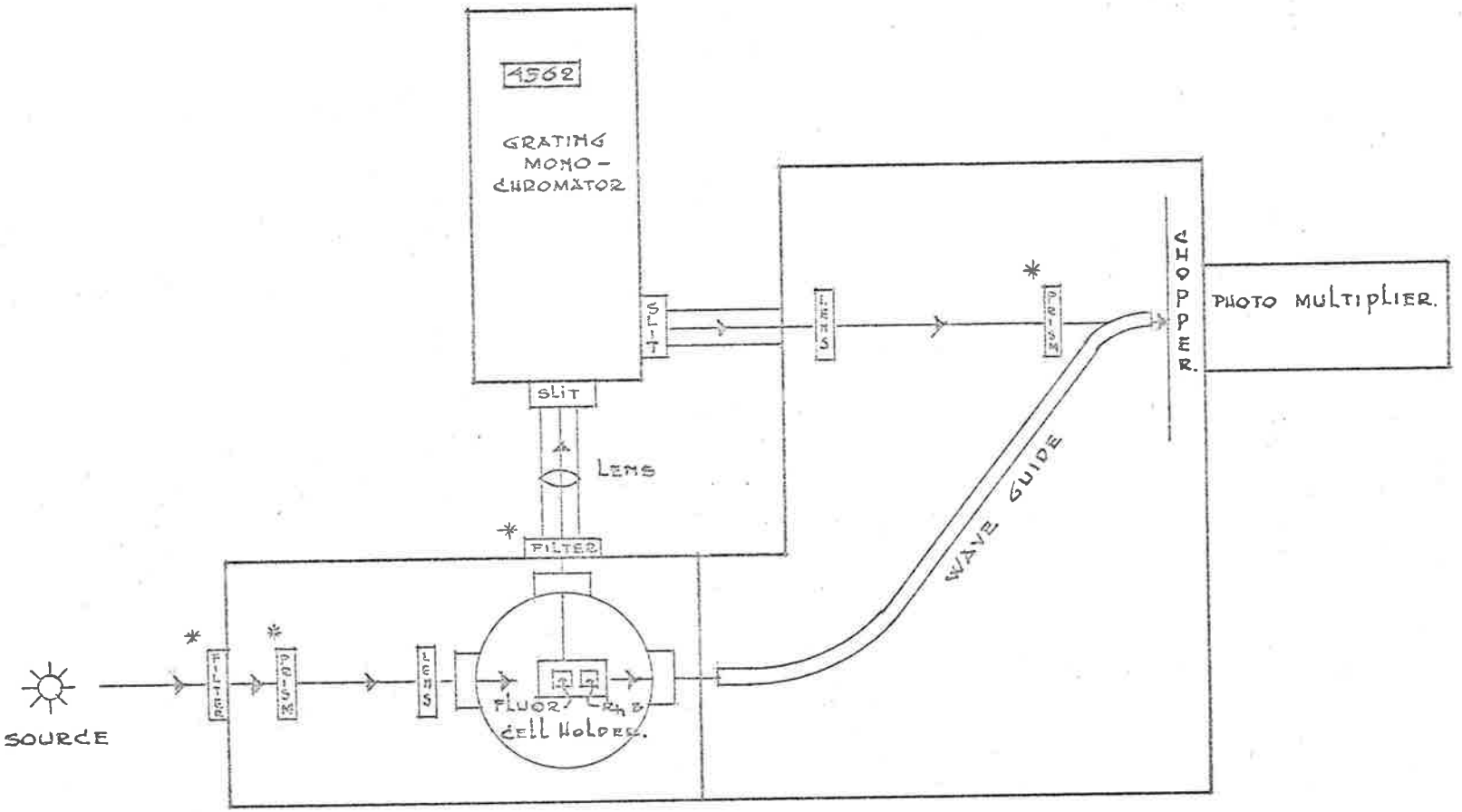

FIG. 5.4 FLUORIMETER. CELL COMPARTMENT.

Rhodamine B solution and emitted at its characteristic wavelength. The number of quanta of light emitted by the Rhodamine B is directly proportional to the quanta of light absorbed, independent of the wavelength of the excitational beam (Yguerabide, 1968). This light is passed through a waveguide (16) to the chopper (18). The waveguide was cast out of CR 39 (diethylene glycol bis(allyl carbonate)) thermosetting resin.

The light emitted by the fluorescent solution passes through a convex lens which focusses on the slit (14) of a Diffraction Products Inc. (River Forrest, Illinois, U.S.A.) grating monochromator (15). An arrangement has been made to include an optical filter (13) in front of the focussing lens to remove light due to scattering of the excitation beam. The grating monochromator was modified to correct for an error in the design. The walls around the counter were built up to prevent light leaking into the monochromator around the wavelength counter. The wavelength is selected by turning a micrometer, attached to a counter, which in turn pushes the grating through an angle. The monochromator was found to be linear over the range from 3000 to 7000 Å. The light of the selected wavelength passes through a slit and a focussing lens onto the chopper.

5.2.3 The detector system.

The fluorimeter detector system is represented in Fig. 5.5. The chopper consists of a rotating metal disc in which were drilled six

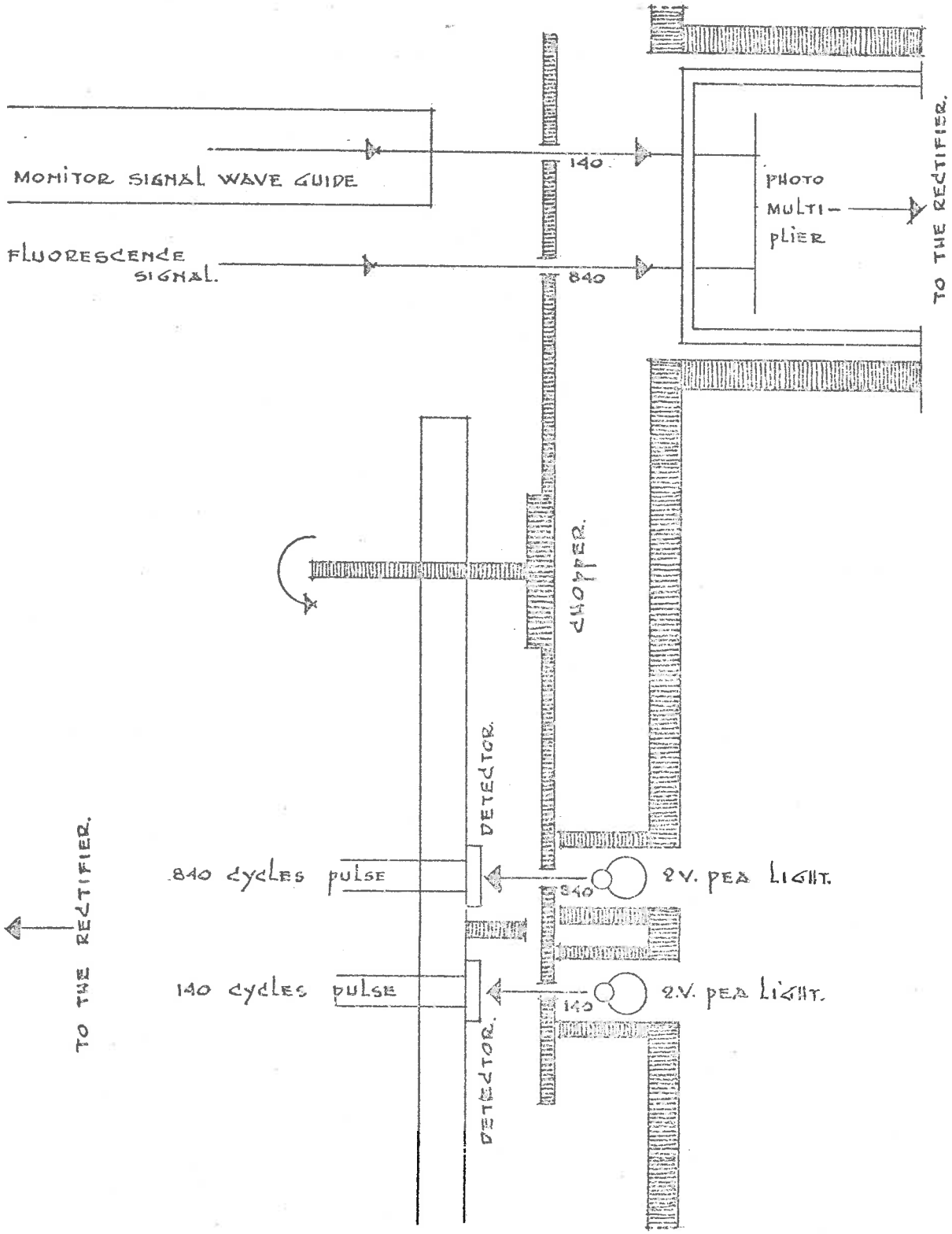

FIG. 5.5 THE FLUORIMETER DETECTOR SYSTEM.

equally spaced holes at 2.75" radius and thirty-six equally spaced holes at 2" radius. The monitor and signal beams are focussed on the 2.75" and the 2" holes respectively. The disc, driven by an electric motor, rotates at approximately 23 rev/sec, so that the monitor and signal beams are chopped at 140 and 840 cycles respectively. The chopped signals are observed on an E.M.I. 6255 (SbCs) photo-multiplier (19) with a high sensitivity in the ultraviolet, and a low dark current.

The light beams from two 2-volt pea lamps are chopped at frequencies equal to the frequencies at which the monitor and signal beams are chopped, and are observed by two light-sensitive detectors. The resulting two reference signals are fed into the rectifier (21) together with the output from the photomultiplier.

5.2.4 The electrical system.

5.2.4.1 The fluorescent signal.

The rectifier is based on the design put forward by Ainsworth and Winter (1964), and separates the signal composed of two superimposed 140 and 840 cycle pulses into two separate DC signals (23). These two signals are passed through an impedence match (24) and fed into the AGC (Attenuated Gain Control (25)). The fluorescent signal is passed through an amplifier, the gain of which is controlled by the monitor signal. This has the effect of dividing the fluorescent signal by the monitor signal. The effects due to lamp intensity fluctuations are thus removed from the spectrum. An arrangement was made for a constant voltage supply

generated within the AGC to replace the monitor signal. This constant signal can be used when no reference beam is used or for tests of the linearity of the AGC output with respect to the input. The output of the AGC produced the Y axis on the Houston Electronics, Houston, Texas, XY recorder. Mr. K. Shepherdson designed the AGC and the impedence match and built these and the rectifier. The circuits for the various elements of the electrical system are shown in Appendix 9.

5.2.4.2 Wavelength.

The electrical system converting the wavelength setting to an electrical signal driving the X axis of the XY recorder is shown in Appendix 8. A Pacific Electric 2-way adjustable-speed electrical motor (1) is used to turn a Beckman Helipot model ESP 100 potentiometer. The potentiometer is coupled to the micrometer of the grating monochromator by means of two rubber fan belts. Since the output voltage of the potentiometer is linearly related to the angle through which it is turned, and the wavelength of the light transmitted by the monochromator is a linear function of the micrometer setting, the voltage input of the recorder is a linear function of the wavelength setting of the monochromator. The X axis of the recorded spectra will thus be linear in wavelength.

5.2.5 Low temperature fluorescence measurements.

The fluorescent solution can be cooled to temperatures of -20°C

by placing the cell holder on a brass plate connected to a rod (11) which is inserted in liquid air. To prevent condensation of water from the atmosphere, the cell holder can be evacuated, or flushed with nitrogen.

5.2.6 Front face fluorescence.

When fluorescence studies are done on concentrated solutions, the observed spectrum shows a definite concentration dependence. This is due to so-called inner-filter effects. The light emitted by the excited molecules is reabsorbed by other molecules and re-emitted. This process can occur many times in concentrated solutions before the light passes out of the cell, causing a distortion of the spectrum, and in general a shift to lower energies. These effects would conceal changes in the fluorescence spectrum due to molecular aggregation.

The frontal or surface fluorescence method (Parker and Rees, 1959, 1962 as used for solid samples can be used successfully on solutions of high optical density. In this method, the fluorescence of the molecules near the front surface of the cell is observed. The experimental set-up for the observation of front face fluorescence is shown in Fig. 5.6.

5.2.7 Polarised fluorescence.

Provisions have been made to include two polarising prisms into the system, one in the path of the exeitational beam, and one (17) into the fluorescence beam. The positioning of these prisms is shown in Fig. 5.4.

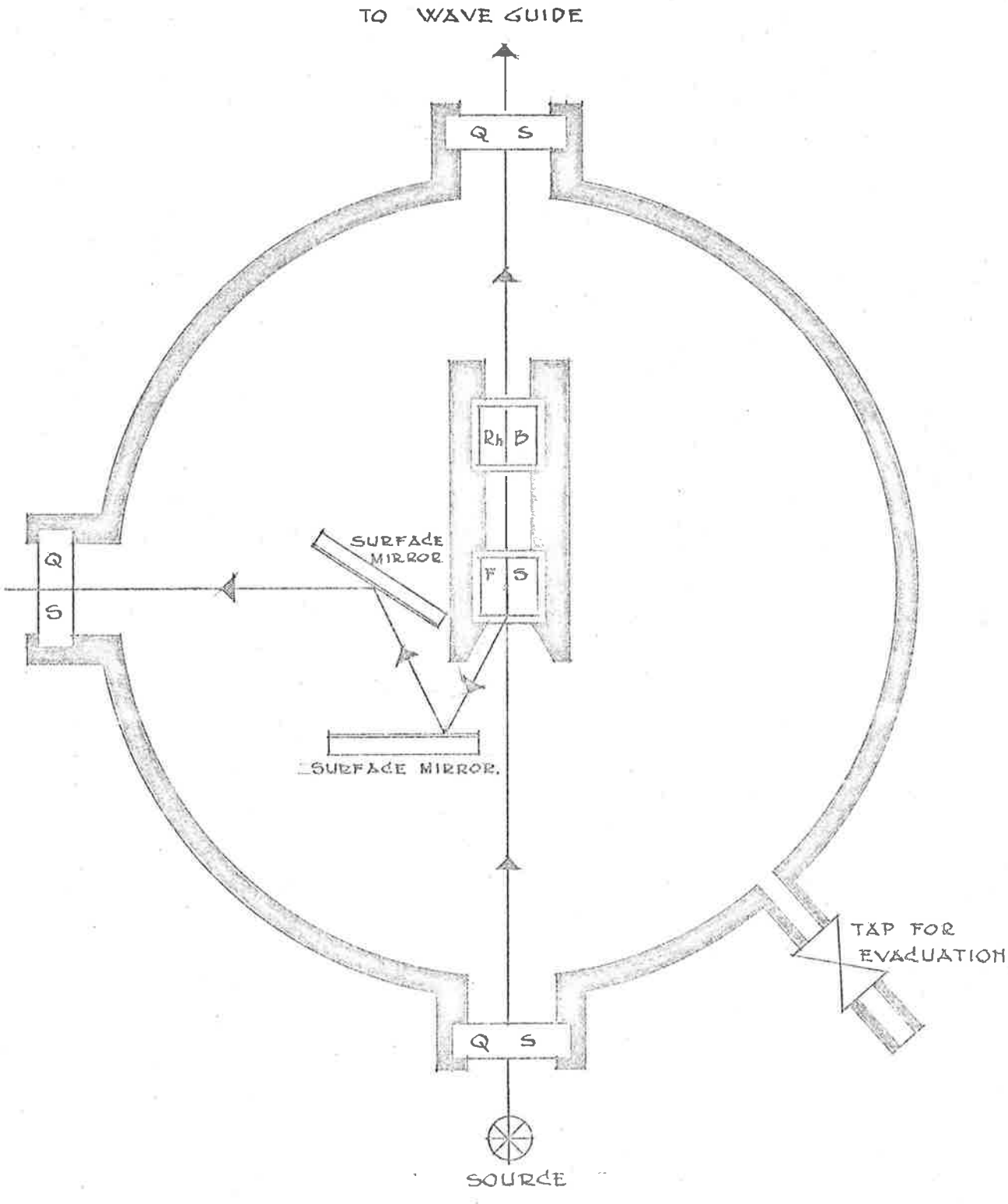

FRONT FACE FLUORESCENCE

FIG. 5.6

5.3 THE TESTING AND CALIBRATION OF THE FLUORIMETER

5.3.1 The xenon arc lamp.

5.3.1.1 Intensity stability.

The intensity fluctuations of the xenon arc lamp, operated at 25 amps, were tested in the following manner. A light beam from the xenon arc lamp was passed through a Rhodamine B solution (8 gm/litre ethylene glycol) the waveguide and the chopper onto the photomultiplier. The signal was resolved and taken from the rectifier and recorded on a 10 volt recorder run at 75 mm/hour. The high tension applied to the photomultiplier was adjusted to give an output of 5 volts. All readings were taken after an initial warm-up period of 30 minutes. The output obtained should be linearly dependent on the lamp intensity apart for the slight non-linearity in the response of the photomultiplier. No noticeable fluctuations in the lamp intensity were observed over the wavelength range from 2000 Å to 5000 Å during a period of 30 minutes for a slit width between 2 mm and 1 mm. When the slit width was reduced to .5 mm slight fluctuations in intensity were observed. The amplitude of the fluctuations was approximately 1% of the output signal over the previously mentioned wavelength range. When the slit was reduced to a minimum, fluctuations of approximately 10% were observed. At this slit width, only one or two lines of the xenon arc lamp would be used as the source. Fig. 5.7 shows the fluctuations as a function of time for a variety of slit widths, and Table 5.1 shows the data for the graphs shown. All cases were chosen

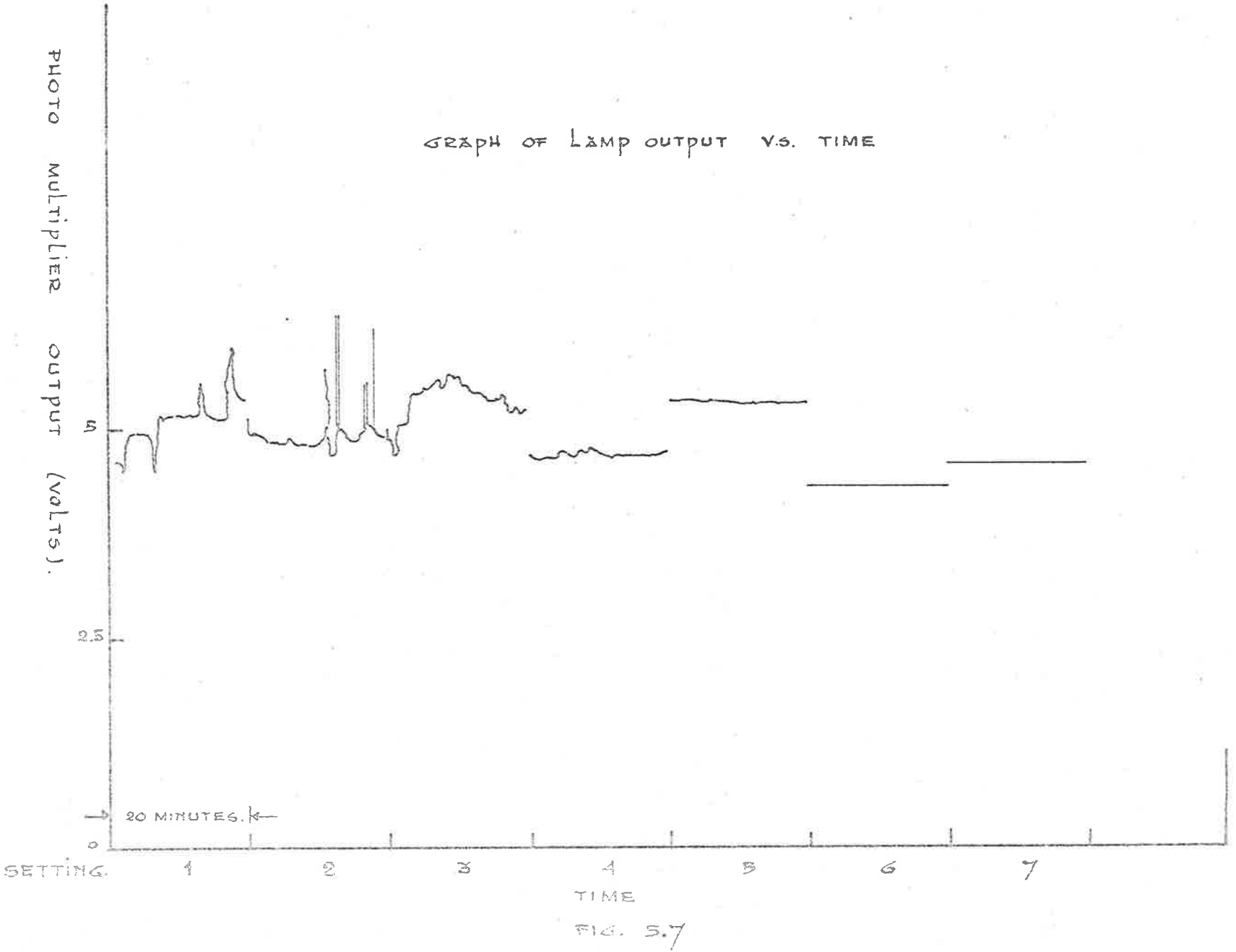
GRAPH OF LAMP OUTPUT V.S. TIME
PHOTO MULTIPLIER OUTPUT (VOLTS).
5
2.5
0
20 MINUTES.
SETTING.
1
2
3
4
5
6
7
TIME

FIG. 5.7

in the ultraviolet as the wavelength of the excitational beam for the caffeine fluorescence is in this region.

TABLE 5.1

NO.	MONOCHROMATOR	WAVELENGTH	SLIT WIDTH (mm)
1	7.50	2710	minimum
2	10.00	2370	"
3	12.50	2150	"
4	7.50	2710	.2
5	7.50	2710	.5
6	7.50	2710	1.0
7	7.50	2710	2.0

It can be concluded that the xenon arc lamp, operated at 25 amps, has no noticeable fluctuations in intensity when the monochromator slit width is adjusted between two and one millimetre. Under these conditions the fluorimeter can be adequately operated without the use of the AGC.

5.3.1.2 Lamp intensity as a function of wavelength.

The intensity of the xenon arc lamp was determined as a function of wavelength. The micrometer of the prism monochromator was set to select the required wavelength. The slit of the monochromator was set at .1 mm so that light of only a very small spectral band width

was used, and this light was passed through a Rhodamine B (8 gm/litre ethylene glycol) solution and the waveguide to the photomultiplier. This means that light of a constant wavelength distribution, characteristic of that emitted by Rhodamine B, and with an intensity directly proportional to the intensity of the light at the wavelength selected, is observed by the photomultiplier. The output voltage of the photomultiplier was measured with the Keithley electrometer. When the micrometer setting of the prism monochromator was varied, the intensity of the light emitted by the lamp and prism monochromator as a unit, is obtained as a function of wavelength.

Because of the non-linear diffraction properties of a prism, the spectral band width allowed to pass through a .1 mm slit varies considerably over the range of wavelengths studied. To obtain the lamp intensity as a function of wavelength, the measured band intensity was divided by the band width. Table 5.2 shows the lamp intensity as a function of wavelength for some selected values of the wavelength.

TABLE 5.2

WAVELENGTH (Å)	BAND INTENSITY (VOLTS)	SPECTRAL BAND WIDTH (Å)	INTENSITY (VOLTS/Å)
3000	.043	1.15	.0374
3500	.155	1.99	.0779
4000	.370	3.27	.1131
4500	.840	4.59	.1830
5000	1.64	5.85	.2803
5500	4.45	7.05	.6312
6000	50.00	8.39	5.959

The intensity distribution in the ultraviolet of the xenon arc lamp is shown in Fig. 5.8.

5.3.2 Calibration of the monochromators.

The position of the grating of the grating monochromator was adjusted so that the monochromator transmitted the two orange D lines of the sodium spectrum at 5890 and 5896 Å. The prism and grating monochromators were then calibrated using known spectral bands of the xenon arc spectrum. The position and intensity of these bands were obtained from the "Handbook of Chemistry and Physics", 41st edition. The cell holder was replaced by a mirror which reflected the light through 90° to the grating monochromator. The two slits of this monochromator were both set at a minimum to reduce the intensity of the light transmitted to the photomultiplier. The output voltage of the photomultiplier was measured on the Keithley electrometer.

An approximate calibration chart of micrometer setting versus wavelength of the light transmitted for the Schoeffel prism monochromator was supplied by the manufacturer. Using this chart and a knowledge of the relative intensities of neighbouring bands, the micrometer was set for a given spectral band of the xenon arc spectrum. The maximum of the band was found using the wavelength setting of the grating monochromator after which the slit of the prism monochromator was reduced and the micrometer adjusted to give a maximum reading on the electrometer. The process was repeated until readings became constant. The monochromators

GRAPH OF LAMPINTENSITY AS A FUNCTION OF WAVE LENGTH.

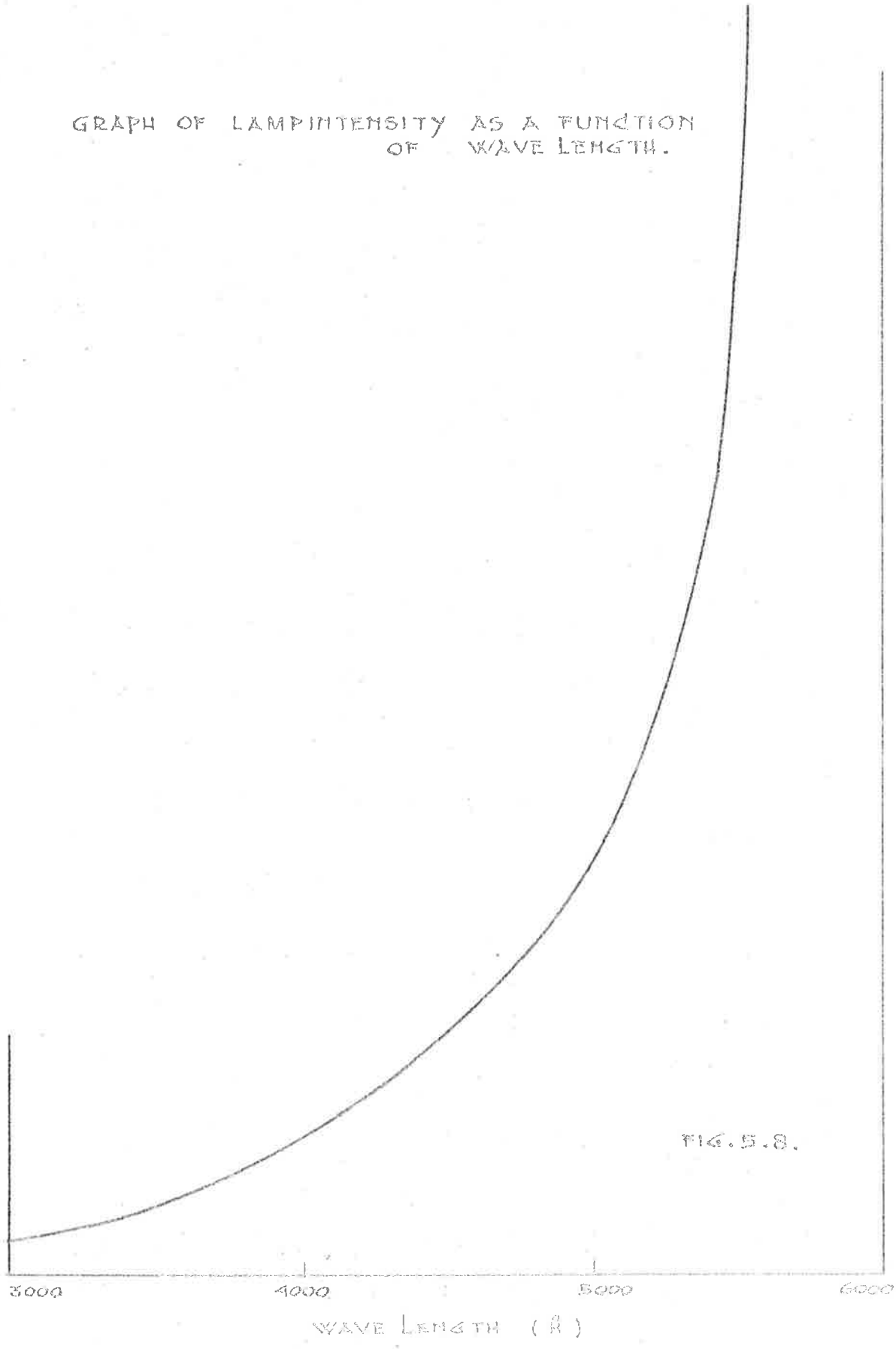

FIG. 5.8.

were calibrated using 61 bands over a range of 3000 to 7000 cm^{-1}. The results obtained for some of the bands are shown in Table 5.3.

The corrections to the micrometer setting were extrapolated to cover the range 1880-7000 Å. The corrected chart is shown in Table 5.4. This chart was checked in August 1970 before the fluorescence spectra were recorded. The wavelength of the light emitted by the grating monochromator is a linear function of the angle through which the micrometer is turned. As a result, the X-coordinate of the recorded spectra will be linear in wavelength.

5.3.3 The detector system.

5.3.3.1 Output of the photomultiplier as a function of the applied voltage.

The output of the photomultiplier was measured as a function of the voltage that was applied to it for a fixed light signal falling on it. The resulting output for one case is shown in Fig. 5.9. The output originally shows an almost exponential dependence on the applied voltage and reaches saturation at an output of 3.2 volts.

5.3.3.2 The output of the photomultiplier as a function of the intensity of the light signal.

The output of the photomultiplier for a constant applied voltage was measured as a function of the intensity of the light of constant wavelength falling onto it. The results are shown in Fig. 5.10.

GRAPH OF PHOTO MULTIPLIER OUTPUT VOLTAGE AS A FUNCTION OF THE VOLTAGE APPLIED ACROSS THE PHOTO MULTIPLIER FOR A CONSTANT SIGNAL.

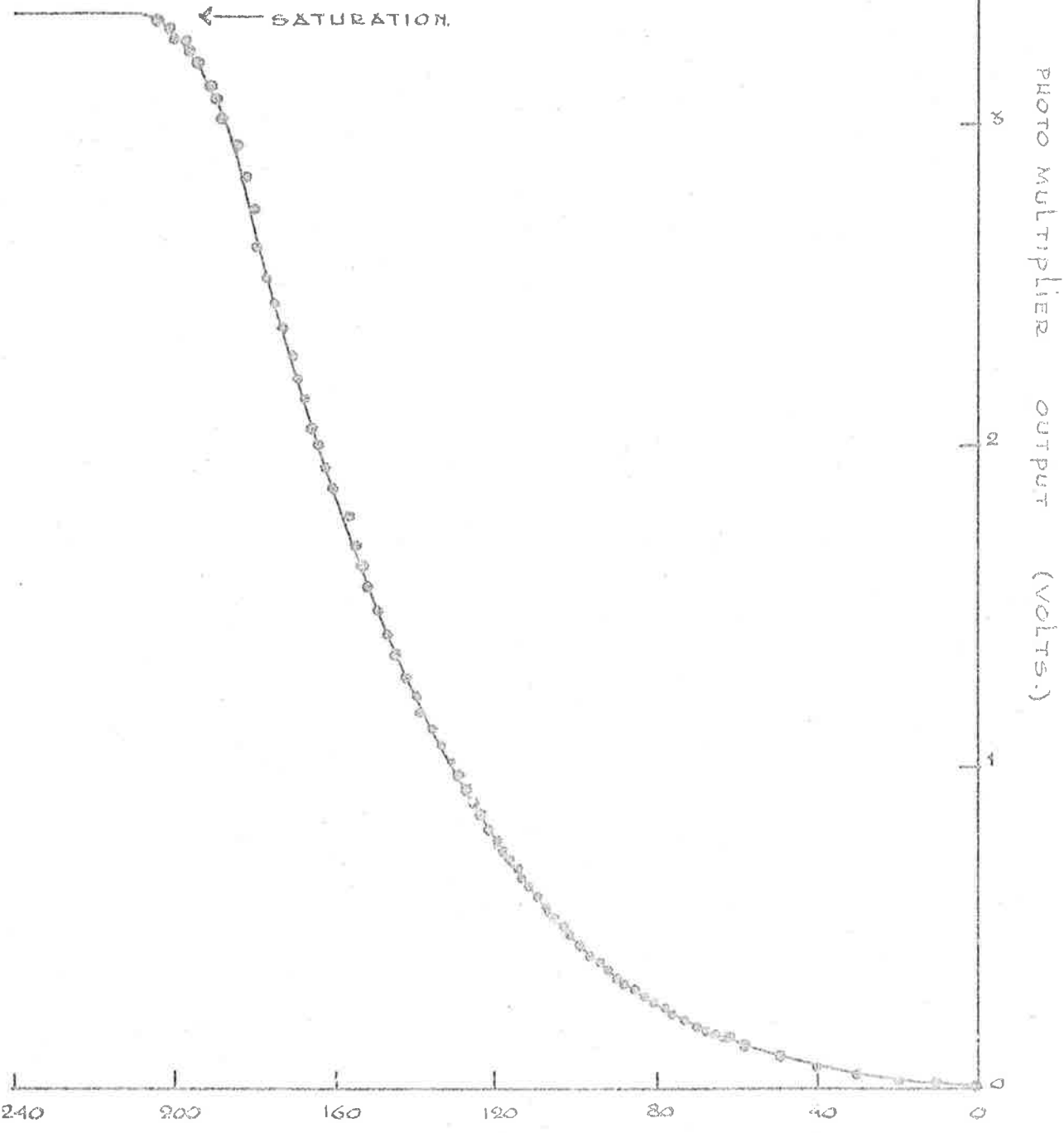

FIG. 5.9

GRAPH OF PHOTOMULTIPLIER OUTPUT AS A FUNCTION OF THE INTENSITY OF THE LIGHT SIGNAL MEASURED.

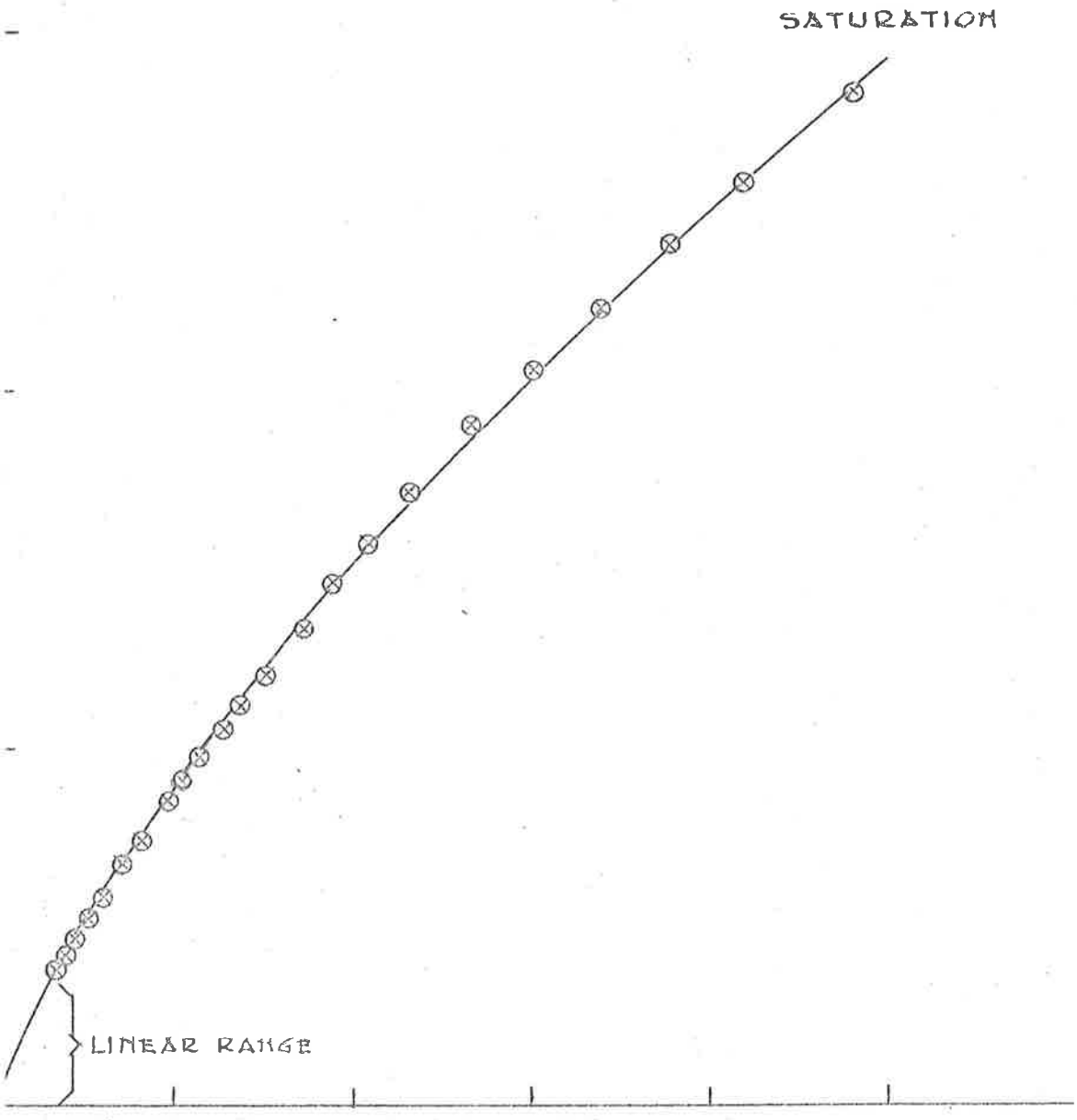

FIG. 5.10.

TABLE 5.3

MONOCHROMATOR SETTINGS FOR SOME OF THE LINES OF THE XENON ARC SPECTRUM

GRATING MONOCHROMATOR XENON ARC BAND (Å)			PRISM MONOCHROMATOR MICROMETER SETTING		
EXPECTED	OBSERVED	DIFFERENCE	EXPECTED*	OBSERVED	DIFFERENCE
3950	3951	+1	3.71	3.60	.11
3968	3970	+2	3.68	3.57	.11
4079	4074	-5	3.50_5	3.41	$.09_5$
4180	4172	-8	3.37	3.27_6	$.09_6$
4331	4326	-5	3.09_5	3.17_2	.08
4603	4604	+1	2.89_5	2.80_5	.09
4697	4695	-2	2.79_5	2.71	$.08_5$
4807	4806	-1	2.70_5	2.61	$.09_5$
4844	4842	-2	2.68	2.58_5	$.09_5$
5292	5294	+2	2.42	2.34_5	$.07_5$
5419	5420	+1	2.35	2.27	.08
6036	6037	+1	1.95	1.88_5	$.06_5$
6098	6099	+1	1.93_3	1.86	$.07_3$
6318	6318	0	1.82_5	1.76	$.06_5$
6595	6594	-1	1.72	1.66	.06
6694	6693	-1	1.69	1.62_5	$.06_5$
6942	6944	+2	1.61	1.54_5	$.06_5$

* Values obtained on interpolation from chart obtained from Schoeffel.

TABLE 5.4

CALIBRATION CHART FOR THE PRISM MONOCHROMATOR

WAVELENGTH mμ	WAVENUMBER KK	MICROMETER	WAVELENGTH mμ	WAVENUMBER KK	MICROMETER
188	53.19	18.15	470	21.28	2.81
190	52.63	17.64	480	20.83	2.71
195	51.28	16.38	490	20.14	2.63
200	50.00	15.28	500	20.00	2.56
210	47.62	13.42	510	19.61	2.48
220	45.45	11.96	520	19.23	2.41
230	43.48	10.75	530	18.87	2.34
240	41.67	9.64	540	18.52	2.28
250	40.00	8.90	550	18.18	2.22
260	38.46	8.17	560	17.86	2.16
270	37.04	7.55	570	17.54	2.10
280	35.71	7.00	580	17.24	2.05
290	34.48	6.50	590	16.95	2.01
300	33.33	6.10	600	16.67	1.97
310	32.26	5.73	610	16.39	1.93
320	31.25	5.40	620	16.13	1.89
330	30.30	5.10	630	15.87	1.83
340	29.41	4.83	640	15.62	1.79
350	28.57	4.58	650	15.38	1.75
360	27.78	4.35	660	15.15	1.72
370	27.03	4.15	670	14.93	1.68
380	26.32	3.96	680	14.71	1.65
390	25.64	3.78	690	14.49	1.61
400	25.00	3.64	700	14.29	1.58
410	24.39	3.49	720	13.89	1.52
420	23.81	3.36	740	13.51	1.46
430	23.26	3.22	760	13.16	1.41
440	22.73	3.11	780	12.82	1.35
450	22.22	3.00	800	12.50	1.30
460	21.74	2.91			

The output of the photomultiplier seems to be a linear function of the light intensity for photomultiplier outputs of up to .3 volts. For higher values of the output voltage, the output of the photomultiplier is non-linear. Saturation is reached at 3.2 volts. All fluorescence spectra were recorded within the linear range of the photomultiplier.

5.3.3.3 The determination of the spectral correction curve for the detector system.

Standard methods for the determination of the response curves for the detector system as a function of wavelength are given by many authors, e.g., Demus and Crosby (1971) and Lee and Seliger (1965). Some of these methods are based on recording spectra, first with the fluorimeter detector system, and then with a system where the response is independent of wavelength, such as thermopiles or quantum counters. The correction curve is derived by dividing the two curves. Other methods are based on comparing the known spectral distribution of a lamp or fluorescence of a compound (such as quinine) with the spectrum measured by the system.

Since the specialized equipment required for these methods is not available at this stage, and since caffeine does not fluoresce in the same region as quinine which is the most reliable standard, a modified method based on the Rhodamine B quantum counter of Yguerabide (1968) was used to determine an approximate correction curve. The correction curve required should include the properties of all elements of the

detector system, the focussing lens, the grating monochromator and the photomultiplier.

The micrometer of the prism monochromator was set to select the wavelength of the light. This light, over a range of 3000-6000 Å, was reflected through 90° by a mirror through the grating monochromator (narrow slits) onto the photomultiplier, and the output of the photomultiplier was recorded on the Keithley electrometer. This gives the lamp detector function.

The lamp intensity (including the function of the mirror) was determined by reflecting the light through 90° by means of the mirror, through the Rhodamine B solution (8 gm/litre ethylene glycol) and the grating monochromator and onto the photomultiplier. The fluorimeter detector function was obtained by dividing the two functions. This function is shown in Fig. 5.11 and Fig. 5.12.

There is some uncertainty in the function in the 20,000-26,000 cm^{-1} region. Yguerabide (1968) studied the spectral distribution of a xenon arc monochromator system using a thermopile and a Rhodamine B quantum counter and found a strong peak at 21,000 cm^{-1} and two smaller peaks at 17,800 cm^{-1} and 25,000 cm^{-1} which seem to match the high points found in the fluorimeter detector function. It seems likely that the high scatter found in the detector function is due to an error in the lamp function. When a comparison with the xenon arc spectrum was made it was found that an unusually high value in the detector function occurred each time the wavelength of the light used coincided with one of the

FLUORIMETER CORRECTION CURVE FOR THE 33000 - 17000 CM^{-1} REGION.

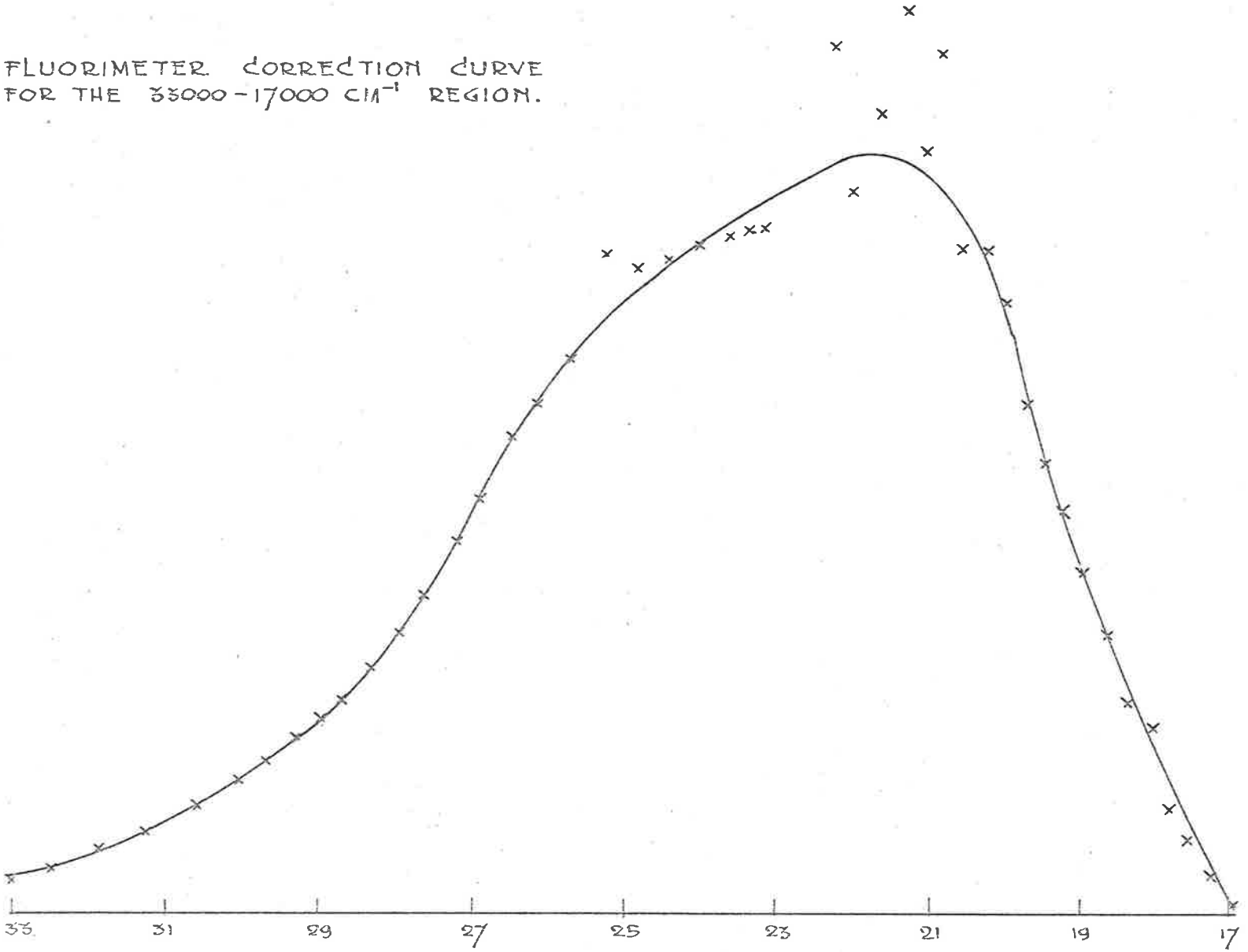

FIG. 5.11.

FLUORIMETER CORRECTION CURVE
FOR THE 29000 - 35000 CM^{-1} REGION.

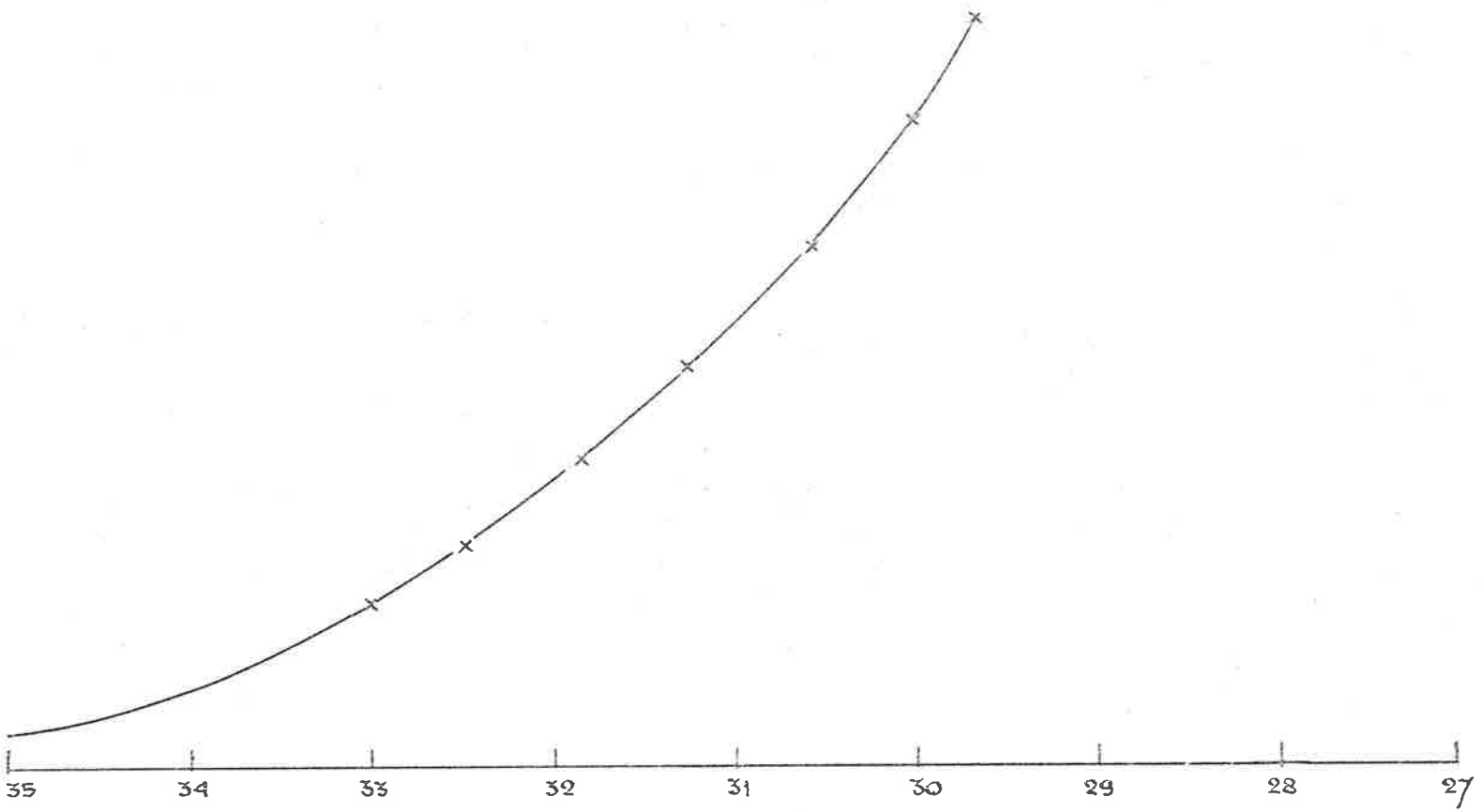

FIG. 5.12

intense bands of the xenon arc spectrum. Since the Rhodamine B solution absorbs strongly ($\approx 99\%$) a slightly wider slit was used in the determination of the lamp function.

The detector function was actually determined by the ratio of the integrated intensities over the band width of the lamp-detector function and lamp function so that a slight difference in slit width would give rise to an unusually high value in this ratio each time the wavelength of the light used coincided with an intense band of the xenon arc spectrum.

A smooth detector function was drawn to cover the 26,000-20,000 cm^{-1} region. Any uncertainty in the detector function does not affect the interpretation of the caffeine fluorescence spectrum in any way since the fluorescence peak of caffeine is at much higher wavelength. It is intended to repeat the determination of the fluorimeter detection function as soon as a lamp of known spectral distribution becomes available.

5.3.4 Testing of the AGC.

5.3.4.1 Linearity.

A constant monitor signal was fed into the AGC while the fluorescent signal, obtained from a variable D.C. voltage supply, was varied over a range from 0 to 11 volts. The output was obtained as a function of input for monitor signals of 5.0 and 3.0 volts. The output was found to be linear for outputs of up to 7.0 volts. The results are shown

in Fig. 5.14.

5.3.4.2 Functioning.

To simulate lamp intensity fluctuations, the monitor and fluorescent signals were coupled through the use of the system shown schematically in Fig. 5.13.

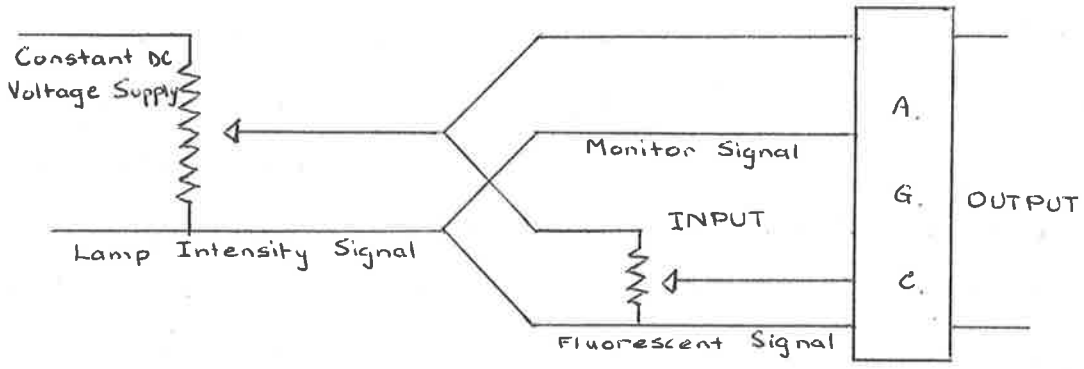

Fig. 5.13

When the lamp intensity signal is varied the monitor and fluorescent signals vary proportionally. The lamp intensity and monitor signals were set to 5 volts and the fluorescent signal for successive runs was set over a range of 1.5 to 5 volts. The lamp intensity signal and the monitor signal were then varied over a range from .1 to 8 volts, with corresponding changes in the fluorescent signal. In the ideal case, when perfect compensation takes place, the output voltage should remain constant. However, in the real case, the output voltage was not constant but varied with the lamp intensity signal. The results are shown in Fig. 5.15. The output voltage was found to be constant in the case where the fluorescent signal was 7/10 of the monitor signal. If the

GRAPH OF THE OUTPUT OF THE A.G.C. AS A FUNCTION OF THE FLUORESCENT SIGNAL FOR CONSTANT MONITOR SIGNALS OF 3.0 AND 5.0 VOLTS.

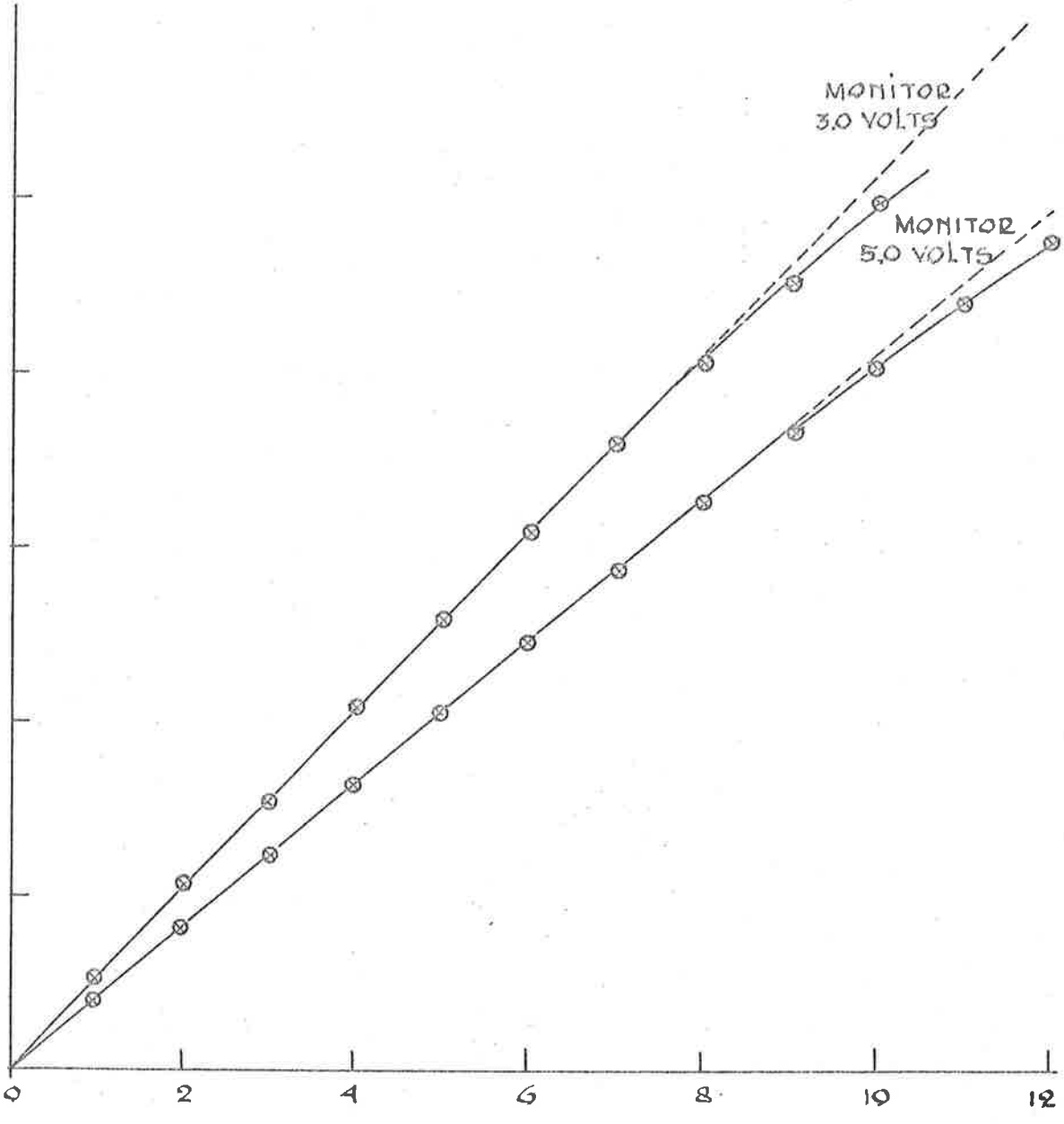

FIG. 5.14.

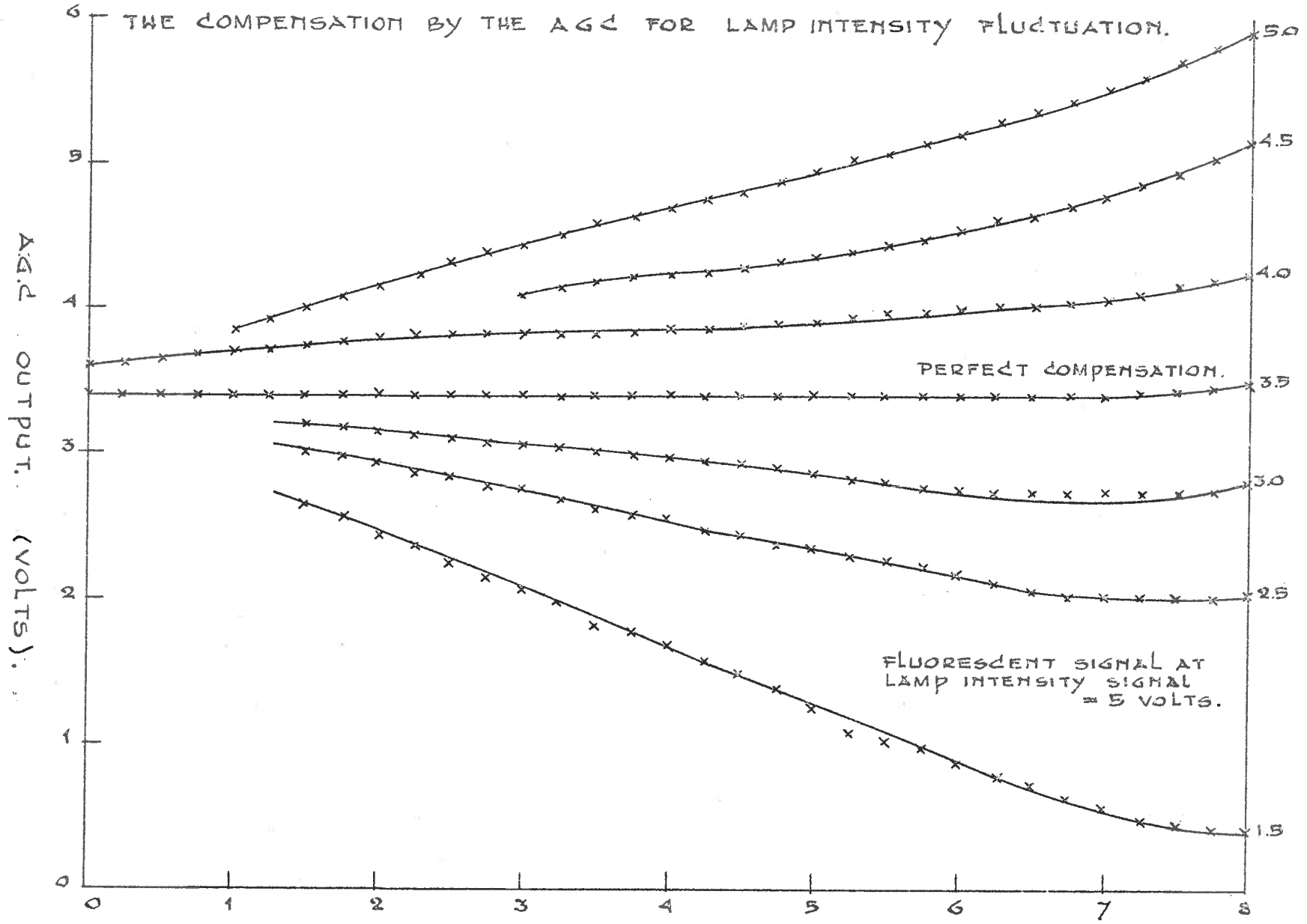
THE COMPENSATION BY THE AGC FOR LAMP INTENSITY FLUCTUATION.
A.G.C. OUTPUT. (VOLTS).
LAMP INTENSITY SIGNAL (VOLTS)
PERFECT COMPENSATION.
FLUORESCENT SIGNAL AT LAMP INTENSITY SIGNAL = 5 VOLTS.
5.0
4.5
4.0
3.5
3.0
2.5
1.5
0
1
2
3
4
5
6
7
8
9

FIG. 5.15

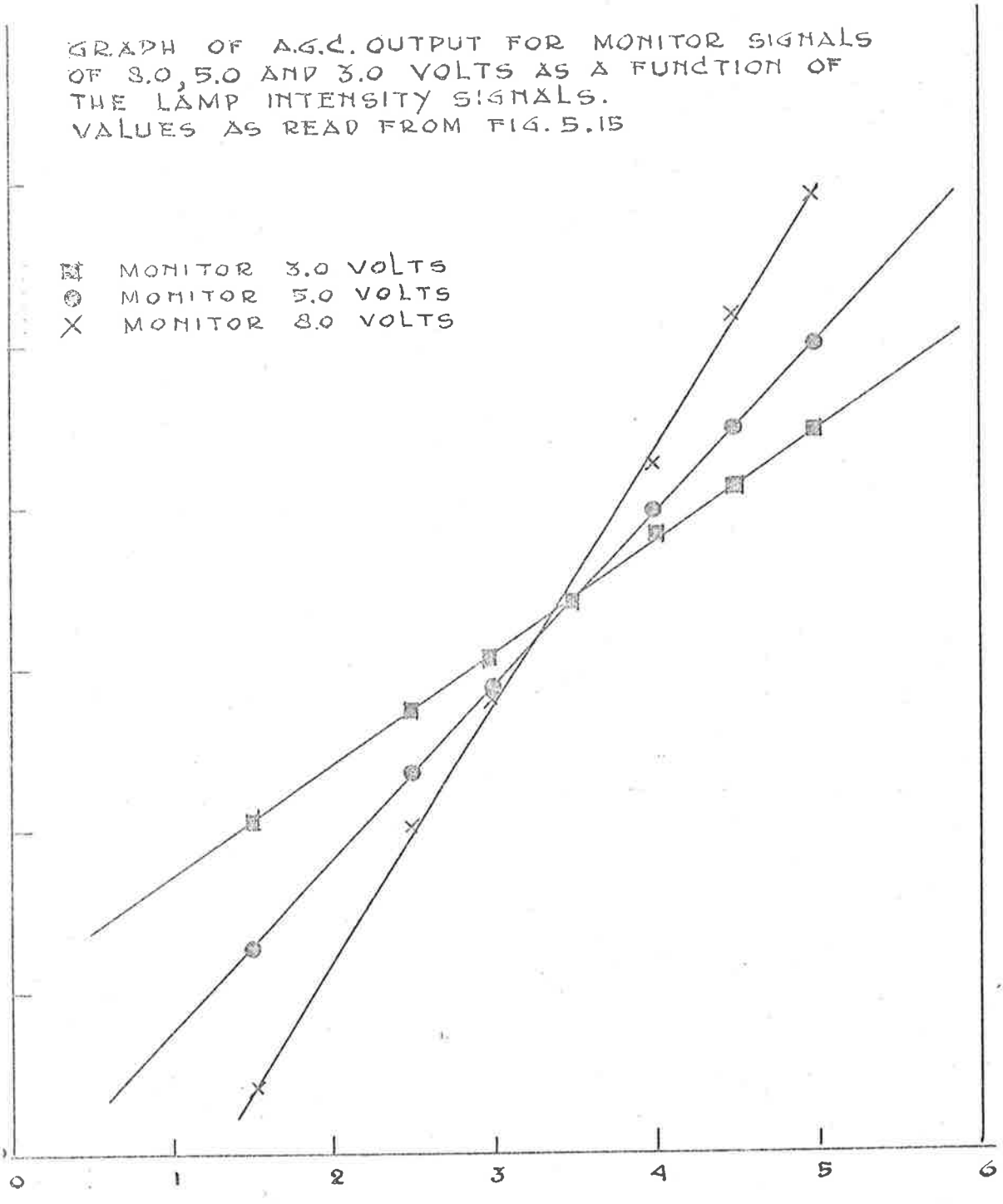
GRAPH OF A.G.C. OUTPUT FOR MONITOR SIGNALS OF 3.0, 5.0 AND 3.0 VOLTS AS A FUNCTION OF THE LAMP INTENSITY SIGNALS.
VALUES AS READ FROM FIG. 5.15
MONITOR 3.0 VOLTS
MONITOR 5.0 VOLTS
MONITOR 8.0 VOLTS
0
1
2
3
4
5
6
LAMP INTENSITY SIGNAL (VOLTS)

FIG. 5.16.

fluorescent over monitor ratio is less than this figure the AGC under-corrects, while for a fluorescent-monitor ratio greater than 7/10 the AGC over-corrects. If the fluorescent signal is greater than the monitor signal, the AGC becomes ineffective. Experimentally the AGC can be used most effectively if the monitor signal is 9/10 of the fluorescent signal at the fluorescence maximum. Fig. 5.16 shows the output at a constant monitor value (as read from Fig. 5.15) versus fluorescent signal. The output in all cases was a linear function of the fluorescent signal, although the baseline needs a correction which depends on the monitor signal.

5.3.4.3 Stability.

Testing over a one hour period, the AGC output was steady to better than .5% and the noise level was found to be negligible.

5.3.5 System used for measurements.

The intensity output of the xenon arc lamp shows little or no fluctuation if a wide spectral band is used. Since caffeine fluoresces only weakly in aqueous solution, wide excitational bands were used. In this case it was found to be convenient not to use a reference monitor beam and to record directly the output of the photomultiplier as a function of wavelength.

5.4 FLUORESCENCE SPECTRUM OF QUININE

Quinine and quinine derivatives have been used extensively as a fluorescence standard (e.g. Chen, 1967; Parker and Rees, 1959; Melhuish, 1961). Their spectral properties are known and the absolute quantum efficiency of quinine bisulphate has been measured. Melhuish (1961) measured the quantum yield of quinine sulphate in 1N H_2SO_4 as .546 for excitation at 3650 Å.

For this reason quinine sulphate was used as a fluorescence standard in this work. A solution of quinine sulphate (5×10^{-3} mole/litre in 1.0N H_2SO_4) was prepared. The solution was filtered and ultracentrifuged. The fluorescence spectrum of this solution was recorded with the reduced fluorimeter (see Section 5.3.5). The experimental details pertaining to this spectrum are shown in Table 5.5.

The spectrum showed no noticeable background noise. The baseline was found to be stable and constant. When a blank of 1.0N sulphuric acid was substituted, a constant background signal was obtained over the range used.

The recorded spectrum was corrected for the properties of the detector system. The corrected spectrum was scaled such that the area under the curve over the range studied remained the same.

The recorded and corrected spectra are shown in Fig. 5.17. These functions are listed together with the correction function in Table 5.6. The corrected spectrum of quinine sulphate was found to have an emission maximum at 4520 Å. This value is in reasonable agreement with fluorescence

THE FLUORESCENCE SPECTRUM OF QUININE SULPHATE IN 1N H_2SO_4

A = UNCORRECTED
B = CORRECTED

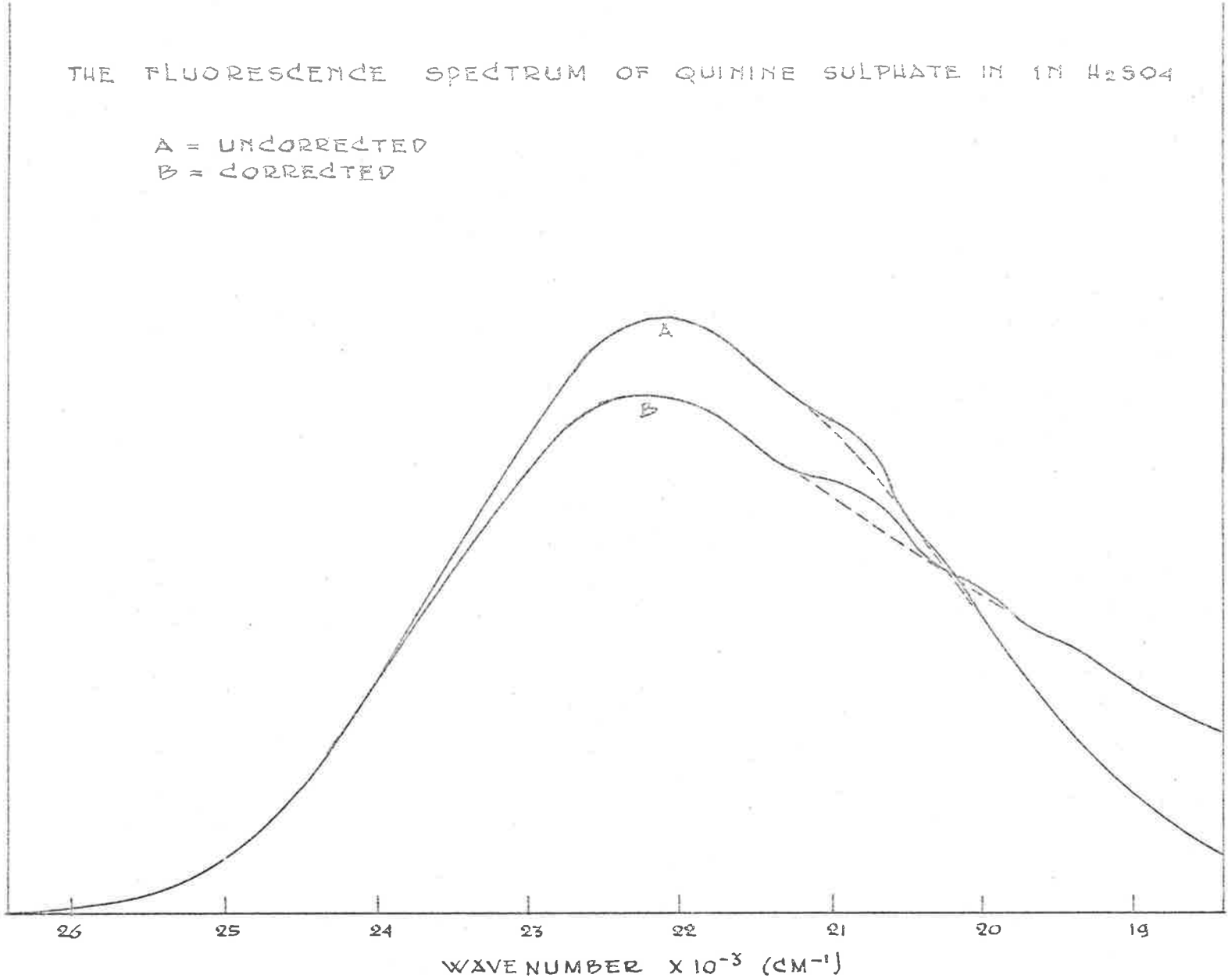

FIG. 5. 17

TABLE 5.5

DATA FOR THE QUININE SPECTRUM

Compound	Quinine sulphate
Concentration	5×10^{-3} mole/litre
Solvent	1.0N H_2SO_4
Source	Xe arc (Osram XBO/4, 450 watt)
Monochromator	Prism (Schoeffel QPM-30)
Exeitational wavelength	3650 Å (micrometer setting 4.25)
Slit width	2 mm
Filters	None
Cell	Quarts silica
Observation	Perpendicular
Emission monochromator	Grating (diffraction products)
Slits	1 mm, .5 mm
Detector	EMI 6255 SbCs photomultiplier
Photomultiplier voltage	610 volts
Output at maximum	.3 volts
Temperature	24°C
Scan speed	50 Å/min.

TABLE 5.6

THE FLUORESCENCE SPECTRUM OF QUININE SULPHATE

5×10^{-3} m/litre in 1N H_2SO_4

WAVELENGTH	WAVENUMBER	FLUORESCENCE INTENSITY	CORRECTION	CORRECTED INTENSITY
3784	26430	3	.735	4
3818	26200	5	.765	6
3852	25960	7	.802	9
3886	25730	13	.840	15
3920	25510	19	.872	22
3954	25290	35	.900	39
3988	25080	57	.924	62
4022	24870	88	.947	93
4056	24650	126	.973	129
4090	24450	170	.989	172
4124	24250	222	1.01	220
4158	24050	283	1.02	277
4192	23860	350	1.04	336
4226	23670	419	1.05	399
4260	23470	487	1.06	459
4294	23290	555	1.08	514
4328	23110	609	1.09	559
4362	22930	665	1.10	605
4396	22750	708	1.11	638
4430	22570	744	1.12	664
4464	22400	768	1.14	673
4498	22230	783	1.15	680
4532	22070	784	1.15	682

(contd.)

TABLE 5.6 (contd.)

WAVELENGTH	WAVENUMBER	FLUORESCENCE INTENSITY	CORRECTION	CORRECTED INTENSITY
4564	21910	779	1.16	671
4600	21740	762	1.17	651
4634	21580	738	1.17	630
4668	21420	713	1.16	614
4702	21270	688	1.16	593
4736	21110	664	1.15	577
4770	20960	648	1.13	573
4804	20810	622	1.11	560
4838	20670	586	1.09	538
4872	20520	531	1.06	501
4906	20390	498	1.04	479
4940	20240	468	1.00	468
4974	20100	436	.970	449
5008	19970	395	.933	423
5042	19830	351	.875	401
5076	19700	301	.812	370
5110	19570	276	.739	373
5144	19440	246	.686	359
5178	19310	218	.642	340
5212	19180	192	.602	319
5246	19060	169	.555	305
5280	18940	151	.511	295
5314	18820	133	.476	280
5348	18710	115	.436	264
5382	18580	100	.392	251
5416	18460	87	.355	245
5450	18350	76	.320	231
5484	18230	64	.285	224

maxima found by other authors (e.g. Fletcher, 1968).

Correlation of measured quinine spectra with the work of other authors is unfortunately difficult due to the dependence of the emission spectrum on the wavelength of excitation.

The shoulders on the low energy side of the quinine spectrum should not have been there. They are likely to have been caused by the non-homogeneous transmission of the grating monochromator. This phenomena has been observed by many authors (e.g. King and Hercules, 1963) and is commonly known as the Wood anomaly. A correction for this should, however, have been included in the correction function. The uncertainty in the 20,000-26,000 cm^{-1} region makes it difficult to determine the exact correction in this region.

5.5 FLUORESCENCE SPECTRUM OF CAFFEINE

The fluorescence spectrum of caffeine was studied in aqueous solution and in cyclohexane. A solution of caffeine (5×10^{-3} m/litre) was prepared. This solution was filtered and ultracentrifuged. The fluorescence spectrum of this solution was recorded with the reduced fluorimeter. The experimental details for the measurement of this spectrum are shown in Table 5.7.

The spectrum showed a background noise of approximately 4%. When a blank solution of distilled water was substituted a constant background signal was obtained over the range studied. The quantum yield of caffeine was estimated to be of the order of .005. Because of the low fluorescence

TABLE 5.7

DATA FOR THE CAFFEINE SPECTRUM

Compound	Caffeine
Concentration	5×10^{-3} m/litre
Solvent	Distilled water
Source	Xe arc (Osram XBO/4, 450 watt)
Excitational wavelength	2700 Å (micrometer setting 7.50)
Slit width	2 mm
Filters	None
Cell	Quarts silica
Observation	Perpendicular
Emission monochromator	Grating (diffraction products)
Slits	3 mm
Detector	EMI 6255 SbCs photomultiplier
Photomultiplier voltage	720 volts
Output maximum	.3 volts
Temperature	24°C
Scan speed	50 Å/min.

yield of caffeine, high amplification and wide slits had to be used, with corresponding amplification of the scattered light. The scattering of the excitation beam was found to be considerable in the 2700-3000 Å region where it partly overlaps with the emission spectrum. Due to this, the emission spectrum had to be extrapolated to cover the range 2860-3000 Å.

The recorded fluorescence spectrum of caffeine was corrected for the properties of the detector system. The corrected spectrum was scaled such that the area under the curve over the studied range remained the same.

The recorded and corrected fluorescence spectra of caffeine are shown in Fig. 5.18. These functions are listed together with the correction function in Table 5.8. The fluorescence spectrum is shown together with the absorption spectrum in Fig. 5.19. The fluorescence spectrum closely resembles the mirror image of the absorption spectrum as would be expected if the state from which the fluorescence takes place is the same as the state to which the molecule is excited in the absorption process. The displacement of the fluorescence spectrum to lower wavelength with respect to the absorption spectrum can be readily explained in terms of reorganisation of the solvent particles.

Caffeine was found not to fluoresce in cyclohexane. This can be explained in terms of the shift of the $\pi^*\leftarrow n$ transition. Because π^*, n states have a relatively long lifetime, deactivation processes other than fluorescence prevail. As a result $\pi^*\leftarrow n$ transitions are noted for

THE FLUORESCENCE SPECTRUM OF CAFFEINE IN AQUEOUS SOLUTION.

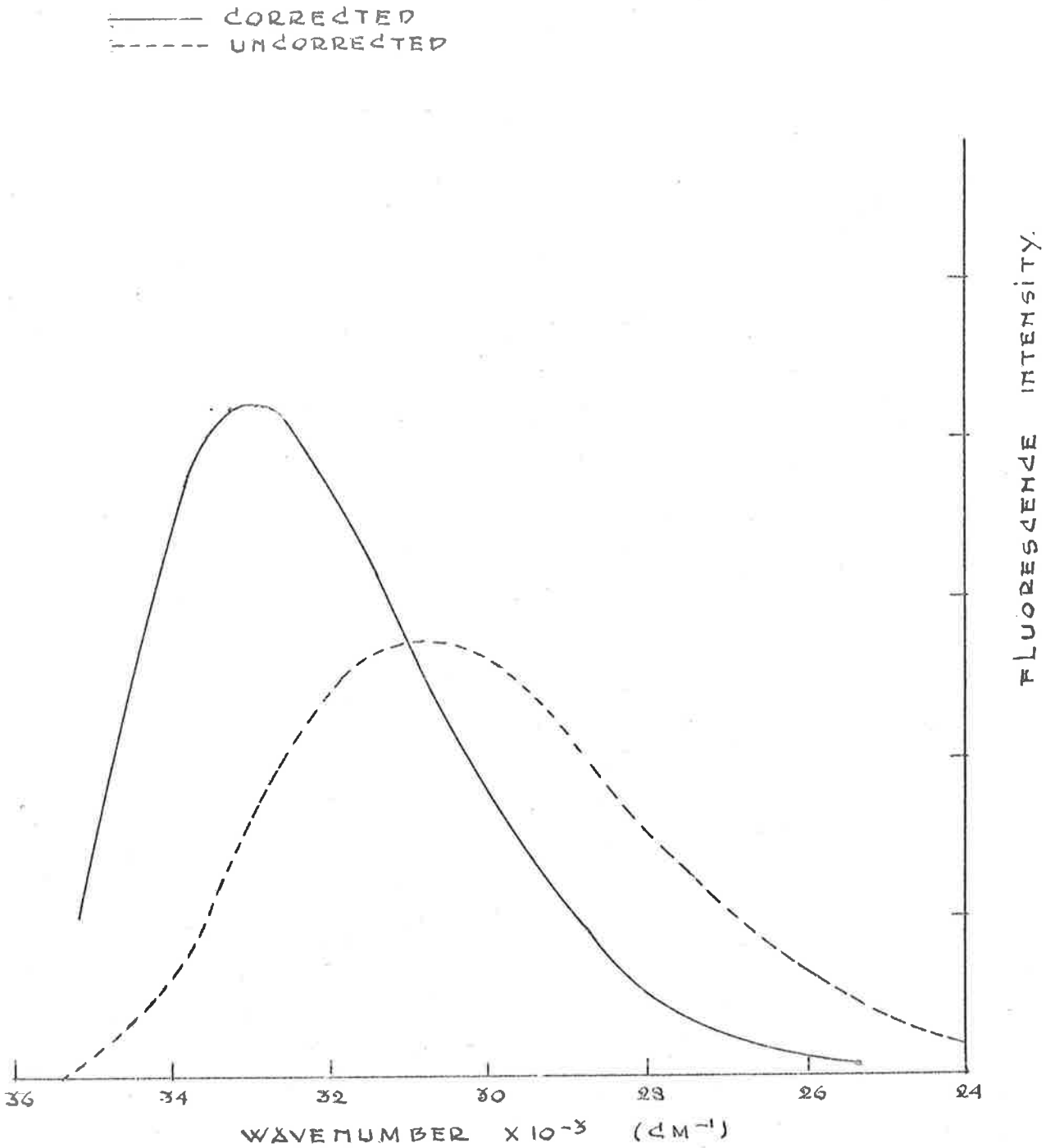

FIG. 5.18

THE ABSORPTION AND THE FLUORESCENCE SPECTRUM OF CAFFEINE IN AQUEOUS SOLUTION.

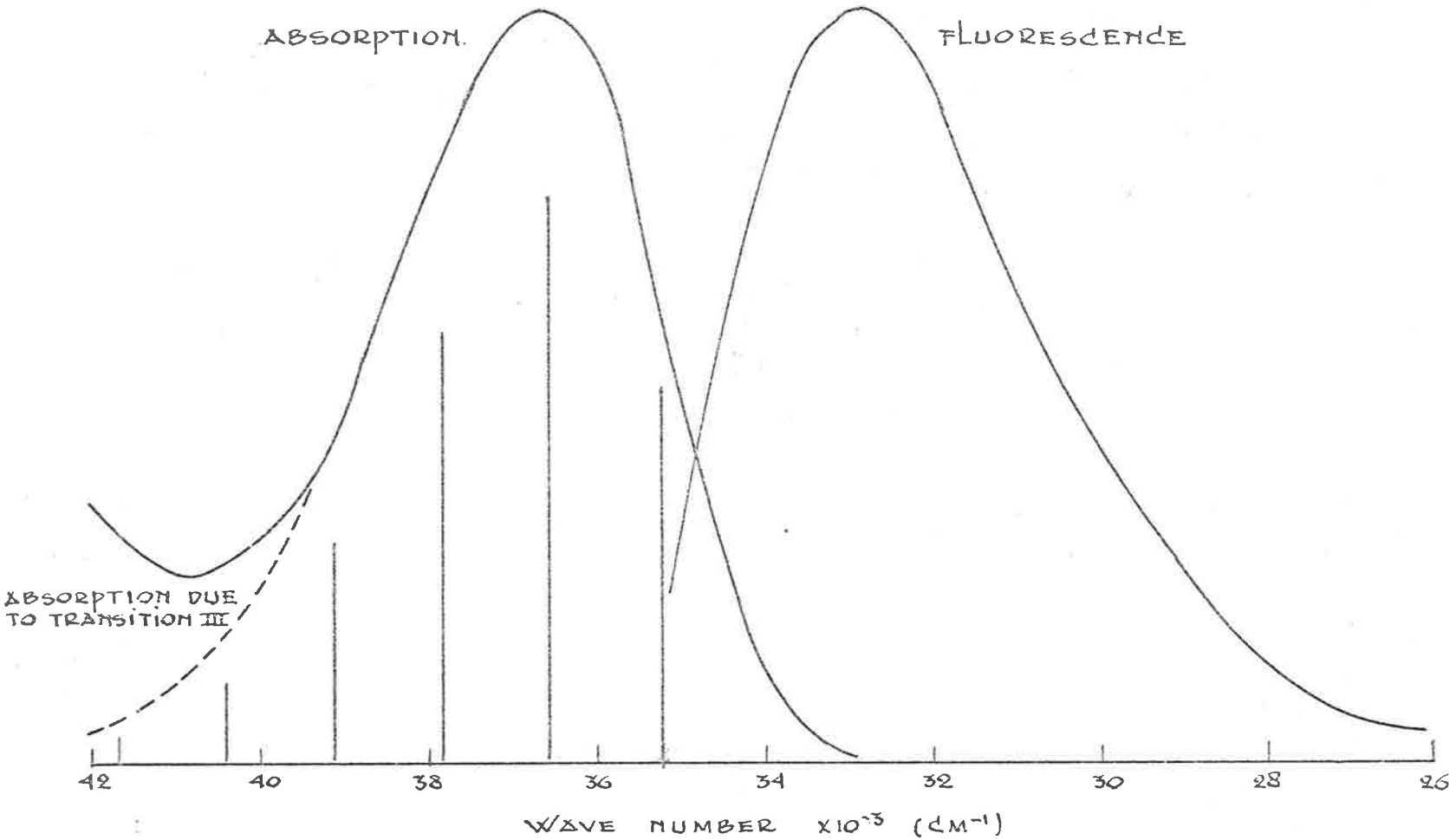

FIG. 5.19

their non-fluorescence (Kasha, 1960; Borrensen, 1963).

In non-polar media the lowest excited state of caffeine is a π^*,n state. The $\pi^*\leftarrow n$ transition has been observed for caffeine in cyclohexane and for caffeine in polyethylene films. In a polar medium the $\pi^*\leftarrow n$ transition decreases in intensity and shifts to higher energy. In aqueous solution and in PVA films the $\pi^*\leftarrow n$ transition is not noticeable, but the fluorescence of caffeine in aqueous solution would indicate that the $\pi^*\leftarrow n$ transition has moved to an energy higher than the $\pi^*\leftarrow\pi$ transition so that the band due to this transition is under the band due to the $\pi^*\leftarrow\pi$ transition (band II). This combined with the low intensity of the $\pi^*\leftarrow n$ transition would make it difficult to detect its presence.

Polarised fluorescence studies could be used to complement this work. If the transition moment directions for the fluorescence are the same as the directions for the absorption process, then it could be concluded that the fluorescence takes place from the π^*,π state. This work should be done as soon as possible to remove any uncertainty in this assignment.

TABLE 5.8

THE FLUORESCENCE SPECTRUM OF CAFFEINE IN AQUEOUS SOLUTION

WAVELENGTH	WAVENUMBER	FLUORESCENCE INTENSITY	CORRECTION	CORRECTED INTENSITY
2840	35211	10	.050	200
2860	34970	20	.073	273
2880	34720	40	.110	365
2900	34480	60	.130	461
2920	34250	100	.161	621
2940	34010	130	.187	695
2960	33780	160	.211	758
2980	33560	230	.260	807
3001	33320	255	.308	827
3021	33010	308	.365	843
3041	32880	342	.406	843
3061	32670	381	.455	838
3082	32450	413	.511	808
3102	32240	446	.576	774
3122	32030	478	.633	755
3142	31830	498	.698	713
3163	31630	517	.763	678
3183	31420	532	.828	642
3203	31210	541	.909	595
3223	31020	551	.974	566
3244	30820	552	1.06	523
3264	30630	551	1.14	485
3284	30450	547	1.22	449
3304	30260	540	1.31	411
3325	30080	530	1.41	375

(contd.)

TABLE 5.8 (contd.)

WAVELENGTH	WAVENUMBER	FLUORESCENCE INTENSITY	CORRECTION	CORRECTED INTENSITY
3345	29900	518	1.51	343
3365	29720	503	1.61	313
3385	29550	487	1.72	283
3406	29360	469	1.85	253
3426	29190	449	1.95	230
3446	29020	429	2.06	208
3466	28850	408	2.16	189
3487	28680	386	2.27	170
3505	28510	365	2.45	149
3528	28350	349	2.58	135
3548	28190	331	2.74	121
3568	28030	312	2.91	107
3589	27870	294	3.08	95
3609	27710	278	3.26	85
3629	27550	264	3.46	76
3649	27400	248	3.69	67
3670	27250	231	3.90	59
3690	27100	218	4.12	53
3710	26950	205	4.33	47
3730	26810	196	4.58	43
3751	26660	186	4.77	39
3771	26520	176	4.95	36
3791	26380	165	5.11	32
3812	26240	154	5.28	29
3832	26100	144	5.47	26
3852	25960	132	5.57	24

(contd.)

TABLE 5.8 (contd.)

WAVELENGTH	WAVENUMBER	FLUORESCENCE INTENSITY	CORRECTION	CORRECTED INTENSITY
3872	25830	122	5.75	21
3893	25690	112	5.91	19
3913	25560	104	6.04	17
3933	25430	98	6.15	16
3953	25300	91	6.27	15
3974	25160	86	6.36	13
3994	25030	78	6.49	12
4010	24920	71	6.57	11
4034	24790	63	6.66	9
4055	24660	57	6.75	8
4075	24540	52	6.83	8
4095	24420	47	6.90	7
4115	24300	43	6.95	6
4136	24180	39	7.01	6
4156	24070	36	7.09	5
4176	23950	33	7.16	5
4196	23840	29	7.22	4
4217	23720	26	7.29	4
4237	23600	22	7.35	3
4257	23490	20	7.40	3
4277	23380	17	7.45	2
4298	23270	14	7.48	2
4318	23160	11	7.57	1

6. CONCLUSIONS

The absorption spectrum of caffeine in aqueous solution was studied. The 36,600 cm^{-1} absorption band of caffeine was found to decrease in intensity as the concentration of caffeine was increased. This decrease in intensity was interpreted as being due to aggregation of caffeine molecules to form dimers and higher aggregates. A monomer-dimer-tetramer type of aggregation was considered to be most likely. The decrease in intensity of the 36,600 cm^{-1} band of caffeine aggregation is similar to the decrease in intensity that is observed in the 38,000 cm^{-1} band of DNA when DNA is denatured.

The absorption spectrum of the caffeine dimer was determined. Apart from the overall decrease in intensity, little change in the spectrum of the dimer compared with that of the monomer was observed. The 36,600 cm^{-1} band of the caffeine dimer spectrum, which had shifted 50 cm^{-1} to higher energy, was found to be slightly broader than the corresponding band in the monomer spectrum. These changes were interpreted as being due to exciton interaction.

An interaction energy of 100 cm^{-1}, which would correspond to an exciton transfer time of 10^{-11} sec., was estimated. This would put the exciton coupling in the caffeine dimer in the intermediate range. If the exciton interaction between the bases in DNA is of a similar magnitude, these interactions would allow the rapid transfer of energy through hundreds of bases before deactivation.

Polarised films of caffeine in PVA and polyethylene were studied. The angle between the transition moment and the axis of alignment of caffeine for the three lowest $\pi^*\leftarrow\pi$ transitions were determined as 50°, 44° and 42° respectively. It is likely that the transition moment for the first $\pi^*\leftarrow\pi$ transition is in the direction of the C_2—C_4 axis, while the transition moments for the other two $\pi^*\leftarrow\pi$ transitions are approximately perpendicular to this direction.

A carbonyl π^*,n band has been observed on the long wavelength side of the 36,600 cm^{-1} band of caffeine in non-polar media. Since π^*,n states have a long lifetime, caffeine was found to be non-fluorescent in non-polar solution. The π^*,n band was found to decrease in intensity and to move to higher energy in polar media. In aqueous solution the π^*,π state has become the lowest excited state, thus enabling caffeine to fluoresce.

APPENDIX 1

PURIFICATION

CAFFEINE

Caffeine (25 gm, B.P. specifications) was obtained from D.H.A. (Australia) and purified by multiple recrystallisation from hot water. Solutions of .250 gm/litre were made up of the original caffeine and the purified caffeine after both had been dried to constant weight in an oven at 110°C for a period of over 48 hours. The optical densities of both solutions were measured on a Shimadzu spectrophotometer at 36,600 cm^{-1} (2730 Å) and were found to be equal (.599) in a .3 mm quartz silica cell for both the original and recrystallised caffeine. Weighings were always made after the caffeine had been dried to constant weight in an oven at 110°C and cooled down for half an hour in a desiccator.

QUININE SULPHATE

Quinine sulphate (20 gm) was dissolved in hot water and active charcoal was added. The hot solution was filtered to remove the charcoal and any insoluble impurities and the quinine sulphate was precipitated, filtered off, and dried. The process was repeated, after which the quinine sulphate was dried to constant weight in the oven at 110°C.

RHODAMINE B

Rhodamine B (5 gm) for use as a photon flux converter was obtained from Hopkins and Williams (England) and used after multiple recrystallisation from hot water.

WATER

The water used for the recrystallisations and the preparation of the solutions was obtained through distilling deionised water through a 35 cm fractionating column. The conductivity of the distilled water was determined as $3.5 \times 10^{-6} \Omega$ /cm.

OPTICAL CELLS

Optical cells were cleaned by soaking in chromic acid for four hours, after which the cells were drained and washed in distilled water. They were then rinsed with doubly distilled alcohol.

APPENDIX 2

```
      PROGRAM GAUSFIT (INPUT,OUTPUT)
      DIMENSION XL(50),XO(7),OD(50),DMM(7),FTD(50),FOD(50,7)
      DIMENSION DIFA(50),FODA(50,7),DIF(50),FTDA(50)
C     THIS PROGRAM FITS A SELECTED SECTION OF THE ELECTRONIC
C     SPECTRUM WITH A SET OF GAUSSIAN CURVES RESEMBLING THE
C     VIBRONIC BANDS CORRESPONDING TO AN ELECTRONIC TRANSITION.
C     ONLY ONE VIBRATION IS ASSUMED.
C     SPACING BETWEEN POINTS
C     POSITION OF FIRST VIBRONIC BAND
      XO(1)=34900
C     VIBRATIONAL SPACING
      DS=1300
C     NUMBER OF POINTS FITTED
      NP=41
C     READ IN OPTICAL DENSITIES
      READ 1,(OD(I),I=1,NP)
    1 FORMAT(3X,11(F3.0,4X))
C     WAVENUMBERS CORRESPONDING TO OPTICAL DENSITY VALUES
      DO11I=1,NP
      XL(I)=33000+(I-1)*200.
   11 OD(I)=OD(I)/XL(I)
      DO10I=2,7
   10 XO(I)=XO(1)+DS*(I-1)
C     INTENSITY OF FIRST VIBRONIC BAND
      DO2N1=780,800,5
      DMM(1)=N1/1E5
C     M**2(DM)
      DO2NM=160,164
      SUM2=200
      DM=NM/100.
C     CALCULATE INTENSITIES OF FURTHER VIBRONIC BANDS
      DMM(2)=DMM(1)*DM
      DMM(3)=DMM(2)*DM/2.
      DMM(4)=DMM(3)*DM/3.
      DMM(5)=DMM(4)*DM/4.
      DMM(6)=DMM(5)*DM/5.
      DMM(7)=DMM(6)*DM/6.
C     BANDWIDTH
      DO3NBW=860,900,5
      SUM1=0.
      DO4I=1,NP
      FTD(I)=0.
      DO5J=1,7
```

APPENDIX 2 (contd.)

```
C       CONTRIBUTION OF BAND TO SPECTRUM
        FOD(I,J)=DMM(J)*EXP(-((XL(I)-XO(J))/NBW)**2)
      5 FTD(I)=FTD(I)+FOD(I,J)
        DIF(I)=FTD(I)-OD(I)
C       EXCLUDE POINTS FROM FIT CRITERION
        IF(I.GE.35)4,15
     15 SUM1=SUM1+DIF(I)*DIF(I)
      4 CONTINUE
C       SELECT BEST FIT
        IF(SUM1.LE.SUM2)9,6
      9 SUM2=SUM1
        NXW=NBW
        DO3I=1,NP
        FTDA(I)=FTD(I)
        DIFA(I)=DIF(I)
        DO3J=1,7
      3 FODA(I,J)=FOD(I,J)
      6 PRINT 7,NXW,DM,SUM1,DMM(1)
      7 FORMAT(* BANDWIDTH*,I5,/,* TRANS. MOM. *F8.5,/,* SUM SQ.*
     X,E13.6,/,* FIRST BAND*,E13.6)
      2 PRINT 8,((FODA(I,J),J=1,7), FTDA(I),OD(I),DIFA(I),I=1,NP)
      8 FORMAT(10F13.11)
        STOP
        END
```

APPENDIX 3

COMPUTER PROGRAM FOR CALCULATION OF EXTINCTION COEFFICIENTS FOR COMPLEX SYSTEM

```
      PROGRAM KEQFIT3(INPUT,OUTPUT)
C
C     THIS PROGRAM CALCULATES EXTINCTION COEFFICIENTS FOR
C     SELECTED AGGREGATION MODELS AND EQUILIBRIUM CONSTANTS
C     BY THE METHOD DESCRIBED IN SECTION 3.2 OF PH.D.
C     THESIS, J.N. KIKKERT (1971) FOR A GIVEN SET OF
C     SOLUTIONS FOR WHICH BOTH CONCENTRATION AND APPARENT
C     EXTINCTION COEFFICIENTS ARE KNOWN.
C
      DIMENSION ET(120,14),EF(120,14),ED(120,14),PC(120,14),C(120)
      DIMENSION CK(120),CK1(120),A(5),PCT(120),X(51),B(36)
      DIMENSION E(4,14),V(4),SUM1(14),SUM2(14),CM(120),ER(4,14)
      REAL MWT
C     SELECT MODEL; TO INCLUDE N-MER SPECY PUT A(N+1)=N
C     EQ. 1,2,3 EQUIL. A(2)=1, A(3)=2, A(4)=3, A(5)=0
C         1,2,4 EQUIL. A(2)=1, A(3)=2, A(4)=0, A(5)=4
C         1,2   EQUIL. A(2)=1, A(3)=2, A(4)=0, A(5)=0
      A(4)=0.
      A(5)=4.
      A(3)=2.
      A(2)=1.
      N=0
C     NUMBER OF SPECIES
      M=3
C     READ IN CONCENTRATIONS AND APPARENT EXTINCTIONS(GM)
      DO1I=1,120
      READ 2,C(I),(ET(I,J),J=1,14)
    2 FORMAT(F7.5,14F5.2)
C     CONVERT TO MOLECULAR VALUES
      CM(I)=C(I)/MWT
      DO11J=1,14
   11 ET(I,J)=ET(I,J)*MWT
      IF(C(I).EQ.0.)3,1
C     COUNTS NUMBER OF SOLUTIONS
    1 N=N+1
C     SET EQUILIBRIUM CONSTANTS
    3 DO6K=13,14
      EQ=K
```

APPENDIX 3 (contd.)

```
C       START TO CALCULATE DISTRIBUTION OF SPECIES FOR THE GIVEN K AND
C       CONCENTRATION
        PM=1.
        DO4I=1,N
        A(1)=CK(I)=CM(I)*EQ
        A(1)=-A(1)
C       ESTIMATE MONOMER CONCENTRATION BY ASSUMING PERCENTAGE
C       MONOMER SAME AS IN PREVIOUS SOLUTION
        CK1(I)=CK(I)*PM
C       FIND MONOMER CONCENTRATION (EQN. 3.2.9)
        CALL NEWRAP(A,5,CK1(I))
C       CALCULATE PERCENTAGES OF SPECIES
        PC(I,1)=PM=CK1(I)/CK(I)
        PC(I,2)=PC(I,1)*A(3)*CK1(I)
        PC(I,3)=PC(I,1)*A(4)*CK1(I)*CK1(I)
        PC(I,4)=PC(I,1)*A(5)*CK1(I)*CK1(I)*CK1(I)
C       PLACE PERCENTAGES IN FIRST M COLUMNS
        PC(I,3)=PC(I,4)
        PC(I,4)=0.
    4   PCT(I)=PC(I,1)+PC(I,2)+PC(I,3)+PC(I,4)
C       SOLVE MATRIX EQUATION PC1(I).E1+PC2(I).E2+...=ET(I)
        CALL LEASTSQ(PC,E,ET,N,M,14,KEY)
C       CALCULATE VARIANCE OF COEFFICIENTS
        CALL VARIAN(PC,N,V)
        DO12J=1,14
        SUM1(J)=0.
        SUM2(J)=0.
        DO12I=1,N
        EF(I,J)=0.
        DO13L=1,M
   13   EF(I,J)=EF(I,J)+PC(I,L)*E(L,J)
        ED(I,J)=ET(I,J)-EF(I,J)
        SUM1(J)=SUM1(J)+ED(I,J)*ED(I,J)
   12   SUM2(J)=SUM2(J)+ABSF(ED(I,J))
        DO20J=1,14
        DO20L=1,M
   20   ER(L,J)=SQRT(SUM1(J)*V(L)/(N-M))
        PRINT 60
   60   FORMAT(1H1,*EXTINCTIONS, PROBABLE ERRORS, SUM OF SQUARES,
     A  SUM OF ABSOLUTE DIFFERENCES*)
        PRINT 15,((E(I,J),J=1,14),(ER(I,J),J=1,14),I=1,M)
        PRINT 15,(SUM1(J),J=1,14)
        PRINT 15,(SUM2(J),J=1,14)
```

APPENDIX 3 (contd.)

```
   15 FORMAT(14(2X,F6.0))
      PRINT 61
   61 FORMAT(1H1,*PERCENTAGES, FITTING ERRORS*)
      PRINT 16,(I,(PC(I,J),J=1,4),PCT(I),(ED(I,J),J=1,14),I=1,N)
   16 FORMAT(I3,5(1X,F6.3),14(1X,F4.0))
      PRINT 62
   62 FORMAT(1H1,*MEASURED EXTINCTIONS*)
      PRINT 17,(I,(ET(I,J),J=1,14),I=1,N)
      PRINT 63
   63 FORMAT(1H1,*FITTED EXTINCTIONS*)
    6 PRINT 17,(I,(EF(I,J),J=1,14),I=1,N)
   17 FORMAT(I4,14(2X,F6.0))
      END

      SUBROUTINE NEWRAP(A,N,X)
C
C     THIS SUBROUTINE FINDS THE SOLUTION TO POLYNOMIAL EQUATIONS
C     BY THE NEWTON-RAPHSON ITERATION METHOD.  AN IMPROVED
C     VALUE OF THE SOLUTION IS FOUND FROM
C              X = X-F(X)/FD(X)
C     THE ORIGINAL VALUE OF X IS OBTAINED FROM THE MAIN PROGRAM.
C
      DIMENSION A(5)
C     ACCURACY LIMIT
      XLIM = X*1E-10
C     WILL FIND SOLUTION WITHIN TEN ITERATIONS
      DO1I=1,10
      XL=X
      X1=1.
C     CALCULATE FUNCTION AND ITS DERIVATIVE
      FD=0.
      DO2J=2,N
      FD=FD+A(J)*(J-1)*X1
      X1=X1*X
    2 F=F+A(J)*X1
C     IMPROVED VALUE OF SOLUTION
      X=X-F/FD
C     CHECK ACCURACY
      IF(ABS(X-XL).LE.XLIM)3,1
    1 CONTINUE
C     NO SOLUTION FOUND
      PRINT 4
    4 FORMAT(*HELP*)
    3 RETURN
      END
```

APPENDIX 4

MATHEMATICAL TREATMENT OF DIMERIC SYSTEM

Consider dimeric system in which the concentration of the monomer is denoted by C_1, that of the dimer C_2, and the total concentration is C. The equilibrium constant is represented by K.

$$C = C_1 + 2C_2 \qquad (1)$$

$$K = \frac{C_2}{C_1^2} \qquad C_2 = KC_1^2 \qquad (2)$$

$$\varepsilon_T C = \varepsilon_1 C_1 + \varepsilon_2 C_2 \qquad (3)$$

where ε_T is the apparent extinction of the solution and ε_1 and ε_2 are the extinction coefficients of the monomer and dimer respectively.

Substituting (1) into (3):

$$\varepsilon_T C = \varepsilon_1 C_1 + \varepsilon_2 (C - C_1)$$

$$= (\varepsilon_1 - \varepsilon_2) C_1 + \varepsilon_2 C \qquad (4)$$

Combining (1) and (2) gives:

$$C = C_1 + 2KC_1^2$$

$$2K^2 C_1^2 + KC_1 - KC = 0 \qquad (5)$$

This is equation 3.9 for the dimeric system.

$$C_1 = \frac{-K + \sqrt{K^2 + 8KC}}{4} \qquad (6)$$

Substituting (6) into (4):

$$\varepsilon_T C = \frac{(\varepsilon_1 - \varepsilon_2)}{4}(-K + \sqrt{K^2 + 8KC}) + \varepsilon_2 C$$

$$\varepsilon_T = \varepsilon_1 - \varepsilon_2 \left(-\frac{K}{4C} + \sqrt{(\frac{K}{4C})^2 + 2(\frac{K}{4C})}\right) + \varepsilon_2 \qquad (7)$$

A plot of $(-\frac{K}{4C} + \sqrt{(\frac{K}{4C})^2 + 2(\frac{K}{4C})}$ versus ε will give a line with a slope of $\varepsilon_1 - \varepsilon_2$ and an intercept of ε_2. To consider what happens at low concentrations put:

$$-\frac{K}{4C} + \sqrt{(\frac{K}{4C})^2 + \frac{2K}{4C}} =$$

$$-\frac{K}{4C} + \sqrt{(\frac{K}{4C})^2 + 2(\frac{K}{4C}) + 1 - 1} =$$

$$-\frac{K}{4C} + \sqrt{(\frac{K}{4C} + 1)^2 - 1}$$

But if $C \rightarrow 0$, $(\frac{K}{4C} + 1)^2 >> 1$

$$\sqrt{(\frac{K}{4C} + 1)^2 - 1} \rightarrow (\frac{K}{4C} + 1)$$

$$\therefore \lim_{C \to 0} (-\frac{K}{4C} + \sqrt{(\frac{K}{4C})^2 + \frac{2K}{4C}} = 1$$

The plot will thus give a graph with an X=0 intercept of ε_2 and an X=1 intercept of ε_1. The baseline denotes the fraction of monomer in the mixture. A least squares fit can be done on the experimental data to obtain the values for ε_1 and ε_2 while the sum of the squares of the deviations can be used as a criterion for selecting a K value. A simple program for these calculations is shown below.

```
      PROGRAM KEQFIT(INPUT,OUTPUT)
      DIMENSION EX(120),ET(120),C(120),CM(120),DC(120),DCS(120)
      DIMENSION X(120)
      REAL MWT
      N=0
      MWT=194.19
      DO1I=1,120
C     READ CONCENTRATION AND EXTINCTION (GM/L)
      READ 2,C(I),EX(I)
    2 FORMAT(F8.6,F4.2)
      EX(I)=EX(I)*MWT
      CM(I)=C(I)/MWT
      IF(C(I).EQ.0.)3,1
    1 N=N+1
    3 DO4K=20,30
C     EQUILIBRIUM CONSTANT
      EQK=K/5
      DO5I=1,N
      X(I)=1./(CM(I)*4.*EQK)
C     FRACTION MONOMER
    5 X(I)=-X(I)+SQRT(X(I)*(X(I)+2.))
C     FIT
      CALL LEASTSQ(X,EX,N,SLP,E2)
      SUM=0.0
      E1=SLP+E2
      DO6I=1,N
      ET(I)=E2+X(I)*SLP
      DC(I)=ET(I)-EX(I)
      DCS(I)=DC(I)*DC(I)
      X(I)=X(I)*100.
C     SUM OF SQUARES
    6 SUM=SUM+DCS(I)
      SUM=SUM/N
      PRINT 7,EQK,E1,E2,SUM
    7 FORMAT(1H1,5X*EQUIL. CONST. = *F11.4/6X,*MON: EX. COEFF.
     A =*F10.4/6X*DIM. EX. COEFF. = *F10.4/6X*MEAN DEVIATION =
     B *F11.4/////1X,*CON(GM/LIT)*3X*CON(MOL/LIT)*2X*PERC. MON
     C .*5X*EXP. EX. COEF.*1X*FIT. EX. COEF.*1X*DIFFERENCE*5X*
     D SQUARE DIF.*)
    4 PRINT 9,(C(I),CM(I),X(I),EX(I),ET(I),DC(I),DCS(I),I=1,N)
    9 FORMAT(1X,7(E11.4,4X))
      STOP
      END
```

```
      SUBROUTINE LEASTSQ(X,Y,N,G,Z)
      DIMENSION X(120),Y(120)
      S=0
      U=0
      T=0
      V=0
      DO3I=1,N
      S=S+Y(I)*X(I)
      T=T+X(I)*X(I)
      U=U+X(I)
    3 V=V+Y(I)
      Z=(T*V-U*S)/(N*T-U*U)
      G=(N*S-U*V)/(N*T-U*U)
      RETURN
      END
```

APPENDIX 5

COMPUTER PROGRAM FOR CALCULATION OF MAJOR AXIS OF MOLECULES

```
      PROGRAM AXIS (INPUT,OUTPUT)
C     THIS PROGRAM CALCULATES A 2D CROSS-SECTION OF A PLANAR MOLECULE
C     THROUGH THE HORIZONTAL PLANE
C     THE MOLECULAR SHAPE IS DEFINED BY THE COORDINATES AND COVALENT
C     RADII OF THE INDIVIDUAL ATOMS
C     THE DENSITY IS SET EQUAL TO 1 INSIDE THE MOLECULE AND 0 OUTSIDE
C     THE MOLECULE
C     THE MAJOR AXIS IS CALCULATED FOR USE IN CONJUNCTION WITH ORIENTED
C     FILM DATA
C     INPUT
C     1ST CARD CONTAINS THE NAME FOLLOWED BY 1 CARD FOR EVERY ATOM CON-
C     TAINING ATOMIC SYMBOL IN COL. 1, X COORD. ATOM IN COL. 16-25,
C     Y COORD. ATOM IN COL. 26-35.
C     ATOMIC SYMBOLS USED ARE N-NITROGEN, O-OXYGEN, C-CARBON, H-HYDROGEN,
C     M-METHYL.
C     THE LAST DATA CARD CONTAINS END
      DIMENSION X(30),Y(30),D(101,101),N1(101),N2(101),AT(6),AS(30)
      DIMENSION CRAD(5),CRADS(5),RAD(30),RADS(30),R(2)
      DATA AT/1HC,1HH,1HN,1HM,1HO,1HE/,CRAD/.77,.37,.73,1.20,.74/
      INTEGER D
      READ 68,COMP1,COMP2
   68 FORMAT(2A10)
      PRINT 60,COMP1,COMP2
   60 FORMAT('MAJOR AXIS CALCULATION A FOR ',/,2A10)
      PRINT 62
   62 FORMAT(1X,'A',6X,'X',10X,'Y',10X,'C.R.')
      DO1I=1,101
      DO1J=1,101
    1 D(I,J)=0.
      N=0
      DO2I=1,30
      READ 3,AS(I),X(I),Y(I)
    3 FORMAT(A1,14X,2F10.8)
C     TEST FOR END
      IF(AS(I).EQ.AT(6))12,7
    7 DO4J=1,5
C     RECOGNIZE ATOM
      IF(AS(I).EQ.AT(J))5,4
C     DEFINE COVALENT RADII
    5 RAD(I)=CRAD(J)
      PRINT 61,AS(I),X(I),Y(I),RAD(I)
   61 FORMAT(1X,A1,3(5X,F6.3))
      GO TO 2
    4 CONTINUE
```

APPENDIX 5 (contd.)

```
      PRINT 8,AS(I)
    8 FORMAT(* UNRECOGNISED ATOMIC SYMBOL*,A3)
      GO TO 50
    2 N=N+1
C     FIND DENSITY MATRIX AROUND ATOM I
   12 DO9I=1,N
      X(I)=X(I)*10.+51.
      Y(I)=Y(I)*10.+51.
      RAD(I)=RAD(I)*10.+0.5
      RADS(I)=RAD(I)*RAD(I)
      IY1=Y(I)-RAD(I)+1
      IY2=Y(I)+RAD(I)
      DO9J=IY1,IY2
      DX=SQRT(RADS(I)-(J-Y(I))*(J-Y(I)))
      IX1=X(I)-DX+1
      IX2=X(I)+DX
      DO9K=IX1,IX2
    9 D(K,J)=1.
C     DENSITY MATRIX DEFINED
      DO10I=1,101
      M=IABS(I-51)
      N1(I)=M/10
   10 N2(I)=M-N1(I)*10
      PRINT 13
   13 FORMAT(1H1)
      PRINT 16,(N1(I),I=1,101)
      PRINT 16,(N2(I),I=1,101)
   16 FORMAT(5X,101I1)
      PRINT 17
   17 FORMAT(/)
      DO14I=1,101
      I1=I-51
C     PRINT DENSITY
   14 PRINT 15,I1,(D(I,J),J=1,101)
   15 FORMAT(1X,I3,1X,101I1)
C     CALCULATE CENTRE OF GYRATION
      NT=0
      RCX=RCY=0.
      DO20I=1,101
      DO20J=1,101
      RCX=RCX+D(I,J)*I
      RCY=RCY+D(I,J)*J
   20 NT=NT+D(I,J)
```

APPENDIX 5 (contd.)

```
      RCX=RCX/NT
      RCY=RCY/NT
C     COORDINATES OF CENTRE OF GYRATION
      RX=RCS-51
      RY=RCY-51
      PRINT 21,RX,RY
   21 FORMAT(1H1,*CENTRE OF GYRATION*/,*X COORDINATE*,F10.4,* Y COOR
     XDINATE,F10.4,6(/))
      SY2=SX2=SXY=0.
C     CALCULATE MAJOR, MINOR AXES
      DO30I=1,101
      DO30J=1,101
      XI=I-RCX
      YJ=J-RCY
      SY2=SY2+YJ*YJ*D(I,J)
      SX2=SX2+XI*XI*D(I,J)
   30 SXY=SXY+XI*YJ*D(I,J)
      SXY=-SXY
      SC=SX2*SY2-SXY*SXY
      SB=-SX2-SY2
      SQ=SQRT(SB*SB-4.*SC)
      R(1)=(-SB+SQ)/2.
      R(2)=(-SB-SQ)/2.
      DO50I=1,2
      C1=1.
      C2=-(SY2-R(I))/SXY
      C=SQRT(C1*C1+C2*C2)
      C1=C1/C
      C2=C2/C
      GO TO (64,65)I
   64 PRINT 66,C1,C2
   66 FORMAT(*MINOR AXIS*,F10.6,*,*,F10.6)
      GO TO 50
   65 PRINT 67,C1,C2
   67 FORMAT(*MAJOR AXIS*,F10.6,*,*,F10.6)
   50 CONTINUE
      STOP
      END
```

APPENDIX 6

APPARENT EXTINCTION COEFFICIENTS CALCULATED FROM THE UV-01 MEASUREMENTS, WITH THE FITTED VALUES

CON	EX	$EX_{COR.}$	$EX_{1,2,3}$	$EX_{1,2,4}$
		2 mm UV-01		
.0422	9667	9776	9766	9781
.0434	9717	9776	9766	9781
.0469	9789	9816	9765	9780
.0544	9708	9764	9764	9777
.0586	9725	9781	9763	9776
.0613	9686	9739	9762	9775
.0710	9717	9764	9760	9772
.0730	9756	9762	9760	9772
.0731	9801	9807	9760	9772
.0767	9752	9752	9759	9771
		1 mm UV-01		
.0807	9739	9803	9758	9770
.1080	9782	9713	9752	9762
.1180	9700	9723	9750	9759
.1200	9740	9760	9749	9758
.1270	9727	9748	9748	9756
.1370	9768	9768	9746	9753
.1380	9729	9729	9745	9753
.1450	9754	9754	9744	9751
.1560	9752	9752	9742	9749

(contd.)

APPENDIX 6 (contd.)

CON	EX	$EX_{COR.}$	$EX_{1,2,3}$	$EX_{1,2,4}$
		.5 mm UV-01		
.1520	9698	9727	9742	9748
.1840	9682	9702	9735	9740
.1910	9735	9754	9734	9738
.1950	9707	9727	9733	9737
.2140	9719	9729	9729	9732
.2230	9715	9725	9727	9729
.2370	9744	9744	9724	9725
.2450	9708	9708	9722	9723
.2500	9746	9738	9721	9722
		.2 mm UV-01		
.3580	9655	9694	9698	9693
.3730	9661	9600	9695	9689
.4120	9649	9678	9686	9679
.4850	9595	9614	9671	9661
.5000	9653	9663	9668	9658
.5330	9610	9620	9661	9649
.6060	9605	9605	9645	9632
.6100	9665	9665	9644	9631
.6290	9624	9624	9640	9627
.6560	9663	9653	9635	9621

(contd.)

APPENDIX 6 (contd.)

CON	EX	$EX_{COR.}$	$EX_{1,2,3}$	$EX_{1,2,4}$
		.1 mm UV-01		
.5900	9597	9663	9634	9625
.6590	9558	9605	9648	9620
.6720	9597	9634	9631	9617
.7650	9556	9577	9612	9596
.8400	9599	9620	9596	9579
.9340	9513	9533	9577	9559
.9580	9556	9576	9572	9554
.9980	9608	9618	9564	9546
1.090	9556	9556	9546	9528
1.150	9496	9506	9535	9516
1.180	9506	9506	9529	9511
		.05 mm UV-01		
1.550	9418	9447	9456	9440
1.610	9412	9440	9446	9431
1.650	9410	9440	9438	9423
1.840	9421	9440	9403	9390
2.020	9424	9442	9372	9361
2.110	9301	9401	9355	9346
2.180	9353	9354	9343	9335
2.400	9288	9288	9306	9301
2.500	9271	9271	9289	9285
2.810	9218	9208	9240	9241

(contd.)

APPENDIX 6 (contd.)

CON	EX	$EX_{COR.}$	$EX_{1,2,3}$	$EX_{1,2,4}$
		.025 mm UV-01		
3.200	9160	9180	9180	9186
3.630	9092	9111	9119	9129
3.840	9061	9080	9089	9102
4.310	9043	9053	9027	9043
4.580	8983	8993	8993	9011
4.730	8950	8960	8975	8994
5.110	8917	8917	8829	8949
5.420	8857	8849	8895	8915
5.470	8837	8828	8889	8910
5.640	8867	8857	8870	8890
		.012 mm UV-01		
6.072	8774	8810	8825	8845
6.382	8758	8789	8793	8813
7.276	8742	8781	8708	8724
7.811	8704	8760	8661	8673
8.438	8678	8688	8609	8616
8.988	8583	8610	8565	8567
9.557	8439	8439	8462	8449
10.42	8560	8570	8523	8519
10.50	8414	8403	8457	8442
11.37	8383	8373	8400	8376
11.98	8306	8284	8363	8331

APPENDIX 7

COMPUTER PROGRAM FOR THEORETICAL CALCULATION OF DIMER SPECTRUM

```
      PROGRAM VIBCOU (INPUT,OUTPUT)
C
C     CALCULATES DIMER SPECTRUM FOR KNOWN COUPLING COEFFICIENTS (EP)
C     AND EXCITATION BAND WIDTH (XL) AS DESCRIBED BY R.L. FULTON AND
C     M. GOUTERMAN, J. CHEM. PHYS.,V41,N8,2280(1964)
C
      DIMENSION B(20,20),C(20,20),EIG(20,5),BO(20),EN(20,20),CI(20,20)
      DIMENSION X(100),SUM(100,3),FPM(2)
C     BANDWIDTH
      BW=1044.
      FINT=1.
C     VIBRATIONAL SPACING GROUND STATE
      V1=1300.
C     VIBRATIONAL SPACING EXCITED STATE
      V2=1300.
C     M
      DM=1.23
      V1S=V1*V1
      V2S=V2*V2
      VS=(V1S+V2S)/2.
C     EXCITATION BAND WIDTH
      XL=V1S*V2S*DM/(VS*VS)
C     MATRIX SIZE
      N=20
C     NUMBER OF SIGNIFICANT VALUES
      NEV=10
      NAX=N-NEV+1
C     INTERACTION ENERGY
      EP=1.
      NFAC=1
      NEX=N-1
C     RELATIVE INTENSITY (+) SERIES
      FPM(1)=.707
C     RELATIVE INTENSITY (-) SERIES
      FPM(2)=.707
      DO28I=1,100
   28 SUM(I,1)=SUM(I,2)=SUM(I,3)=0.
C     CALCULATE B TERMS (EQN.16)
      DO11I=1,NEV
      K=I-1
      BO(I)=XL*(2.*K)/NFAC/(2.**K)*EXP(-XL*XL/2.)
      BO(I)=SQRT(BO(I))
   11 NFAC=NFAC*I
```

APPENDIX 7 (contd.)

```
C       PQ=+1 FOR(+)EQN., PQ=-1 FOR(-)EQN.
        DO10NQ=1,2
        PQ=3-2*NQ
C       SET UP MATRIX EQUATION (EQN.17)
        DO1I=1,N
        DO2J=1,N
      2 B(I,J)=0.
        K=I-1
      1 B(I,I)=K+0.5+PQ*(-1)**K*EP
        DO3I=2,NEX
        K=I-1
      3 B(I,I-1)=B(I-1,I)=XL*SQRT(.5*K)
C       FIND EIGENVALUES AND EIGENFUNCTION
        CALL MLEW(N,B,C,EIG)
        DO5I=NAX,N
C       PRINT EIGENVALUES AND EIGENFUNCTION
      5 PRINT 4,PQ,EIG(I,1),(C(J,I),J=1,NEV)
      4 FORMAT(F4,5X,F10.6,5X,10F10.6)
        XLS=.5*(1.+XL XL)
C       CALCULATE INTENSITIES AND ENERGIES OF VIBRONIC BANDS EQNS(19&20)
        DO12I=1,NEV
        DO13J=NAX,N
        EN(I,J)=(I-1)+EIG(J,1)-XLS
        EN(I,J)=EN(I,J)*V1+37.15E3
     13 CI(I,J)=(BO(I)*C(1,J))**2 FINT/2.
        PRINT 6,(EN(I,J),J=NAX,N)
        PRINT 6,(CI(I,J),J=NAX,N)
      6 FORMAT(10F12.6)
     12 PRINT 7
      7 FORMAT(/)
C       EVENLY SPACED WAVENUMBER VALUES
        DO22K=1,100
     22 X(K)=(K-46) 100.+37.2E3
        DO21I=1,NEV
        DO21J=NAX,N
        IF(CI(I,J).LE.1E-4)21,23
     23 DO21K=1,100
C       INCLUDE GAUSSIAN SHAPE (EQN. 23)
     21 SUM(K,NQ)=SUM(K,NQ)+EXP(-((X(K)-EN(I,J))/BW)**2)*CI(I,J)*FPM(NQ)
     10 CONTINUE
        DO40K=1,100
        SUM(K,3)=SUM(K,1)+SUM(K,2)
        DO40NQ=1,3
     40 SUM(K,NQ)=SUM(K,NQ)*X(K)
        PRINT 24,(X(K),(SUM(K,NQ),NQ=1,3),K=1,100)
     24 FORMAT(4(5X,E13.6))
        STOP
        END
```

APPENDIX 8

VAPOUR PRESSURE OSMOMETRY

THEORY

The thermoelectric determination relies on the difference between the vapour pressure of a solution and the corresponding pure solvent. From Raoult's Law:

$$\frac{\Delta P}{P_o} = X_1 g \qquad (1)$$

ΔP = vapour pressure difference

X_1 = mole fraction of solute

g = osmotic coefficient

P_o = vapour pressure of the pure solvent.

If one considers that the decrease in vapour pressure due to solute addition can be balanced by an increase due to a temperature rise, then applying the Clausian Clapeyron equation

$$\frac{d(\ln P)}{dT} = \frac{\Delta H_{vaps}}{RT^2} \qquad (2)$$

one obtains the ideal relation represented by

$$\Delta T_{ideal} = \frac{RT^2}{\Delta H_{vaps}} g X_1 \qquad (3)$$

where ΔH_{vaps} = heat of vaporisation of the solvent

R = gas constant

T = cell temperature.

Thus ΔT for a given solution can be related to the mole fraction of the

solute; consequently the molecular weight of the solute can be calculated from a knowledge of the weight concentration of the solution.

Allowing for heat losses by conduction through the vapour phase leading to a steady state one obtains

$$\Delta T_{ss} = \frac{\varphi X}{(L/RT^2) + (RT\lambda/DL)(P-p)/P} \qquad (4)$$

where λ = thermal conductivity of vapour/air mixture

D = diffusion coefficient of solvent vapour through air

P = total pressure of the cell

p = vapour pressure of solvent.

This equation was first derived by Baldes. In most cases this equation gives too high a value for the temperature difference since no allowance has been made for conduction through the thermistor wires and convection. Iyengar (1954) introduced the correction factor, φ, which is an approximate constant for the apparatus nearly independent of the solvent used.

$$\Delta T_{ss} = \frac{\varphi X}{(L/RT^2) + (RT\lambda/DL)(P-p/P)(1+\varphi)} \qquad (5)$$

At low concentrations the mole fraction can be assumed to be directly proportional to molality and equation (5) can be written in the form:

$$\Delta T_{ss} = K_c m \qquad (6)$$

where K_c is a cell constant which can be determined experimentally.

The temperature difference between a solvent and solution drop is best measured through the use of a set of matched thermistors although

thermocouples have been used (Van Dam, 1964). The two thermistors comprise two arms of a Wheatstone bridge in which the third arm is an adjustable resistor, and the fourth arm a fixed resistor. The basic electrical diagram is shown in Fig. A1.

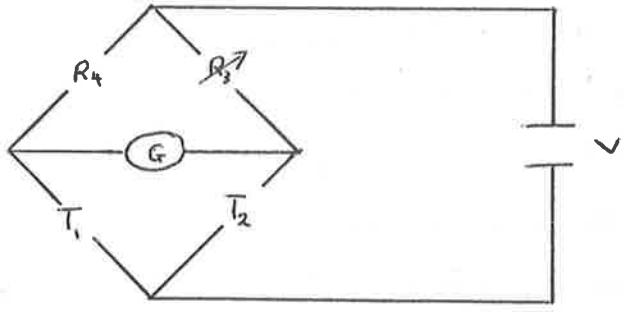

Fig. A1

Solvent drops are placed on both thermistors and the bridge is balanced through the use of the variable resistor R_3. When the solvent drop on one of the thermistors is replaced by a solution drop, the bridge becomes unbalanced, and the current measured is proportional to the change in resistance. The temperature resistance property of a thermistor is given by $R = Ae^{-\beta/T}$. For small temperature changes the change in resistance of the thermistor is directly proportional to the change in resistance and equation (6) becomes

$$i = K'm \qquad (7)$$

where i is the output current.

DISCUSSION

Vapour pressure osmometry studies of aqueous solutions have been

limited to the measurement of concentrations of 10^{-2} mole/litre to accuracies of approximately 5%, and most commercially available vapour pressure osmometers can be used up to this limit, although Dohner, Wachter and Simon (1967) have built a highly sophisticated apparatus which can improve these limits by a factor of ten. In the present work it is hoped to be able to measure the osmotic coefficient of caffeine for a concentration range of 10^{-1} mole/litre to 10^{-2} mole/litre accurate to 1%. Had this accuracy been reached then vapour pressure osmometry could have been used to study the aggregation of caffeine. T'so et al (1963, 1964) used vapour pressure osmometry to study the aggregation of purine, uridine, cytidine, 6-methyl purine and 5-bromo-uridine.

Most commercial vapour pressure osmometers use bead thermistors in conjunction with a DC bridge. In this work an AC bridge was used, and when the bead thermistors were used for measurements on aqueous solutions large capacitances, which could not be balanced, were found to arise. Due to this the less sensitive STC F15 glass thermistors had to be used.

INSTRUMENTATION

Matched F15 thermistors were obtained from STC (U.K.) with the specifications:

a) the resistance was matched to better than 1%;

b) the temperature coefficient was matched to better than 1%.

After some experimentation, an apparatus, a cross-section of which is shown in Fig. A2, was designed with the following features. The thermistor

CROSS-SECTION OF THE VAPOUR PRESSURE OSMOMETER MEASURING COMPARTMENT.

SCALE DOUBLE FULL SIZE.

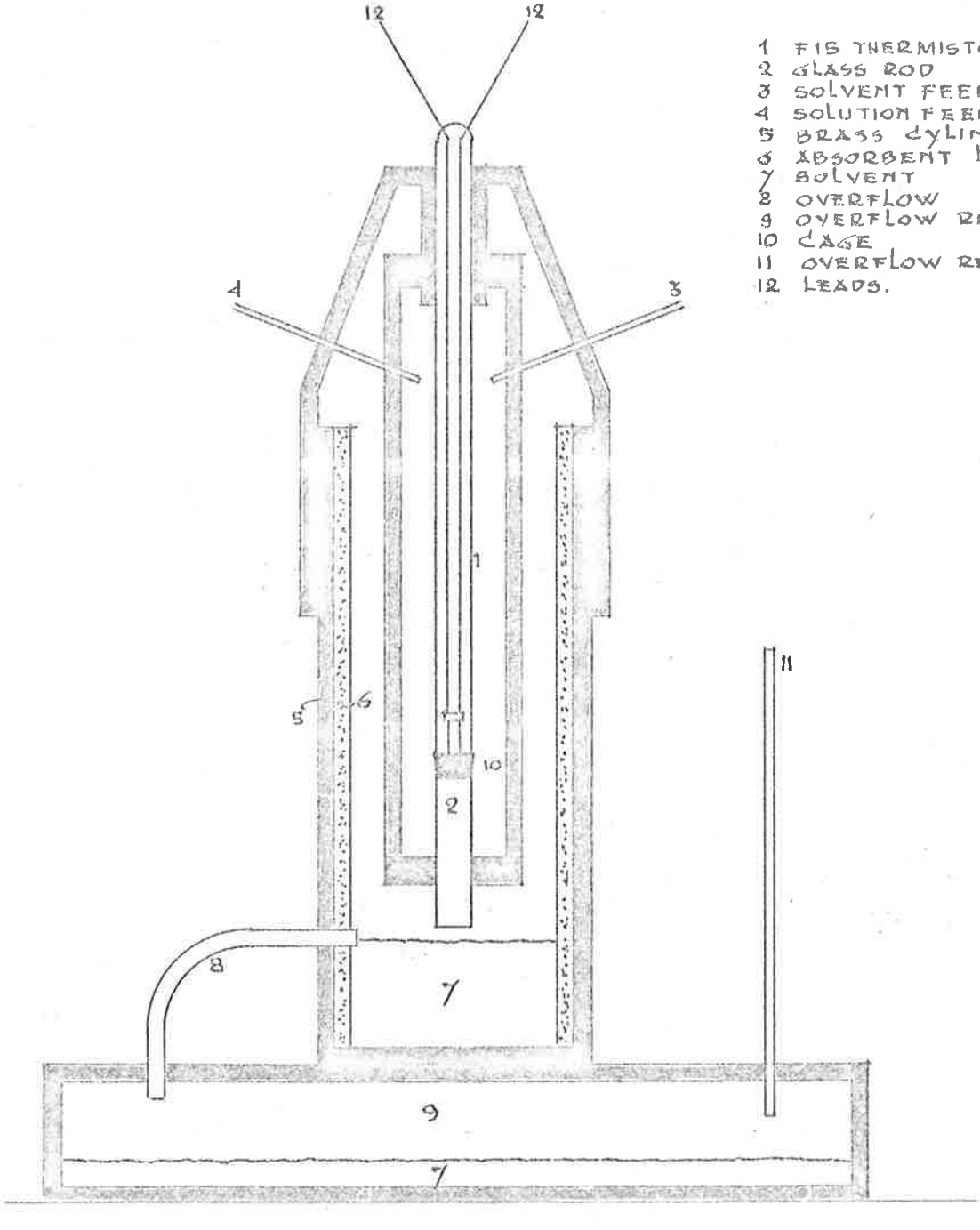

1 FIS THERMISTOR
2 GLASS ROD
3 SOLVENT FEEDER TUBE
4 SOLUTION FEEDER TUBE
5 BRASS CYLINDER.
6 ABSORBENT LINING.
7 SOLVENT
8 OVERFLOW
9 OVERFLOW RESERVOIR
10 CAGE
11 OVERFLOW REMOVER TUBE
12 LEADS.

FIG. A2

beads of the two F15 glass thermistors rest on $\frac{1}{4}$" diameter glass rods on which small copper wire baskets are placed. The solution and solvent drops are passed through a polythene tube and run down the stem of the thermistor into the basket. The polythene tube is coiled inside the cell to obtain a maximum degree of thermostatting of the solvent and solution drops before delivery.

The basket on top of the glass rod arrangement results in a highly reproducible drop-size, while little rinsing is required. Drop-size control is considered vital to the reproducibility of VPO readings (Meeks and Goldfarb, 1967).

Each thermistor is contained in a brass cylinder, the walls of which are lined with blotting paper. This produces an atmosphere rich in solvent vapour. An overflow maintains a constant solvent level in each of the thermistor cells. The thermistor apparatus was placed in a polyethylene container which was immersed in a water bath thermostatted to a constant temperature within 5×10^{-3} °C. The polyethylene container was lined with several layers of aluminium foil to reduce electrical interference.

An AC thermistor bridge based mainly on the circuit used by Nancollas and Hardy (1967) was built by Eilco Electronics, Adelaide, South Australia. The circuit diagram for the system is shown in this article. ~~Appendix 9~~. To eliminate temperature fluctuation effects on the bridge the two main 150 KΩ resistors were replaced by Karma wound mica plate resistors, while the whole circuit is contained in an insulated box in

which the temperature is controlled to .005°C through an arrangement involving a temperature probe, a proportional voltage supply, a lamp as a heating unit and a 35 cubic ft. displacement fan to circulate inside the bridge casing. The thermistor bridge output was found to have a noise level and stability many orders greater than required by the limits of this project.

Fig. A3 shows the output of the thermistor bridge as a function of the resistance difference between the two bridge arms for the lowest sensitivity setting. Results for the other temperature settings are proportionally similar.

Since the thermistor bridge is linear over a limited range it was found to be more convenient to compensate for the reduction in the resistance of the solution thermistor by including a decade box (1000Ω - $.1\Omega$) in the circuit.

With solvent drops on both thermistors the bridge was balanced. When the solvent drop on one thermistor was replaced by a solution drop a small temperature rise occurred resulting in a decrease in resistance of the thermistor. This decrease in resistance was then compensated for by an increase in the resistance of the decade box until the bridge was balanced again. This method has the advantage over the usual method, which relies on reading the variation in the thermistor bridge current off a graph, that a direct value in the resistance difference is obtained. The accuracy of the reading is not limited by the accuracy of a recorder or the scale of the recorder.

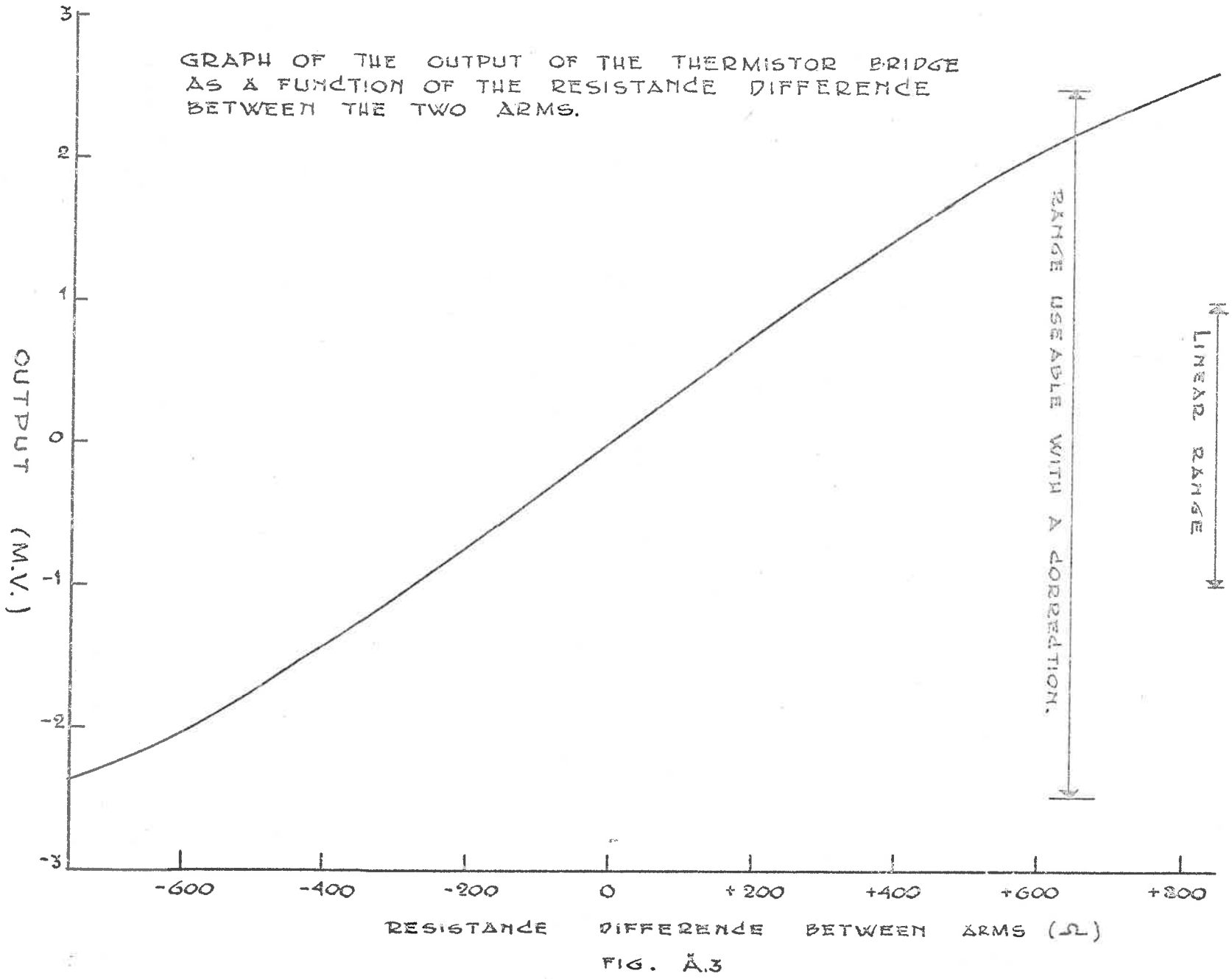
GRAPH OF THE OUTPUT OF THE THERMISTOR BRIDGE AS A FUNCTION OF THE RESISTANCE DIFFERENCE BETWEEN THE TWO ARMS.
OUTPUT (M.V.)
3
2
1
0
-1
-2
-3
-600
-400
-200
0
+200
+400
+600
+800
RESISTANCE DIFFERENCE BETWEEN ARMS (Ω)
RANGE USEABLE WITH A CORRECTION.
LINEAR RANGE

FIG. A.3

RESULTS AND CONCLUSIONS

A set of aqueous sucrose solutions was prepared. A solution of .02 mole/litre was prepared and the resistance decrease produced by this solution was recorded. In each case equilibration took about 10 minutes and the resistance difference was extrapolated to t = 0. The resistance difference values obtained were 11.0 ± .2, 11.4 ± .2, 11.2 ± .1 and 11.2 ± .1. The reproducibility of the other solutions was found to be similar. The relation between the resistance decrease and the concentration was found to be non-linear. The long equilibration time is most likely due to the use of the glass-coated F15 thermistor.

When the thermistors became defective it was found to be impossible to obtain a replacement pair of thermistors within the time available for this project.

Although the accuracy required seems to be obtainable, the long time required for the steady state to develop makes the present method unsuitable. Unless the method can be improved to reduce the time taken for the steady state to be reached, the present use of the F15 thermistor will have to be abandoned. In this case it would be more feasible to use a DC bridge.

APPENDIX 9

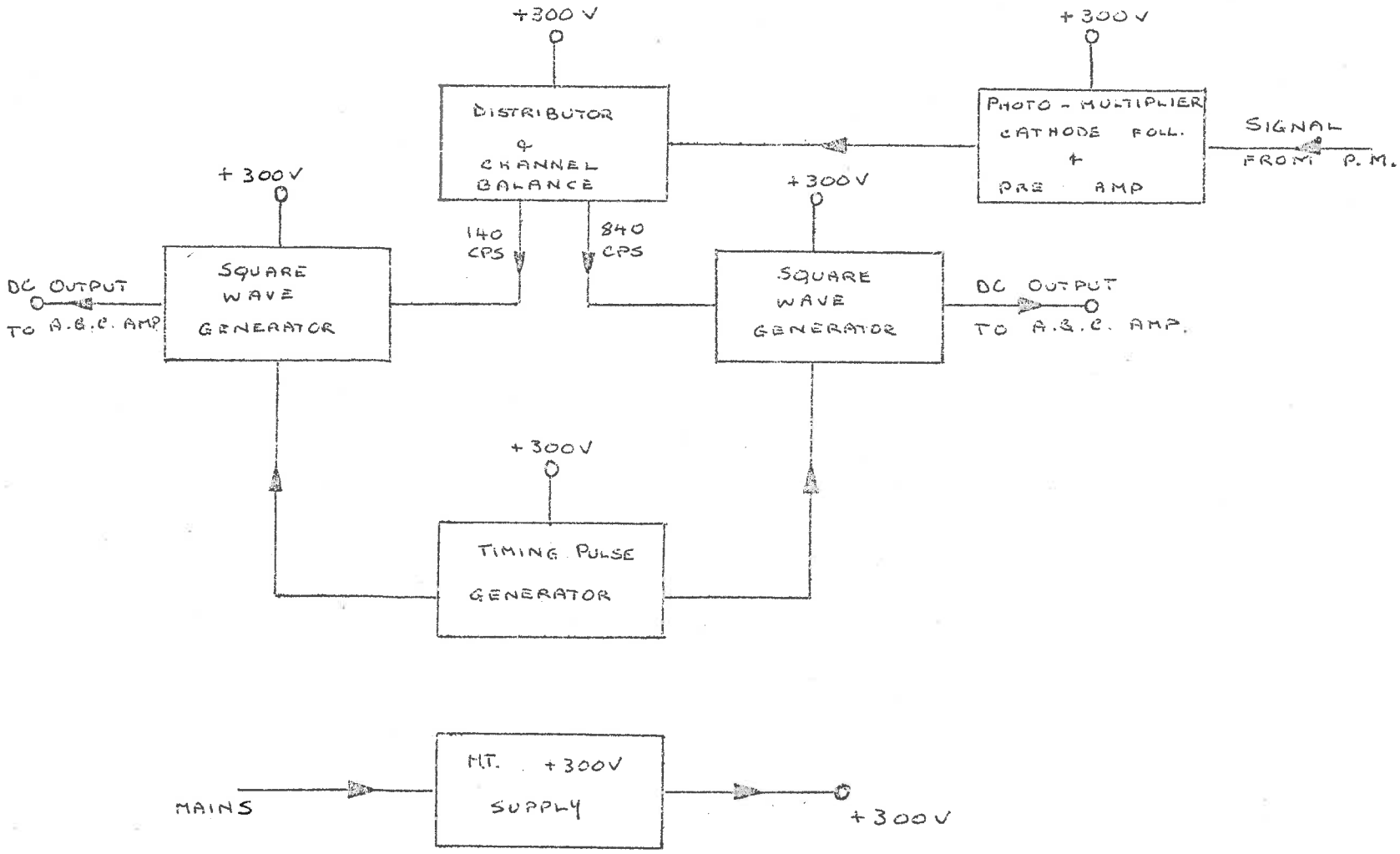
+300 V
DISTRIBUTOR & CHANNEL BALANCE
+300 V
PHOTO - MULTIPLIER CATHODE FOLL. + PRE AMP
SIGNAL FROM P.M.
+300 V
140 CPS
840 CPS
+300V
DC OUTPUT TO A.B.C. AMP
SQUARE WAVE GENERATOR
SQUARE WAVE GENERATOR
DC OUTPUT TO A.B.C. AMP.
+300V
TIMING PULSE GENERATOR
MAINS
M.T. +300V SUPPLY
+300V

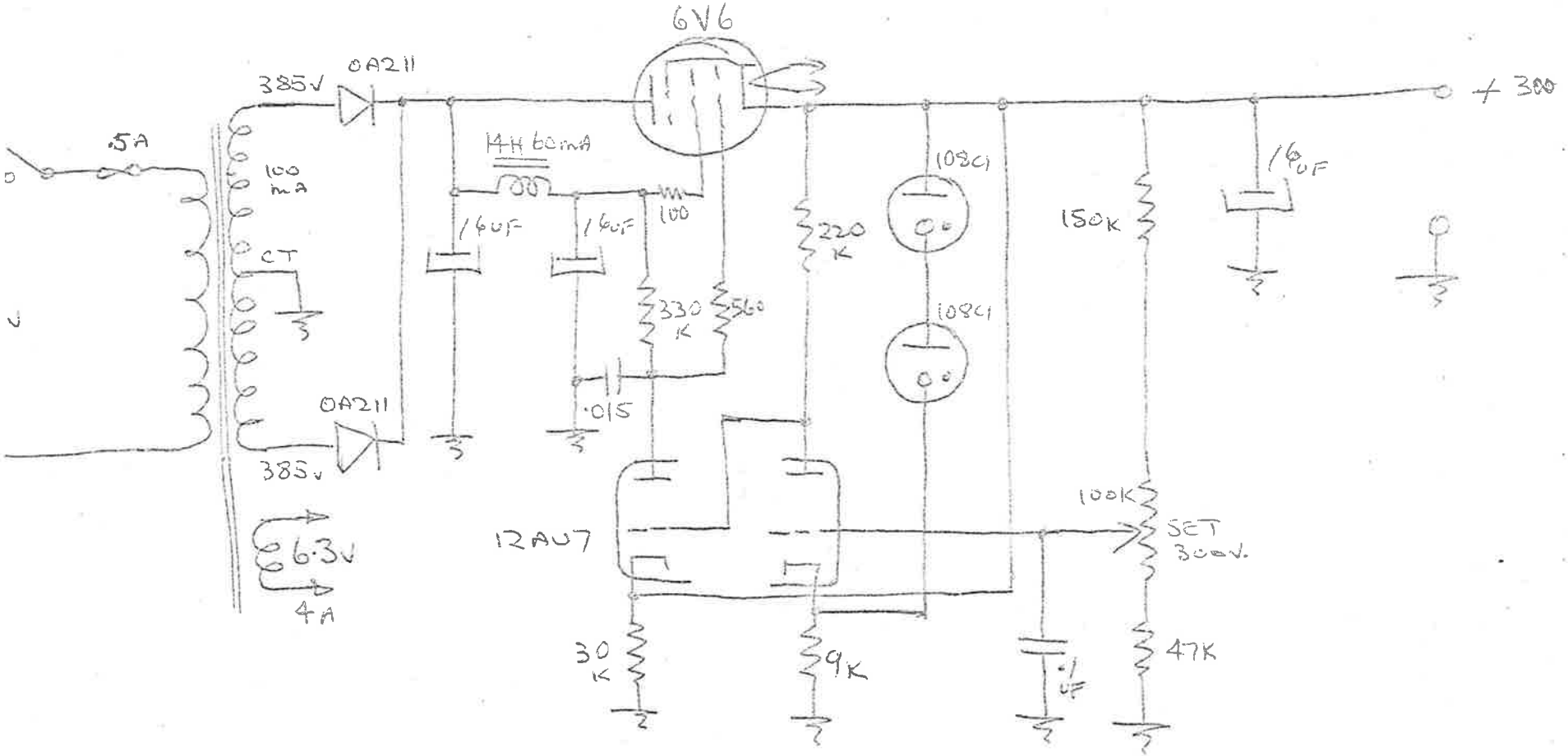

+300V STABILISED SUPPLY.

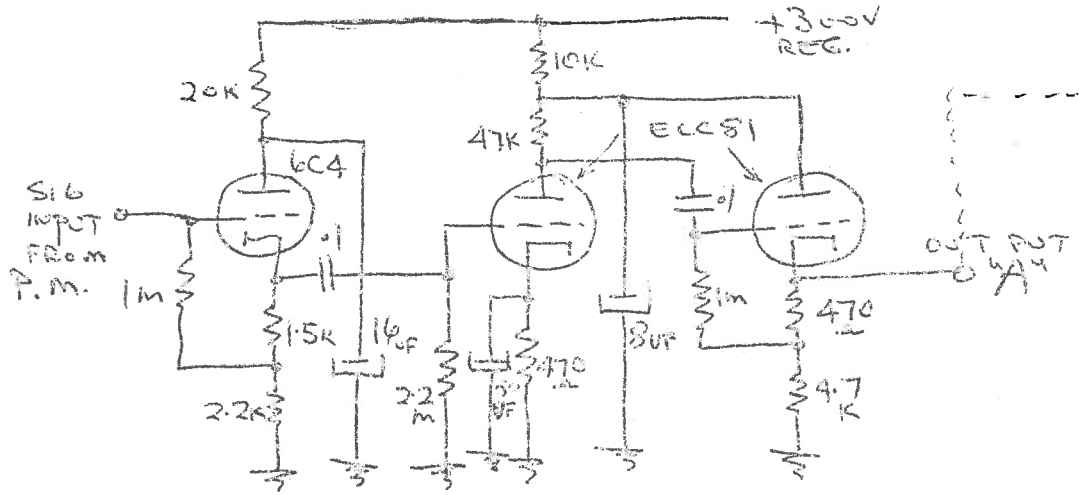

P. M. CATHODE FOLLOWER, PRE AMPLIFIER.

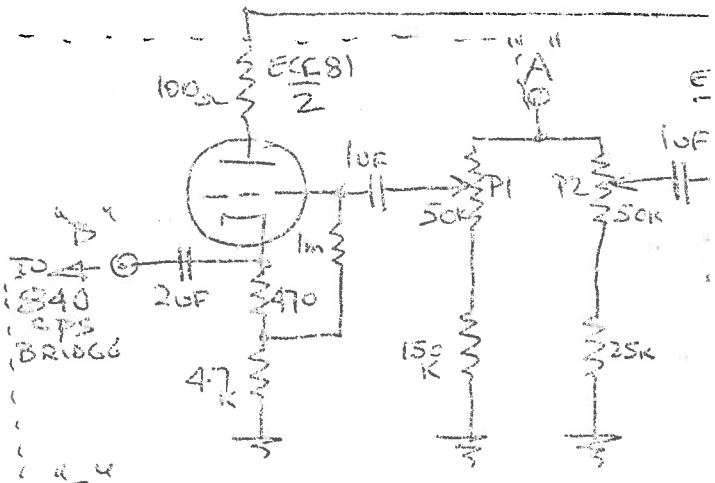

DISTRIBUTOR AND C

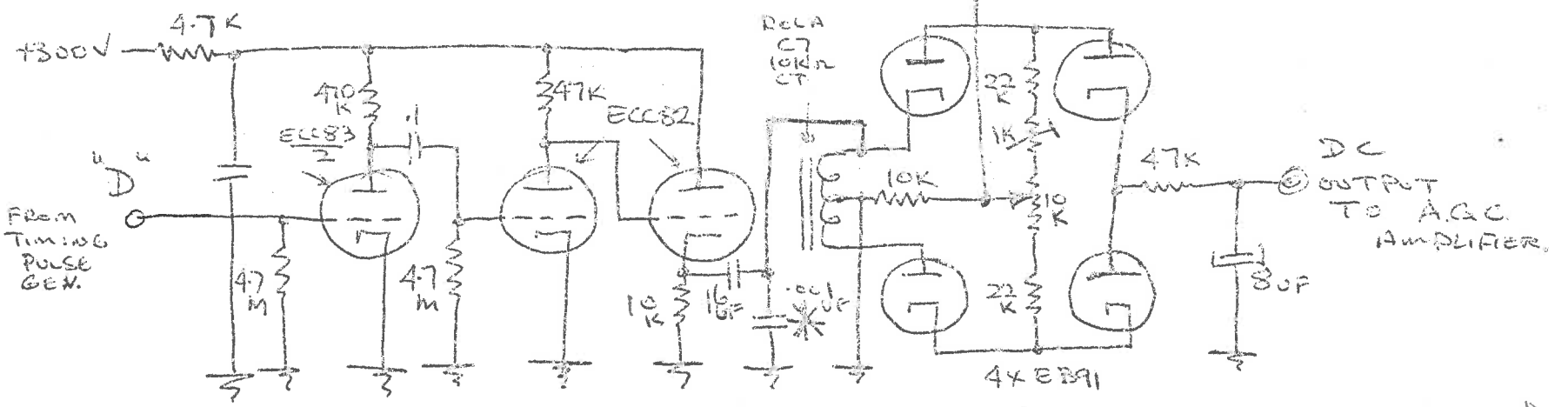

840cps SQUARE WAVE GENERATOR, DIODE BRIDGE.

NOTE 140cps SQUARE WAVE GEN & BRIDGE SAME AS ABOVE EXCEPT CAPACITOR MARKED * IN .01UF.

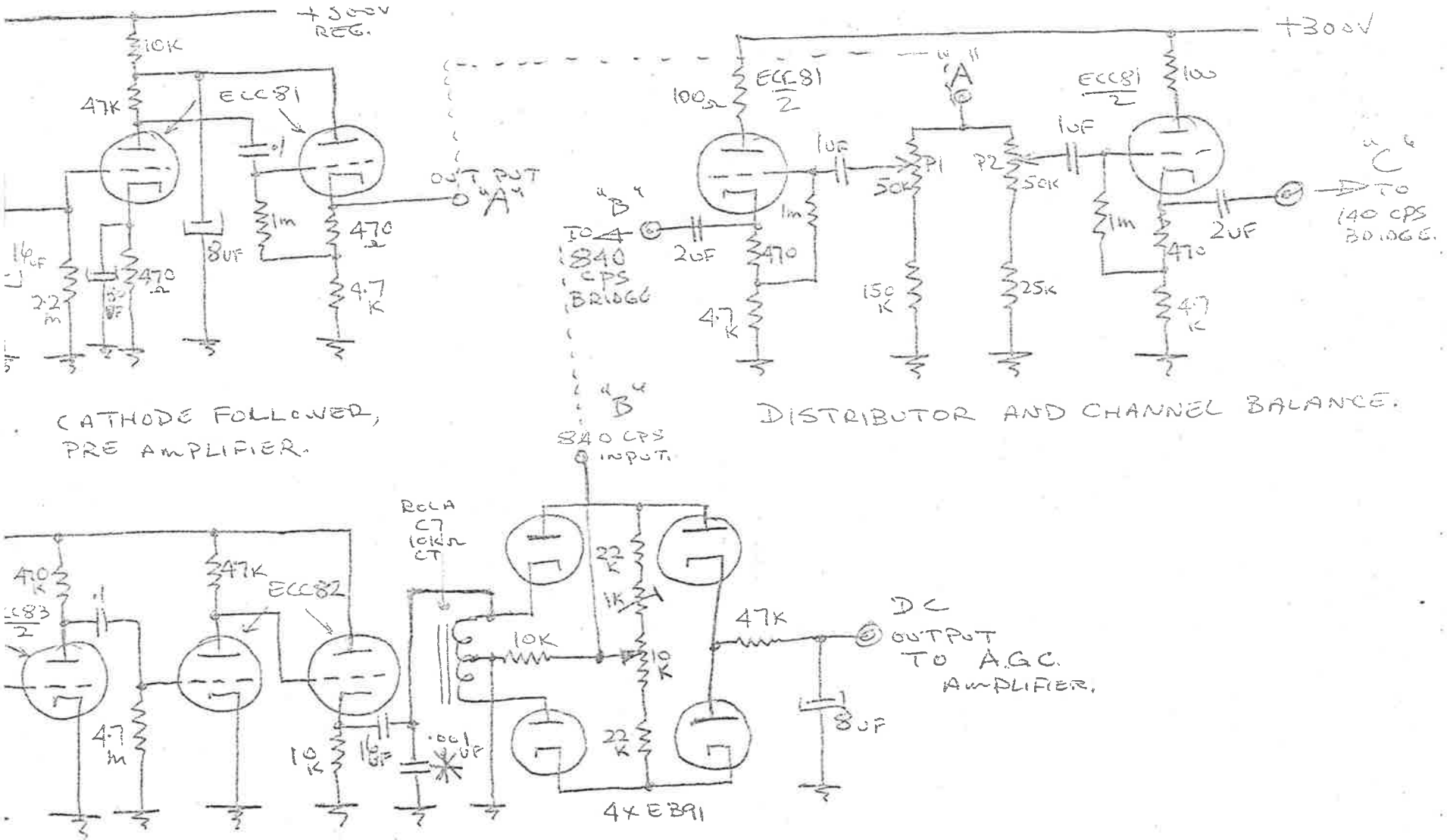

CATHODE FOLLOWER, PRE AMPLIFIER.

DISTRIBUTOR AND CHANNEL BALANCE.

0cps SQUARE WAVE GENERATOR, DIODE BRIDGE.

0cps SQUARE WAVE GEN & BRIDGE SAME AS ABOVE
CEPT CAPACITOR MARKED * IN .01UF.

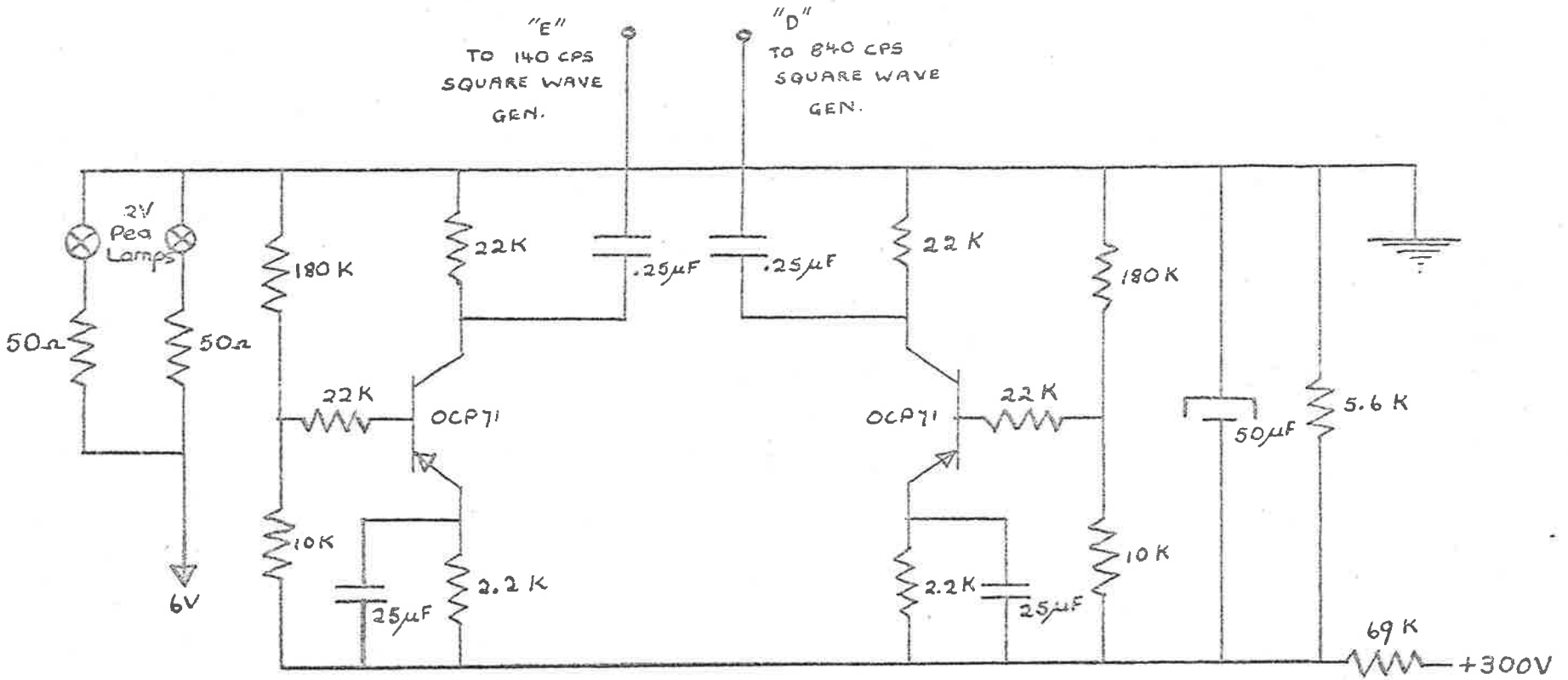

TIMING PULSE GENERATOR

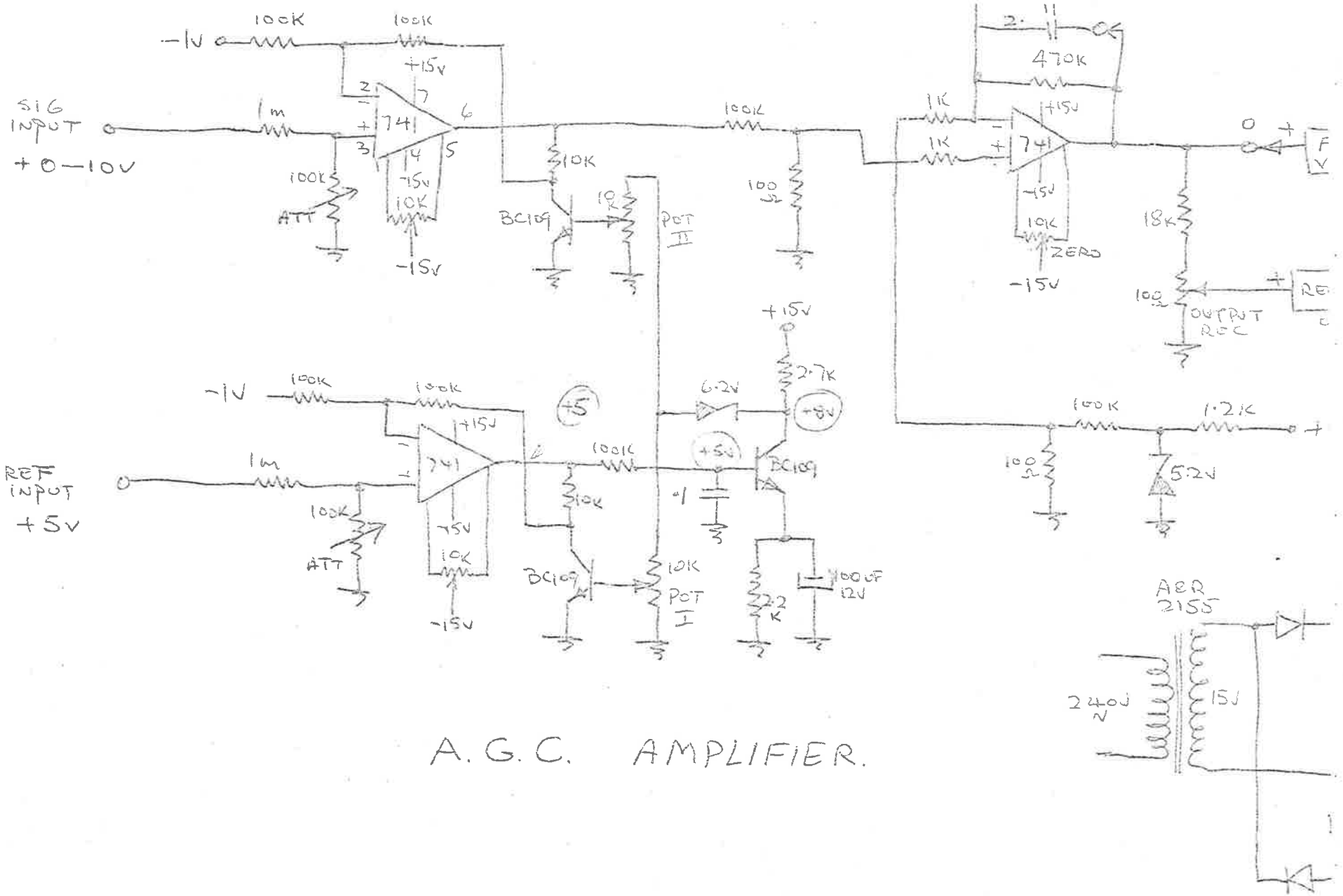

A. G. C. AMPLIFIER.

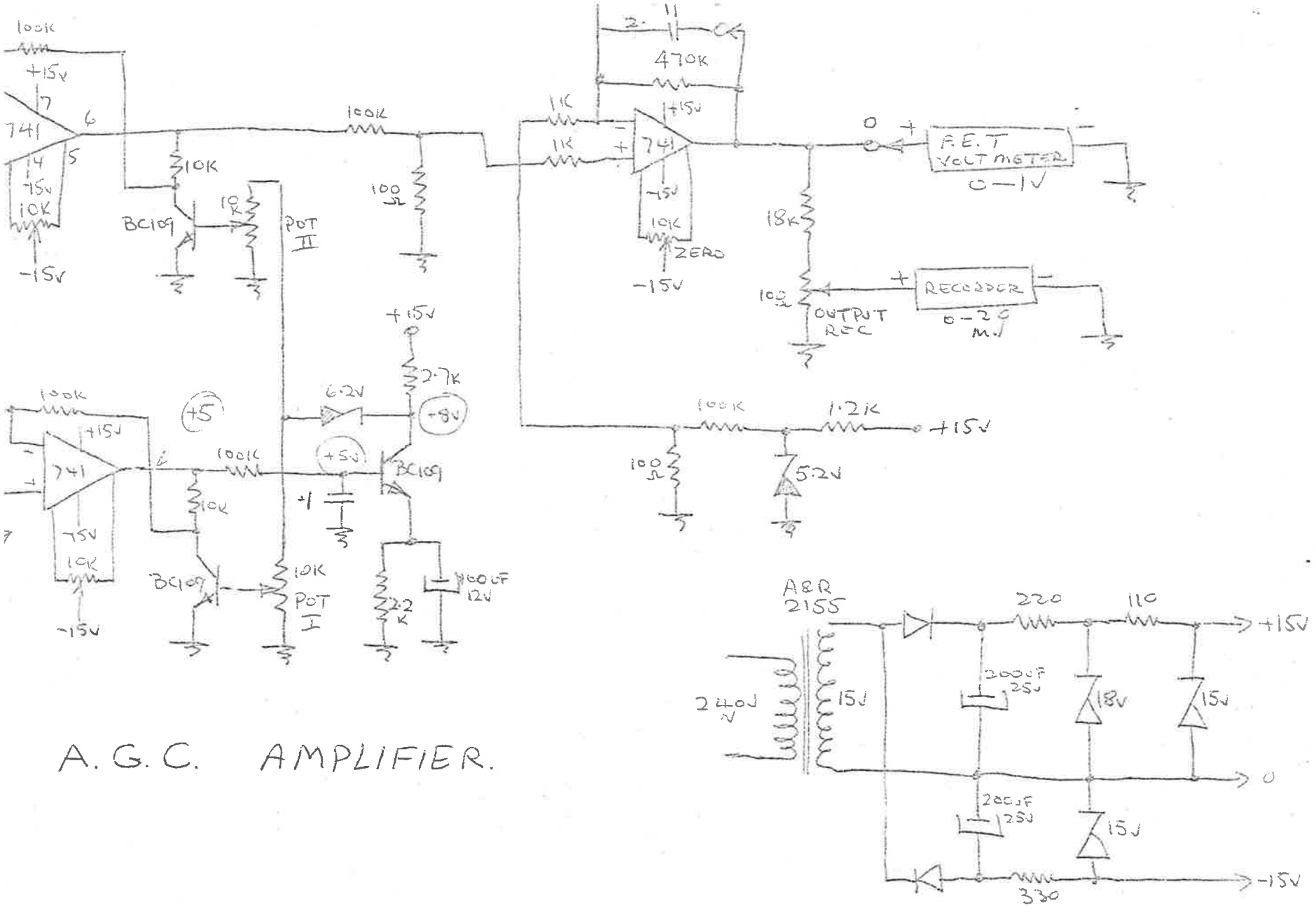

A. G. C. AMPLIFIER.

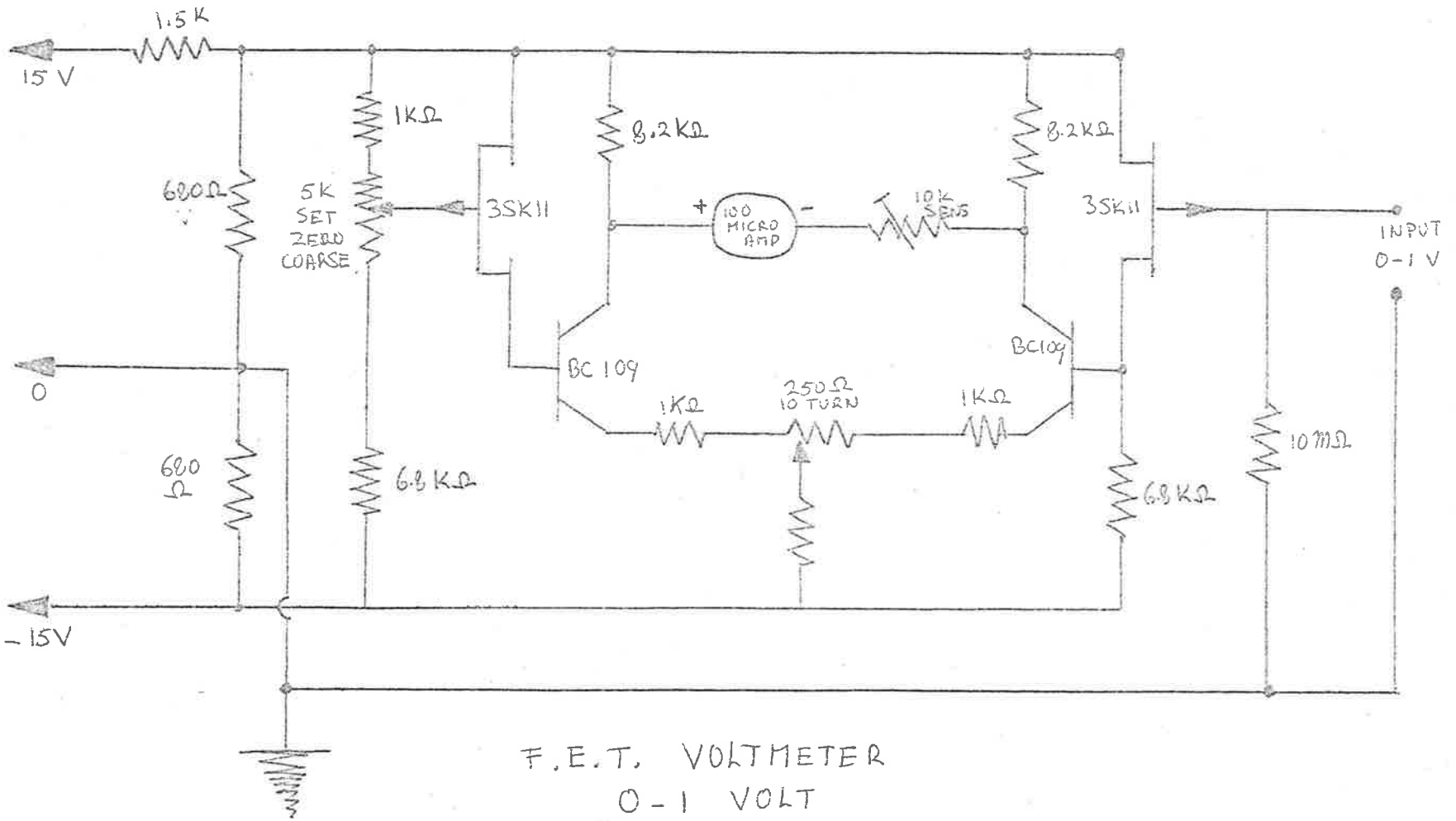

F.E.T. VOLTMETER
0 - 1 VOLT

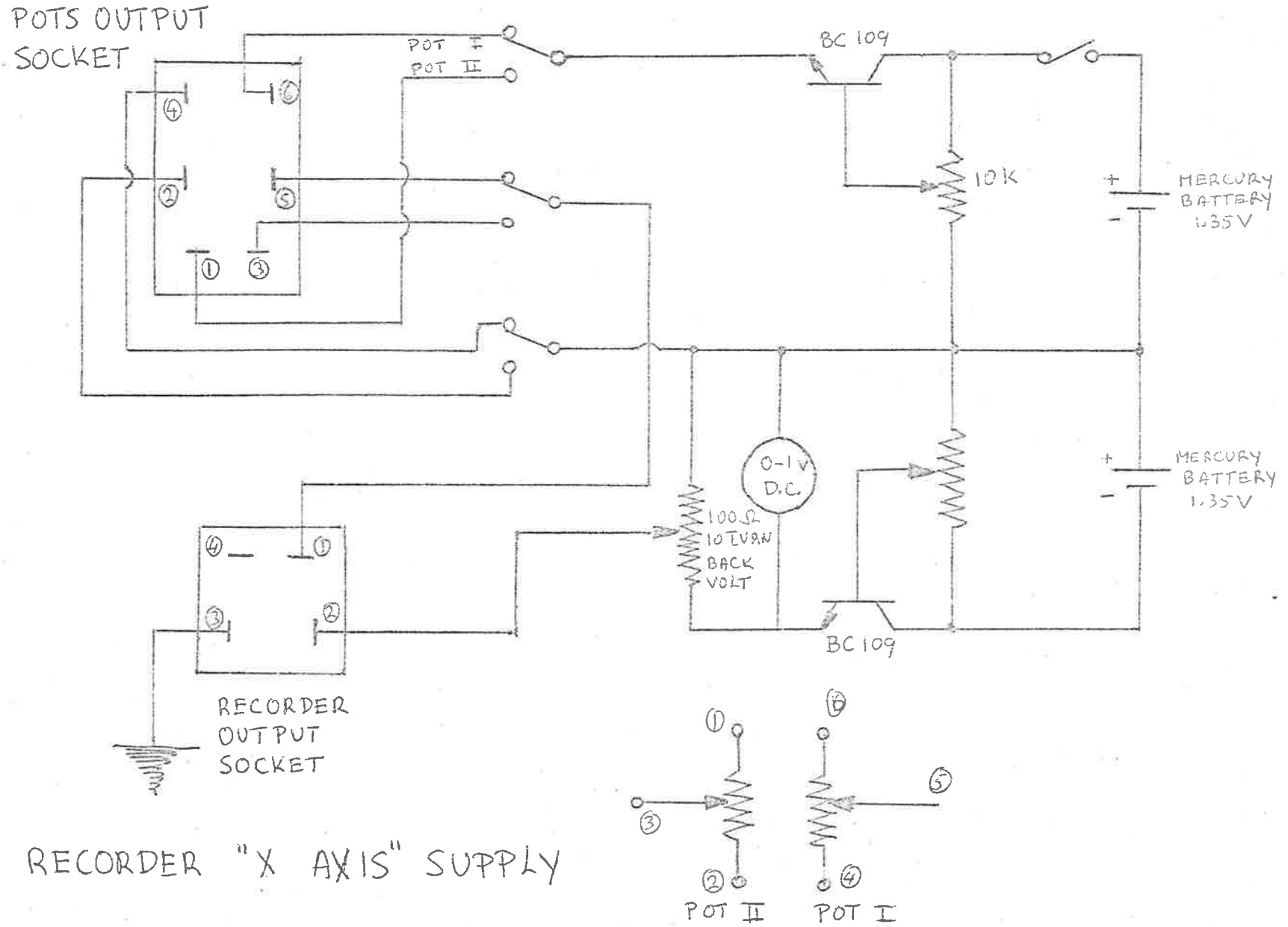

RECORDER "X AXIS" SUPPLY

REFERENCES

Ainsworth, S. and Winter, E. "An Automatic Recording Polarisation Spectrofluorimeter", Applied Optics, 3, 3 March (1964).

Bailey, M.L. "Semi-Empirical π-Electron Calculations", Theoret. Chim. Acta 13, 56 (1969).

Bailey, M.L. "PPP Calculations of the Absorption Spectra of Purines and Pyrimidines", Theoret. Chim. Acta 16, 309 (1970).

Bauman, R.P. "Absorption Spectroscopy", John Wiley (1962).

Börrensen, H.C. "On the Luminescence Properties of Some Purines and Pyrimidines", Acta Chem. Scand. 17, 921-29 (1963) No. 4.

Börrensen, H.C. "The Fluorescence of Guanine and Guanosine", Acta Chem. Scand. 21, 920 (1967).

Callis, P.R. Ph.D. Thesis (1966), University of Washington.

Callis, P.R., Rosa, E.J. and Simpson, W.T. "Search for Accidental Degeneracy in Purines", J. Am. Chem. Soc. 86, 2292 (1964).

Cavalieri, L.F., Bendich, A., Tinker, J.E. and Brown, G.B. "UV Absorption Spectra of Purines, Pyrimidines and Triazolopyrimidines" J. Am. Chem. Soc. 70, 3875 (1948).

Cavalieri, L.F., Fox, J.J., Stone, A. and Chang, N. "On the Nature of Xanthine and Substituted Xanthines in Solution", J. Am. Chem. Soc. 76, 1119 (1954).

Chandross, E.A., Ferguson, J. and McRae, E.G. "Absorption and Emission Spectra of Anthracene Dimers", J. Chem. Phys. 45, (10) 3546 (1966).

Chen, R.F. "Some Characteristics of the Fluorescence of Quinine", Analytical Biochemistry 19, 374 (1967).

Chen, H.H. and Clark, L.B. "Polarisation Assignment in the Electronic Spectrum of Purine", J. Chem. Phys. 51, 1862 (1969).

Clark, L.B. and Tinoco, I. Jr. "Correlation in the Ultraviolet Spectra of Purine and Pyrimidine Bases", J. Am. Chem. Soc. 87, 11 (1965).

Clementi, I. I.B.M. Research Paper RJ-256 (1963).

Cohen, B.J., Goodman, L. "The Luminescence of Purines", J. Am. Chem. Soc. 87, 5487 (1965).

Danesi, P.R., Magini, M. and Scibona, G. "Osmotic and Vapour Pressure Behaviour of Solutions Containing a Solute that Undergoes Aggregation", J. Phys. Chem. 72, (10) 3437 (1968).

Davydov, A.C. "Theory of Absorption Spectra of Molecular Crystals", J. Expt. Theor. Phys. 18, 210 (1948).

Del Bene, J. and Jaffe, H.H. "Use of the CNDO Method in Spectroscopy. II. Five-Membered Rings", J. Chem. Phys. 48, 1807, 4050 (1968); "Use of the CNDO Method in Spectroscopy. III. Mono-Substituted Benzenes and Pyridines", J. Chem. Phys. 49, 1221 (1968).

Demas, J.N. and Crosby, G.A. "Measurement of Photoluminescence; Quantum Yields", J. Phys. Chem. 75, N8, 991 (1971).

Denbigh, K. "The Principles of Chemical Equilibrium", University Press, Cambridge (1964).

DeVoe, H. and Tinoco, I. Jr. "The Hypochromism of Helical Polynucleotides", J. Mol. Biol. 4, 518 (1962).

Dohner, R.E., Wachter, A.H. and Simon, W. "Apparatur zur Molekulargewichtsbestimmung an hochverdünnten (10^{-4} M) Lösungen mittels Dampfdruckosmometrie", Helvetica Chim. Acta 50, 138 (1967).

Drobnik, J. and Augenstein, L. "Spectroscopic Studies of Purines. I. Factors Affecting the First Excited Levels of Purine", Photochemistry and Photobiology 5, 13 (1966A).

Drobnik, J. and Augenstein, L. "Spectroscopic Studies of Purines. II. Properties of Purine Substituted at the Second and Sixth Carbons", Photochemistry and Photobiology 5, 83 (1966B).

Drobnik, J., Augenstein, L. and Kleinwächter, V. "Spectroscopic Studies of Purines. III. Properties of Purines Substituted at the Sixth and Ninth Positions", Photochemistry and Photobiology 6, 113 (1967

Falk, M.M. "The UV Spectra of Native and Denatured DNA", J. Am. Chem. Soc. 86, 1226 (1964).

Fletcher, A.N. "Fluorescence; Emission Band Shift with Wavelength of Excitation", J. Phys. Chem. 72, 2742 (1968).

Fraser, R.D.B. "A Laboratory Manual of Analytical Methods of Protein Chemistry", (Ed. by P. Alexander and R.J. Block), Pergamon Press Ltd., London, Vol. 2, 285 (1960).

Fraser, R.D.B. "The Interpretation of Infrared Dichroism in Fibrous Protein Structures", J. Chem. Phys. 21 (9), 1511 (1953).

Fraser, R.D.B. "Interpretation of Infrared Dichroism in Axially Oriented Polymers", J. Chem. Phys. 28 (6), 113 (1958).

Frenkel, J. "The Transformation of Light into Heat In Solids", Phys. Rev. 37, 17 & 1276 (I & II) (1931).

Fröberg, C.E. "Introduction to Numerical Analysis", Addison-Wesley (1965), page 19.

Fucaloro, A.F. Ph.D. Thesis (1969), University of Arizona.

Fulton, R.L. and Gouterman, M. "Vibronic Coupling", J. Chem. Phys. 35, 1059 (1961).

Fulton, R.L. and Gouterman, M. "Vibronic Coupling. II. Spectra of Dimers", J. Chem. Phys. 41, N8, 2280 (1964).

Gilbert, N.E. "Electricity and Magnetism", Revised Edition, New York (1941).

Gill, S.J., Downing, M. and Sheats, G.F. "The Enthalpy of Self-Association of Purine Derivatives in Water", Biochemistry 6, No. 1, 272 (1967).

Goeppert-Mayer, M. and Sklar, A.L. "Calculations of the Lower Excited Levels of Benzene", J. Chem. Phys. 6, 645 (1938), included in Parr (1963).

Guttman, D. and Higuchi, T. "The Reversible Association of Caffeine and Some Caffeine Homologs in Aqueous Solution", J. Am. Pharm. Assoc. (Scientific Ed.), 46 (1), 4 (1957).

Handbook of Chemistry and Physics, 41st Edition, page 2890, Chemical Rubber Company, Cleveland, Ohio.

Haugen, G.R. and Melhuish, W.H. "Association and Self-Quenching of Proflavine in Water", Trans. Faraday Soc. 60, 386 (1964).

Haupt, G.W. "An Alkaline Solution of Potassium Chromate as a Transmittancy Standard in the Ultraviolet", J. Opt. Soc. Am. 42, 441 (1952).

Haylward, G. and Findlay, T.J.V. "Chemical Data Book", 2nd Edition, John Wiley, page 40.

Hercules, D.M. (Ed.) "Fluorescence and Phosphorescence Analysis", Interscience (1966).

Hinse, J. and Jaffe, H.H. "Electronegativity. I. Orbital Electronegativity of Neutral Atoms", J. Am. Chem. Soc. 84, 540 (1962).

Hirschfelder, J.O., Curtis, C.F. and Bird, R.B. "Molecular Theory of Gases and Liquids", John Wiley, New York, London (1964).

Iyengar, B.R.Y. "The Steady-State Temperature Difference in the Hill-Baldes Technique", Recueil, 73, 789 (1954).

Jablonski, A. "Zur Theorie der Polarisation der Photolumineszens von Farbstoffl"osungen", Z. Phys. 96, 236-46 (1935).

Jones, R.N. and Sandorfy, C. "Infrared and Raman Spectrometry: Applications", Technique of Organic Chemistry 11, 279 (1956).

Kankare, J.J. "Computation of Equilibrium Constants for Multicomponent Systems from Spectroscopic Data", Anal. Chem. 42, N12 (1970).

Kasha, M. "Energy Transfer Mechanisms and the Molecular Exciton Model for Molecular Aggregates", Rad. Res. 20, 55 (1963).

Kasha, M. "Paths of Molecular Excitation", Rad. Res. Suppl. 2, 243 (1960).

Kausmann, W. "Quantum Chemistry", Academic Press Inc., New York (1957).

Kelly, G.R. Honours Report, University of Adelaide (1970).

King, R.M. and Hercules, D.M. "Correction for Anomalous Fluorescence Peaks Caused by Grating Transmission Characteristics", Anal. Chem. 35, 1099 (1963).

Klopman, G. and O'Leary, B. "All-Valence Electrons S.C.F. Calculations", Fortschritte der Chemischen Forschung 15, N4, 445 (1970).

Kratky, O. "Deformation Mechanisms Der Faserstoffe", Kolloid Z. 64, 213 (1933).

Kurucsev, T. and Strauss, V.P. "Derivation and Interpretation of the Spectrum of the Dimer of Acridine Orange Hydrochloride; Dilute Aqueous Solution and Oriented Film Studies", J. Phys. Chem. 74, 3081 (1970).

Kwiatkowski, S. "Electronic Structure and Spectra of Organic Molecules: I. SCF-MO Calculations on Aniline and Phenylenediamines", Acta Physica Polon. 29, 477 (1966).

Lee, J. and Seliger, H.H.S. "Absolute Spectral Sensitivity of Phototubes and the Application to the Measurement of the Absolute Quantum Yields of Chemiluminescence and Bioluminescence", Photochemistry and Photobiology, 4, 1015 (1965).

Lindenberg, J. "Consistency Requirements in the PPP Model", Chem. Phys. Letters 1, 39 (1967).

McRae, E.G. "Molecular Vibrations in the Exciton Theory for Molecular Aggregates", Aust. J. Chem. 14, 329, 344, 354 (1962).

Mason, S.F. "Purine Studies II. The UV Absorption Spectra of Some Mono- and Poly- Substituted Purines", J. Chem. Soc. 2071 (1954).

Mason, S.F. "The Electronic Spectra of N Heterocaromatic Systems: VI. The $\pi \rightarrow \pi^*$ Transitions of Monocyclic Amino- and Mercaptoazines", J. Chem. Soc. 219 (1960).

Meeks, A.C. and Goldfarb, I.J. "Time Dependence and Dropsize Effects in Determining the Number Average Molecular Weight by V.P.O.", Anal. Chem. 39, No. 8, 908 (1967).

Melhuish, W.H. "Quantum Efficiencies of Fluorescence of Organic Substances: Effect of Solvent and Concentration of the Fluorescent Solute", J. Phys. Chem. 65, 229 (1961).

Merrifield, R.E. "Vibrational States of Dimers", Radiation Research 20, 154 (1963).

Murrell, J.N. "The Theory of the Electronic Spectra of Organic Molecules", Methuen, London (1963).

Nancollas, G.H. and Hardy, J.A. "A Thermistor Bridge for use in Calorimetry", J. Sci. Instrum. 44 (4), 290-1 (1967).

Nishimoto, K. and Foster, L.S. "SCF Calculations of Aromatic Hydrocarbons. The Variable B Parameter", Theoret. Chim. Acta 3, 407 (1965).

Nishimoto, K. and Foster, L.S. "SCF-MO Calculation of Heteroatomic Systems with the Variable B Parameter", Theoret. Chim. Acta 4, 155 (1966).

Parker, C.A. and Rees, W.T. "Fluorescence Spectrometry", Analyst 87, 83-111 (1962).

Parker, C.A. and Rees, W.T. "Photolysis of Thionine in Rigid Medium", J. Chim. Phys. 56, 761-70 (1959).

Parr, R.G. "Quantum Theory of Molecular Electronic Structure", W.A. Benjamin Inc., New York (1963).

Platt, J.R. "Spectroscopic Moment: A Parameter of Substituent Groups Determining Aromatic Intensities", J. Chem. Phys. 19, 263 (1951).

Pople, J.A. and Beveridge, D.L. "Approximate Molecular Orbital Theory", McGraw-Hill (1970).

Pople, J.A., Santry, D.P. and Segal, G.A. "Approximate Self-Consistent Molecular Orbital Theory", J. Chem. Phys. 43, 129 (1965).

Pullman, A. and Pullman, B. "Electronic Structure of the Purine and Pyrimidine Bases of Nucleic Acids and of their Interactions", Adv. Quantum Chem. 4, 267 (1968).

Pullman, B., Claverie, P. and Caillet, J. "V.D. Waals-London Interactions and the Configuration of Hydrogen-Bonded Purine and Pyrimidine Pairs", Biochemistry 55, No. 4, 904 (1966A).

Pullman, B., Claverie, P. and Caillet, J. "V.D. Waals-London Interactions Between Stacked Purines and Pyrimidines", J. Theoret. Biol. 12, 419 (1966B).

Pullman, B. Claverie, P. and Caillet, J. "Intermolecular Forces in Association of Purines with Polybenzoid Hydrocarbons", Science 147, 1305 (1965).

Ramette, R.W. and Sandell, E.B. "Rhodamine B Equilibria", Bull. Chem. Soc. Japan 78, 4874 (1956).

Rich, A. and Kasha, M. "The $n \rightarrow \pi^*$ Transition in Nucleic Acids and Polynucleotides", J. Am. Chem. Soc. 82, 6197 (1960).

Rosa, E.J. Ph.D. Thesis, University of Washington (1966).

Siebrand, W. "Vibrational Structure of Electronic States of Molecular Aggregates", J. Chem. Phys. 40 (8), 2223 (1964).

Simpson, W.T. and Peterson, D.L. "Coupling Strength for Resonance Force Transfer of Electronic Energy in V.D. Waals Solids", J. Chem. Phys. 26, 588 (1957).

Smirnov, L.V. "Molecular Dichroism by the Method of Artificial Orientation of Molecules", Optika i Spektroskopiya 3, 123-33 (1957

Spencer, M. "The Stereochemistry of Deoxyribonucleic Acid: I. Covalent Bond Length and Angles", Acta Cryst. 12, 59 (1959).

Stewart, R.F. and Davidson, N. "Polarised Absorption Spectra of Single Crystals of 1-methyl Thymine, 9-methyl Adenine and their Hydrogen Bonded Complexes", Biopolymers Symp. 1, 465 (1964).

Stewart, R.F. and Davidson, N. "Polarised Absorption Spectra of Purines and Pyrimidines", J. Chem. Phys. 39, 255 (1963).

Stewart, R.F. and Jensen, R.H. "Redetermination of the Crystal Structure of Uracil", Acta Cryst. 23, 1102 (1967).

Stewart, R.F. and Jensen, L.H. "Crystal Structure of Methyladenine", J. Chem. Phys. 40, 2071 (1964).

Stoesser, P.R. and Gill, S.J. "Calorimetric Study of Self-Association of 6-methylpurine in Water", J. Phys. Chem. 71 (3), 564 (1967).

Sutor, D.J. "The Structure of the Pyrimidines and Purines. VII. The Crystal Structure of Caffeine", Acta Cryst. 11, 453 (1958).

Tanisaki, Y. "Dichroism of Dyes in Stretched PVA Sheets. II. The Relation Between the Optical Density Ratio and the Stretch Ratio. An Attempt to Analyse Relative Directions of Absorption Bands", Bull. Chem. Soc. Japan 32, 75 (1959).

Tanisaki, Y. "The Correction of the Relation of the Optical Density Ratio to the Stretch Ratio on the Dichroic Spectra", Bull. Chem. Soc. Japan 38, 1798 (1965).

Tanisaki, Y. and Kubodera, S. "Dichroism Analysis. Part I. Vibronic Transitions of Some Naphthols", J. Mol. Spectroscopy 24, 1 (1967).

Thakkar, A.L., Tenameyer, L.G., Hermann, R.E. and Wilham, W.L. "Self-Association of Caffeine in Aqueous Solution; H Nuclear Magnetic Resonance Study", Chemical Communications 9, 524 (1970).

Thulstrup, E.W. and Eggers, J.H. "Moment Directions of the Electronic Transitions of Fluoranthene", Chem. Phys. Lett. 1, 690 (1968).

Thulstrup, E.W., Michl, J. and Eggers, J.H. "Polarization Spectra in Stretched Polymer Sheets. II. Separation of $\pi - \pi^*$ Absorption of Symmetrical Molecules into Components", J. Phys. Chem. 74, 3868 (1970A).

Thulstrup, E.W., Michl, J. and Eggers, J.H. "Polarization Spectra in Stretched Polymer Sheets. III. Physical Significance of the Orientation Factors and Determination of $\pi - \pi^*$ Transition Moment Directions in Molecules of Low Symmetry", J. Phys. Chem. 74, 3878 (1970B).

T'so, P.O., Melvin, I.S. and Olson, A.C. "Interaction and Association of Bases and Nucleosides in Aqueous Solution", J. Am. Chem. Soc. 85, 1289 (1963).

T'so, P.O. and Chan, S.I. "Interaction and Association of Bases and Nucleosides in Aqueous Solution. II. Association of 6-methylpurine and 5-bromouridine and Treatment of Multiple Equilibria", J. Am. Chem. Soc. 86, 4176 (1964A).

T'so, P.O., Chan, S.I., Schweizer, M.P. and Helmkamp, G.K. "Interaction and Association of Bases and Nucleosides in Aqueous Solution. III. An NMR Study of the Self-Association of Purine and 6-methylpurine", J. Am. Chem. Soc. 86, 4182 (1964B).

T'so, P.O., Chan, S.I. and Schweizer, M.P. "Interaction and Association of Bases and Nucleosides in Aqueous Solution. IV. PMR Studies of the Association of Pyrimidine Nucleosides and their Interactions with Purine", J. Am. Chem. Soc. 87, 5241 (1965).

T'so, P.O., Broom, A.D. and Schweizer, M.P. "Interaction and Association of Bases and Nucleosides in Aqueous Solution. V. Studies of the Association of Purine Nucleosides by VPO and PMR", J. Am. Chem. Soc. 89, 3612 (1967).

Tsunoda, T. and Yamaoka, T. "Study of the Orientation of Light-Sensitive Tetrazonium Salt in Poly(Vinyl Alcohol)", J. Polymer Sci. Part A, 3 (1965).

Turner, D.W. "Ionisation Potentials", Advan. Physic. Org. Chem. 4, 31 (1966).

Van Dam, J. "Determination of Molecular Weights by Means of Thermoelectric Vapour Phase Osmometry", Rec. des Travaux Chimiques des Pays-Bas 83, No. 2, 129 (1964).

Voet, D., Gratzer, W.B., Cox, R.A. and Doty, P. "The Absorption Spectra of Nucleotides, Polynucleotides and Nucleic Acids in the Far UV", Biopolymers 1, 193 (1963).

Yguerabide, J. "Fast and Accurate Method for Measuring Photon Flux in the Range 2500-6000 Å", Rev. Sci. Instrum. 39 (7), 1048 (1968).